Study of the effects of solvent and temperature on the self-assemble surface patterns in Azopolymer films

Shahla Golghasemi Sorkhabi

UNIVERSITE BRETAGNE LOIRE

université angers

Thèse de Doctorat

Shahla Golghasemi Sorkhabi

Mémoire présenté en vue de l'obtention du
grade de Docteur de l'Université d'Angers
sous le sceau de l'Université Bretagne Loire

École doctorale : *3MPL*

Discipline : *Physique*
Spécialité : Optique
Unité de recherche : *UMR 6200*

Soutenue le *4 septembre 2017*
Thèse N° :

Study of the effects of solvent and temperature on the self-assemble surface patterns in Azopolymer films

JURY

Rapporteurs :	Saifollah RASOULI, associate professor, IASBS, (Iran). Ezzedin MOHAJERANI, Professor, Shahid Behehsti University, (Iran)
Examinateurs :	Saifollah RASOULI, associate professor, IASBS, (Iran). Ezzedin MOHAJERANI, Professor, Shahid Behehsti University, (Iran) Mohammad Sadegh Zakerhamidi, associated Professor, University of Tabriz (RIAPA), (Iran)
Invité(s) :	Behrooz Rezaei, **associated Professor, University of Tabriz (**RIAPA), (Iran)
Directeur de Thèse :	Régis Barillé, Professeur, Université d'Angers, (France)
Co-directeur de Thèse :	Sohrab Ahmadi-Kandjani, Assistant professor, University of Tabriz (RIAPA), (Iran)

UNIVERSITE BRETAGNE LOIRE

université angers

Thèse de Doctorat

Shahla golghasemi Sorkhabi

Study of the effects of solvent and temperatures on the self-assemble surface patterns in azopolymer films

Résumé

Dans cette thèse nous présentons différents motifs formés par auto-organisation de matériaux azopolymères soumis à un rayonnement lumineux.
Nous avons montré que de nombreux réseaux de surface photoinduits, jusqu'à 10, peuvent être enregistrés sur la même zone d'un film azopolymère pourvu que la polarisation du faisceau d'écriture soit bien choisie. Cet effet a permis la création d'une grande variété de motifs complexes. Dans cette thèse, nous montrons de telles structures complexes formées à la surface de couches minces d'azopolymère via un ensemble de réseaux superposés (jusqu'à 16 sur la même zone). Nous créons ainsi des structures dites quasi-cristal à 2 dimensions. La surface d'azopolymère est alors utilisée comme un moule afin d'être répliquée avec un élastomère. La couche d'élastomère ainsi produite possède la même structure que le moule en azopolymère.
Cette couche est flexible, transparente et étirable et nous l'avons utilisé pour le dépôt de nano-objets uniques.
Les caractéristiques de deux surfaces photoinduites de deux azopolymères chiraux ont été comparées: une surface aléatoire de type gaussien et une surface avec des réseaux quasi-aléatoires.
Ces motifs ont été obtenus avec une technique simple de type 'bottom-up' en éclairant la couche mince d'azopolymère avec un seul faisceau laser. La surface avec des réseaux quasi-aléatoires peut être utilisée pour le couplage de la lumière dans plusieurs directions dans un film ultra-mince. Ces deux surfaces ont été utilisées comme moule et répliquées sur un élastomère transparent. Elles montrent un très bon piégeage de la lumière. Plus précisément, le piégeage de la lumière est 20% meilleur avec les réseaux quasi-aléatoires qu'avec la surface aléatoire de type gaussien et il est de l'ordre de 40%.

Mots clés
Azopolymère, structuration en surface, piégeage de lumière

Abstract

In this thesis we present various patterns formed by self-organization of azopolymer materials subjected to light radiation.
We have shown that many photoinduced surface gratings, up to 10, can be recorded on the same area of an azopolymer film, provided that the polarization of the writing beam is well chosen.
This effect allowed the creation of a wide variety of complex patterns. In this thesis, we show such complex structures formed on the surface of thin layers of azopolymer, via a set of superimposed networks (up to 16 on the same zone). We thus create so-called quasi-crystal structures with 2 dimensions. The azopolymer surface is then used as a mold to be replicated with an elastomer. The elastomer layer produced has the same structure as the azopolymer mold.
This layer is flexible, transparent and stretchable and we used it for the deposition of unique nano-objects.
The characteristics of two photoinduced surfaces of two chiral azopolymers were compared: a Gaussian type random surface and a surface with quasi-random lattices. These patterns were obtained with a simple bottom-up technique, by illuminating the thin layer of azopolymer with a single laser beam. The surface with quasi-random lattices can be used for the coupling of light in several directions in an ultra-thin film. These two surfaces were used as molds and replicated on a transparent elastomer. They show a very good trapping of light. More precisely, the trapping of the light is 20% better with the quasi-random gratings than with the random surface of the Gaussian type and it is of the order of 40%.

Key Words
Azopolymer, Surface structuration, light trapping

Acknowledgments

It has truly been a privilege and rewarding experience to work in the creative atmosphere of the group of Dr.Sohrab Ahmadi-Kandjani and Prof. Regis Barille. First and foremost I would like to thank them for their continuous guidance, support and encouragement and for being inexhaustible sources of ideas and inspiration. Without them this work would have been impossible. I am grateful to Prof. Asghar Asgari, who gave me expert guidance, generous professional support and invaluable ideas. I am deeply indebted to Dr. Sylvie DABOS-SEIGNON. She was very kind to me and always helpful during my time in Angers and helped me with many AFM images for our studies. I am also grateful to Dr. Sonia Zielinska and Dr. Ewelina Ortyl (Department of Polymer Engineering and Technology, Wroclaw University of Technology) for the preparation and synthesis of the compounds used in this thesis. I would like to thank our colleagues Dr. Matthieu Loumaigne and Fabien Cousseau (Moltech, University of Angers) for their efforts regarding the theoretical calculations and simulations of our experimental results.

I'd like to thank the members of my thesis jury. My special thanks go to Prof. Ezeddin Mohajerani, Prof. Saifollah Rasouli and Dr. Mohammad Sadegh Zakerhamidi for carefully reading the manuscript and for their insightful comments.

I would like to thank R. MALLET; Service Commun d'Imageries et d'Analyses Microscopiques (SCIAM), Angers, for AFM and SEM images presented in this thesis.

I'd like to thank my professors in RIAPA/University of Tabriz for their help and support during this project. I appreciate the support of my friends and collegues at both Moltech and Riapa.

Last, but certainly not least, and the most important, I would like to give my special thanks and all my love to my family, without their undying love, support, understanding, and unwavering faith I would not have be who i am or where i am.

This thesis was funded by the Ministry of Science, Research & Technology of IRAN, University of Tabriz and the culture and language center of the embassy of France.

Abstract

In this thesis we present various patterns formed by self-organization of azopolymer materials subjected to light radiation.

We have shown that many photoinduced surface gratings, up to 10, can be recorded on the same area of an azopolymer film, provided that the polarization of the writing beam is well chosen. This effect allowed the creation of a wide variety of complex patterns. In this thesis, we show such complex structures formed on the surface of thin layers of azopolymer, via a set of superimposed networks (up to 16 on the same zone). We thus create so-called quasi-crystal structures with 2 dimensions. The azopolymer surface is then used as a mold to be replicated with an elastomer. The elastomer layer produced has the same structure as the azopolymer mold. This layer is flexible, transparent and stretchable and we used it for the deposition of unique nano-objects.

The characteristics of two photoinduced surfaces of two chiral azopolymers were compared: a Gaussian type random surface and a surface with quasi-random lattices. These patterns were obtained with a simple bottom-up technique, by illuminating the thin layer of azopolymer with a single laser beam. The surface with quasi-random lattices can be used for the coupling of light in several directions in an ultra-thin film. These two surfaces were used as molds and replicated on a transparent elastomer. They show a very good trapping of light. More precisely, the trapping of the light is 20% better with the quasi-random gratings than with the random surface of the Gaussian type and it is of the order of 40%.

On the other hand, using a non-coherent irradiance associated with the solvent-droplet-induced-dewetting method, we have shown a method for producing ordered nano-patterns based on dewetting. These nanostructures can be categorized as nano-doughnuts and are composed of a hole surrounded by a ring. Moreover, using the property of the azopolymer films, having a large

macroscopic photoinduced motions, the nanostructures can be optimized and reshaped via a judiciously chosen light field.

Finally, in this thesis, a new type of colloidal nanoparticles of the 'janus' type composed of azopolymer and PMMA were synthesized. These nanoparticles look like soccer balls. Because of the photo-fluidization of the azopolymer, a restricted portion of the azopolymer layer at the surface of the nanoparticles can be modified by light in order to obtain unique morphologies such as; "porcupine" particles or "pineapple" particles.

Résumé

Dans cette thèse nous présentons différents motifs formés par auto-organisation de matériaux azopolymères soumis à un rayonnement lumineux.

Nous avons montré que de nombreux réseaux de surface photoinduits, jusqu'à 10, peuvent être enregistrés sur la même zone d'un film azopolymère pourvu que la polarisation du faisceau d'écriture soit bien choisie. Cet effet a permis la création d'une grande variété de motifs complexes. Dans cette thèse, nous montrons de telles structures complexes formées à la surface de couches minces d'azopolymère via un ensemble de réseaux superposés (jusqu'à 16 sur la même zone). Nous créons ainsi des structures dites quasi-cristal à 2 dimensions. La surface d'azopolymère est alors utilisée comme un moule afin d'être répliquée avec un élastomère. La couche d'élastomère ainsi produite possède la même structure que le moule en azopolymère. Cette couche est flexible, transparente et étirable et nous l'avons utilisé pour le dépôt de nano-objets uniques.

Les caractéristiques de deux surfaces photoinduites de deux azopolymères chiraux ont été comparées: une surface aléatoire de type gaussien et une surface avec des réseaux quasi-aléatoires. Ces motifs ont été obtenus avec une technique simple de type 'bottom-up' en éclairant la couche mince d'azopolymère avec un seul faisceau laser. La surface avec des réseaux quasi-aléatoires peut être utilisée pour le couplage de la lumière dans plusieurs directions dans un film ultra-mince. Ces deux surfaces ont été utilisées comme moule et répliquées sur un élastomère transparent. Elles montrent un très bon piégeage de la lumière. Plus précisément, le piégeage de la lumière est 20% meilleur avec les réseaux quasi-aléatoires qu'avec la surface aléatoire de type gaussien et il est de l'ordre de 40%.

D'autre part en utilisant un éclairement non cohérent associé à la méthode 'solvent-droplet-induced-dewetting', nous avons montré une méthode pour fabriquer des nano-motifs ordonnés

basés sur le démouillage. Ces nanostructures sont assimilables à des nano-beignets et sont composées d'un trou entouré d'un anneau. De plus, en utilisant la propriété des films d'azopolymère à avoir de grands mouvements macroscopiques photoinduits, les nanostructures peuvent être optimisées et remodelées via un champ lumineux judicieusement choisi.

Enfin, dans cette thèse, un nouveau type de nanoparticules colloïdales de type ‘janus’ composées d'azopolymère et de PMMA ont été synthétisées. Ces nanoparticules ressemblent à des ballons de football. A cause de la photo-fluidisation de l’azopolymère, une partie restreinte de la couche d'azopolymère en surface de la nanoparticule peut être modifiée par la lumière afin d'obtenir des morphologies uniques comme par exemple des particules “hérissons” ou des particules “ananas”.

Table of Contents

List of Figures

List of Tables

General Introduction

Our environment is a composite of numerous amazing self-organized patterns. The waves of the sea, the little ripples on the shore, the sweeping curve of the sandy bay between the headlands, the outline of the hills, the shape of the clouds, patterns on the skin of animals, the nest of social insects, bacterial colonies, all these are so many riddles of form, so many problems of morphology, and all of them the physicist can more or less easily read and adequately solve. In optics self-organized regular patterns emerge from uniform or randomly structured input optical fields. These patterns can be used in image formation and manipulation techniques to increase the sensitivity or resolution of optical systems, the manufacturing of optical neural networks and associative memories and the use of fractal and wavelet algorithms for image compression.

In this regard, Azobenzene and its derivatives are fascinating molecules display that the reversible photoisomerization between the more stable trans and the less stable cis isomers. Although photoisomerization can result in important changes of properties for azobenzene molecules on their own, such as a large change in molecular shape and dipole moment, changes that can be imparted to polymers and liquid crystals when azobenzene is part of their structures or is associated with them are more interesting. Surface relief grating (SRG) formation in azo-polymeric materials is a new form of grating formation in optical materials. SRG is a young branch of research and lot of questions remain unanswered. Migration (diffusion) of azo-molecules from bright region of two coherent beams interference to its dark region result grating formation on the surface of polymer film. As such, engineering azopolymer materials can lead to photoisomerization induced by light, to create different and unique self-induced patterns on the surface of thin films. The subject of our study concerns the self-organization of azo-molecules to form a regular patterns through single or multiple exposures in a azopolymer film.

In this thesis, we present a simple experimental method, based on irradiation of azopolymer thin films with an interference pattern of laser beam, for formation of complex quasi-crystal structures on the surface of thin films. Also, using a set of newly synthesized chiral azopolymers, a 2D quasi Gaussian surface and a quasi-random periodic surface (quasi-random gratings) are formed on the surface of thin films, based on molecular nano-motor lithography. Advantages of both surfaces for energy conversion are discussed and two examples of applications, requiring a high light coupling in a thin film, are presented. Next, a simple bottom-up approach is used to produce doughnut shaped nanostructures on the surface of azopolymer thin films, by the choice of a solvent-droplet-induced-dewetting method and an incoherent unpolarized light illumination. Also, due to the presence of highly photoactive azobenzene derivative in the material, illumination of these nano-structures by a polarized laser light shows the possibility of a further growth and reshaping of the structures. Furthermore, using the method of control dewetting on a pre-patterned substrate, formation of nano-structures are directed and ordered.

The last part of the study deals with a new and excited group of colloidal azopolymer particles, composed of PMMA and azopolymer, resembling a buckyball, and their unique deformations under illumination via laser light, with different polarizations. We propose the investigation of such particles for the study of the SRG formation phenomena and the basic understanding of the light-matter interaction.

The vitality and sustained interest of this field can easily be noticed from the many research papers on azobenzene-based materials that continue to appear.

Overview of the thesis

The first chapter is devoted to the presentation of self-organization and a general review of azo-polymer film deformation. The idea of surface relief grating formation, proposed models will be

developed in this chapter. The basic background is set to help the general readership understand the fundamental aspects involved in and the ideas and interests behind the azo materials used in this study. In this chapter we will also present the concept and advantages of Random and Quasi-random surfaces, as an active field in disorder photonics. Following, we introduce Dewetting as a different approach to induce patterns on the surface of azopolymer thin films. Next, we review and discuss colloidal polymeric particles as the subject of a wide range of studies and developments. The last part of chapter I, recalls soft lithography as a simple and inexpensive method, well suited for the fabrication of surface structures for polymers, gels and organic monolayers.

In the second chapter, we present azopolymer materials used in this study, along with their characteristics. Plus, this chapter contains the list of solvents, experimental methods, nanoparticles, optical setups and the equipments (microscops, profilometer and …) employed in this project. Last part of chapter II explains the synthesis process of the new group of azoparticles.

The third chapter is devoted to describing the results of studies. In first part, we present the fabrication of surface quasi-crystal structures on azo polymer films through successive inscription of multiple surface relief gratings. Following, this structures were used as a mold for replication, via soft lithography, on a transparent elastometer (PDMS) and its applicibility in nanoparticle deposition.

In second part of chapter III we discuss the formation of Quasi-random or Gaussian random structures on azopolymer films, by the method of single beam irradiation. Special characteristics and properties of these structures are discussed and the possibility of application of these surface structures in real life fields like, Organic light-emitting diode (OLEDs) or solar cells, for a better efficiency of light diffusion or light harvesting, are evaluated.

In third part of chapter III we focus on surface structuring through dewetting. In this part, using solvent-droplet-induced-method doughnut shaped nanostructures are induced on the surface of azopolymer thin films. Due to the nature of azopolymer material, there is a possibility of further growth and reshaping of said nano structures under laser irradiation.

In final part of chapter III we review the newly synthesized azoparticles. Properties and behavior of these particles under single and double beam illumination are studied and the resulted deformations and unique shapes are presented.

In the appendix, mathematical description of SRGs on the thin films and PDMS replica are discussed in great details. Also, a quantitative analysis of the evolution of the nanocavities' dimensions with stretching the PDMS quasi-crystal was done and a method for extraction of cavities' dimension on the PDMS sample was presented. Finally, a simulation of the random Gaussian surface was obtained with a stochastic process, resulting from an acting random molecular surface process.

Chapter I:
Introduction of Pattern Formation

I.1. Introduction

The scientific study of self-organizing systems is relatively new, although questions about how organization arises have of course been raised since ancient times. Many natural systems show organization (e.g. galaxies, planets, chemical compounds, cells, organisms and societies). There has been a tremendous increase in the study of self-organization in optical systems.

This thesis is devoted to review optical patterns and surface relief grating (SRG) formation as a path to form complex structures for different applications. We will also discuss one beam deformation of azo-materials on a new series of azo-polymers. Two unique surface structures are introduced; a Gaussian random pattern and a surface with quasi-random gratings. Following, new set of structures are obtained using the solvent-droplet-induced-dewetting method. The resulted structures resemble a dough-nut, with the ability for further reshaping.

In the end, we present a new group of synthesize colloidal polymeric particles consist of PMMA and azopolymer. Due to the unique structure of these particles, under illumination by a laser beam, the resulted shapes are utterly interesting and unique.

I.2. Patterns/self-organizations

Pattern formation is a truly interdisciplinary science. The similarity in fundamental mechanisms and the accompanying mathematics brings together scientists from many disciplines such as; biology, chemistry, fluid dynamics, material science, mathematics, medicine, geophysics, ecology, physics and surface science. Natural patterns turn up all over. From sea shells and spiral galaxies to the structure of human lungs, the patterns of chaos are all around us. Fractals are patterns formed from chaotic equations and contain self-similar patterns of complexity increasing with magnification. If a fractal pattern is divided into parts, one gets a nearly identical reduced-size copy of the whole. The mathematical beauty of fractals is that infinite complexity is formed with relatively simple equations. By iterating or repeating fractal-generating equations many times, random outputs create beautiful patterns that are unique, yet recognizable. Some of the most stunning natural examples are found of fractals on our planet.

Like Romanesco Brocoli; this variant form of cauliflower is the ultimate fractal vegetable. Its pattern is a natural representation of the Fibonacci or golden spiral, a logarithmic spiral where every quarter turn is farther from the origin by a factor of phi, the golden ratio.

Ammonite Sutures; Extinct for 65 million years, ammonites were marine cephalopods that built chambered spiral shells. The walls between these chambers, called sutures, were complex fractal curves. The shells of ammonites also grow as a logarithmic spiral, a pattern that appears often in nature, as with romanesco broccoli.

Mountains; result of tectonic forces pushing the crust upward and erosion tearing some of that crust down. The resulting pattern is a fractal. Such as the Rainbow Mountains Of China, earth's paint palette. Leaves of plants that follow simple recursive formulas in generating their branching shapes and leaf patterns. Patterns of peacock Feathers, which Peacocks used to attract mates. Snowflakes; crystallizing water that forms repeating patterns in snowflakes and on frosty surfaces. The patterns have

inspired claims about the power of consciousness to affect matter, as well as one of the first described fractal curves, the Koch snowflake, and so many other examples all around us (Fig.I.1).

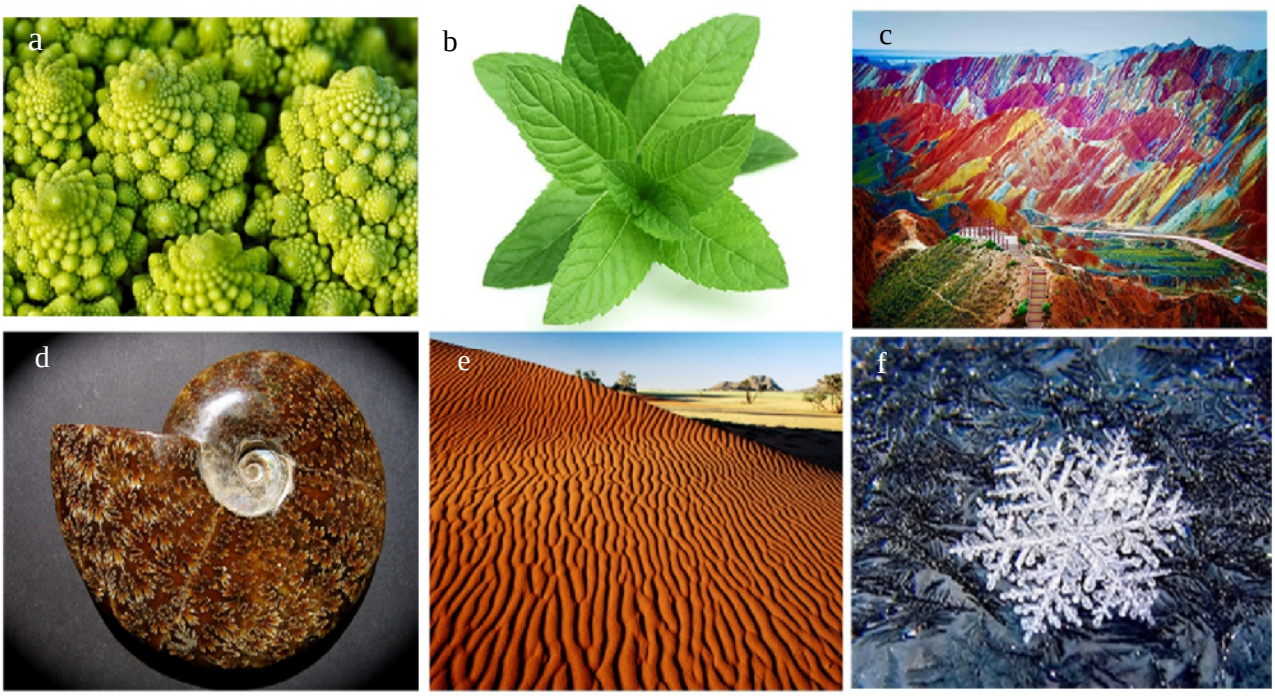

Fig. I-1: Few examples of self-organized patterns in nature. a) golden spiral of RomanescoBrocoli, b) Leaves of plants c) Rainbow Mountains Of China d) logarithmic spiral ofAmmonite Sutures e)Ripples pattern of a desert dune f) Pattern of a snowflake

There is always an element of subjectivity in perceiving patterns. There are surely certain spatial images that are most categorized as patterns; the repeating designs of wallpaper or carpets, for example. This prompts the idea that a pattern might be regarded as a regularly repeating array of identical units. This concept can be broadened slightly, and include in general definition an arrays of units that are similar but not necessarily identical, and which repeat but not necessarily regularly or with a well-defined symmetry. An example is the ripples of sand at the seaward edge of a beach or in a desert (Fig.I.1.e). No two ripples are identical, and they are not positioned at exactly repeating intervals (which is to say, periodically in space) but nonetheless, it isn't too hard to persuade one that this might be reasonably called a pattern, since one can recognize within it elementary units (the ripples) that recur again

throughout space. A mountain range has features of all sizes, from little crevasses to huge sweeping valleys, but there is still something about the way it looks from above that allows one to see a pattern.

Form is a more individual affair. It could be defined loosely as the characteristic shape of a class of objects. Like the elements of a pattern as described above, objects with the same form do not have to be identical, or even similar in size; they simply have to share certain features so they can be recognized as typical. Shells of sea creatures are like this. The shells of organisms of the same species all tend to have a certain form that can be recognized and identified even by a relatively untrained eye, despite the fact that no two shells are identical. The same is true of flowers, and of the shapes of mineral crystals. The true form of these objects is that which remains after all the slight and inevitable variations between individuals have been averaged away[1].

The problem of creating patterns and forms that we tend to recognize as such is therefore not one of how to generate the symmetry that they often possess, but of how to reduce the perfect symmetry that total randomness engenders, to give rise to the lower symmetry of the pattern. How do the water molecules moving at random in the atmosphere coalesce into a six-petalled snowflake? Patterns like this are the result of symmetry breaking[1].

The study of complexity provides new insights into how patterns develop in nature. One exciting finding is that order often arises spontaneously from disorder; patterns can emerge through a process of self-organization[2].

Self-organized systems are structure formations without any clear association from outside of the system. Any system that takes a form that is not imposed from outside (by walls, machines or forces) can be said to self-organize. In other words, a self-organization results from the interactions among the components of the system and is an internal phenomenon. The

organization can develop in either time or space, maintain a stable form or show transient phenomena. The size of self-organized patterns typically is much larger than the size of individual components and in some natural patterns their ratio can reach 10^4-10^5. General resource flows within self-organized systems are expected (dissipation), although not critical to the concept itself. For example in spite of conflicting actions between insects, collective structures which fulfil numerous functional and adaptive requirements are produced[3]. Noise (fluctuations) can allow metastable systems to escape one basin and to enter another, thus over time the system can approach an optimum organization or may swap between the various patterns, depending upon the size and nature of the perturbations. For instance, individual insects are not able to process a large quantity of information but simply their response to stimulus from other individuals or environment (these stimulus don't carry any signs, simply they are attractive or repulsive, activating or inhibiting) lead to Pattern formation. The individual units just have access to local information[4].

The field of self-organization seeks general rules about the growth and evolution of systemic structure, the forms it might take, and finally methods that predict the future organization that will result from changes made to the underlying components (past construction sets the stage for new building actions)[5].

Several researches have been developed on the study of the structure formation through self-organization in optical systems because optics has several advantages such as flexibility and the simplicity of handling. Organic materials have been shown to be quite useful for the fabrication of integrated-optics devices. Responsive polymer-based materials, like azopolymers, are capable of altering their chemical and/or physical properties upon exposure to external stimuli.A brief description of these compounds are given in the next section.

I.3. Azobenzene

Azobenzene is a chemical compound composed of two phenyl rings linked by an N=N double bond. The term azobenzene or simply azo is often used to refer to a wide class of molecules that share the core azobenzene structure, with different chemical functional groups extending from the phenyl rings (technically, these compounds should be referred to as diazenes). The azobenzene compounds strongly absorb light, and were historically used as dyes in a variety of industries. One of the most intriguing properties of azos is photo-isomerization behavior between two isomers, the trans and cis configurations[6]. The two isomers can be switched with particular wavelengths of light: ultraviolet or blue light, which corresponds to the energy gap of the π-π* (S_2 state) transition, for trans-to-cis conversion, and blue light, which is equivalent to that of the n-π* (S_1 state) transition, for cis-to-trans isomerization. For a variety of reasons, the cis- isomer is less stable than the trans (for instance, it has a distorted configuration and breaks the aromaticity of the trans configuration) Thus, cis-azobenzene will thermally relax back to the trans via cis-to-trans isomerization. The trans isomer is more stable by approximately 50 kJ/mol, and the barrier to photo-isomerization is on the order of 200 kJ/mol (Fig.I.2)[7, 8].

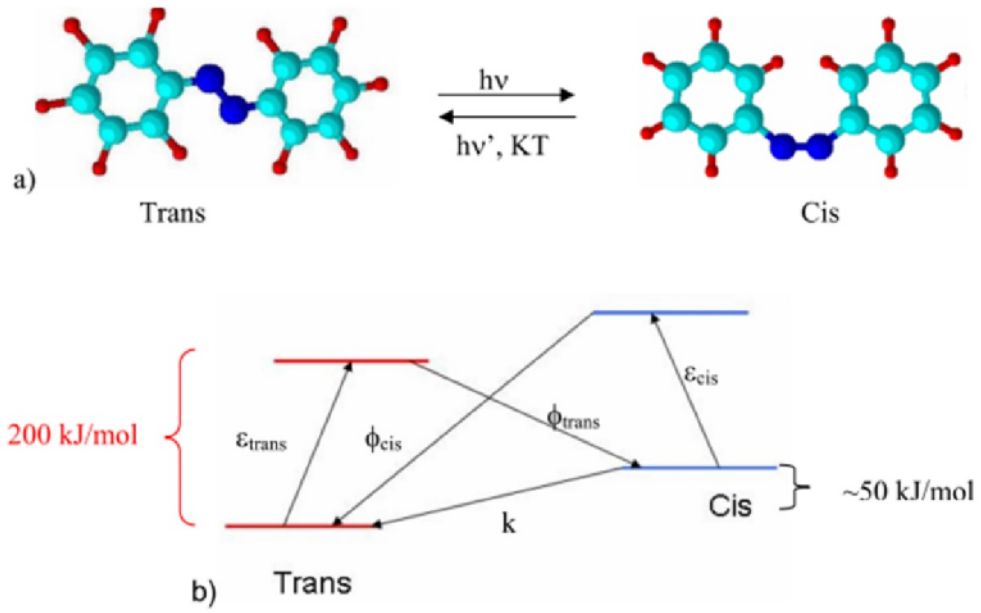

Fig. I-2 : a) Azobenzene can be converted from the trans to the cis state photochemically, and will revert back to the stable trans state thermally. Alternately, the cis to trans conversion can be effectuated with a distinct wavelength of light. (b) Simplified state model for azobenzenechromophores. The exinction coefficients are denoted ε, whereas the quantum yields for the photoisomerizations are labelled φ. The rate of thermal relaxation is denoted by k.

The exact wavelength at which azobenzene isomerization occurs depends on the particular structure of each azo molecule, but they are typically grouped into three classes[6]: the azobenzene-type molecules, the amino-azobenzenes, and the pseudo-stilbenes (Fig. I.3).

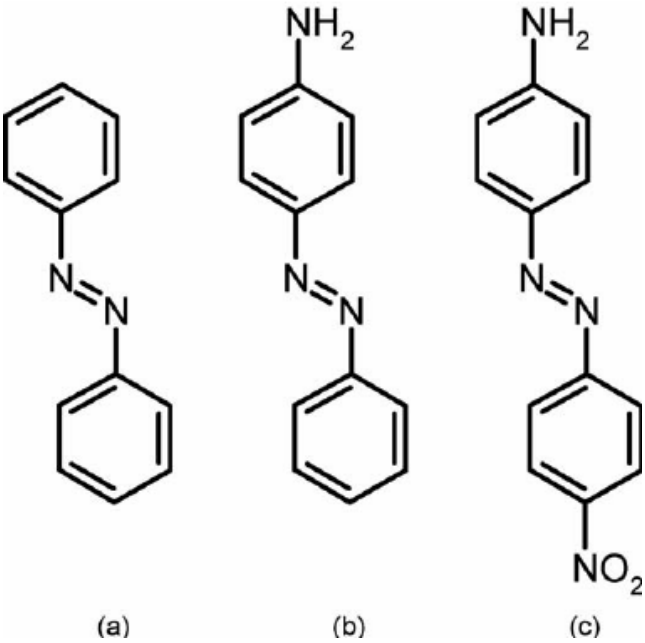

Fig. I-3 : Examples of azobenzene molecules that fall into the three spectroscopic classes: (a) azobenzenes (b) aminoazobenzenes, and (c) pseudo-stilbenes

These azos are yellow, orange, and red, respectively, owing to the subtle differences in their electronic absorption spectra. The compounds similar to the unsubstitutedazobenzene exhibit a low-intensity n-π* absorption in the visible region, and a much higher intensity π-π* absorption in the ultraviolet. Ortho- or para-substituted azo dyes with electron-donating groups (such as aminos), are classified as amino-azobenzenes, and tend to closely spaced n-π* and π-π* bands in the visible. The pseudo-stilbene class is characterized by substituting the 4 and 4' positions of the two azo rings with electron-donating and electron-withdrawing groups (that is, the two opposite ends of the aromatic system are functionalized). This push-pull configuration results in a strongly asymmetric electron distribution, which modifies a host of optical properties. In particular, it shifts the absorption spectra of the trans- and the cis- isomers, so that they effectively overlap. Thus, for these compounds a single wavelength of light in the visible region will induce both the forward and reverse isomerization. Under illumination, these molecules will be constantly cycling between the two isomeric states. The thermal back-

relaxation varies greatly depending on the compound: usually hours for azobenzene-type molecules, minutes for aminoazobenzenes, and seconds for the pseudo-stilbenes. The energy barrier for this thermal isomerization is on the order of 90 kJ/mol[9], [10]. The thermal back-relaxation is generally first-order, although the distribution of highly constrained configurations that arise in a glassy polymer matrix can lead to anomalously fast decay components [11]–[13]. Accordingly, higher matrix crystallinity increases the decay rate[14].

The mechanism of isomerization has been the subject of some debate, with two pathways identified as viable: a rotation about the N=N bond, with disruption of the double bond, or via an inversion, with a semi-linear and hybridized transition state (Fig.I.4). It has been suggested that the trans-to-cis conversion occurs via rotation into the S_2 state, whereas inversion gives rise to the cis-to-trans conversion. It is still under discussion which excited state plays a direct role in the series of the photoisomerization behavior. However, the latest research on femtosecond transition spectroscopy has suggested that the S_2 state undergoes internal conversion to the S_1 state, and then the trans-to-cis isomerization proceeds. The conversion from trans to cis reduces the distance between the ends of the moiety (between the 4 and 4' positions): from 0.99 nm in the trans state to 0.55 nm in the cis state[15]–[17]. This change in geometry results in a change in the molecular dipole, increasing it from essentially zero in the trans state to 3.1 D in the cis form (for the parent azobenzene) [2]. The free volume requirement of the cis is larger than the trans[18], with estimates of approximately 0.12 nm^3 required for isomerization to proceed via an inversion of the azo bond[12], [19], and 0.28 nm^3 for a rotation about the azo bond[20]. This large molecular change generates a nanoscale force, which has been successfully measured in single-molecular force spectroscopy experiments[21], [22].

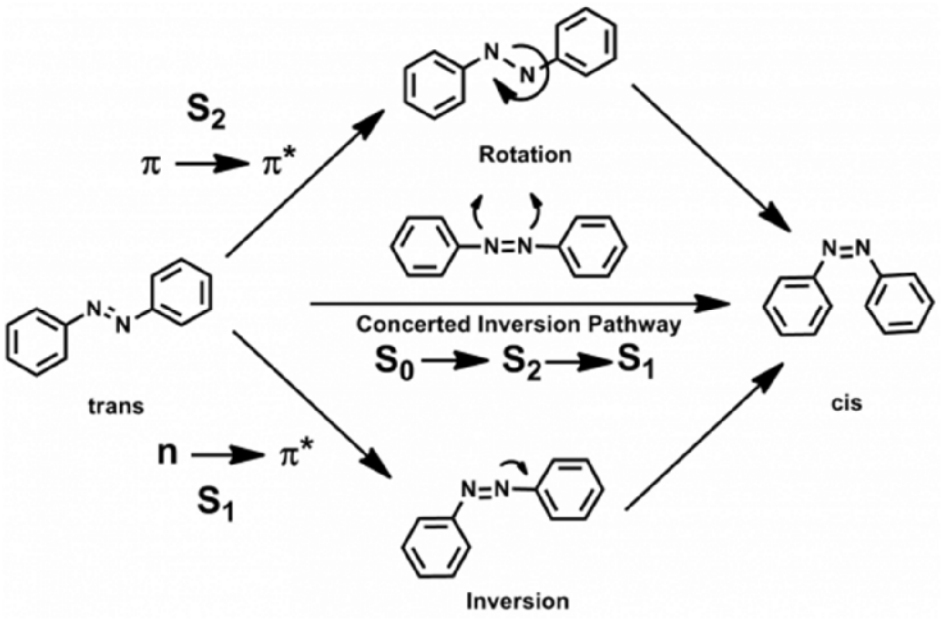

Fig. I-4 : Rotation and inversion mechanisms pathways for azobenzene isomerization process

I.4. Photo-induced orientation

The photo-isomerization of azobenzene is a unique form of light-induced molecular motion. This motion can also lead to motion on larger length scales. For instance, polarized light will cause the molecules to isomerize and relax in random positions. However, those relaxed (trans) molecules that fall perpendicular to the incoming light polarization will no longer be able to absorb, and will remain fixed (the probability of photon absorption varies as cos2Φ, where Φ is the angle between the light polarization and the azo dipole axis). Thus, there is a statistical enrichment of chromophores perpendicular to polarized light (orientational hole burning) (Fig.I.5). The photo-orientation is reversible: isotropy can be restored using circularly polarized light, or a new orientation direction can be selected by irradiation with a new polarization.

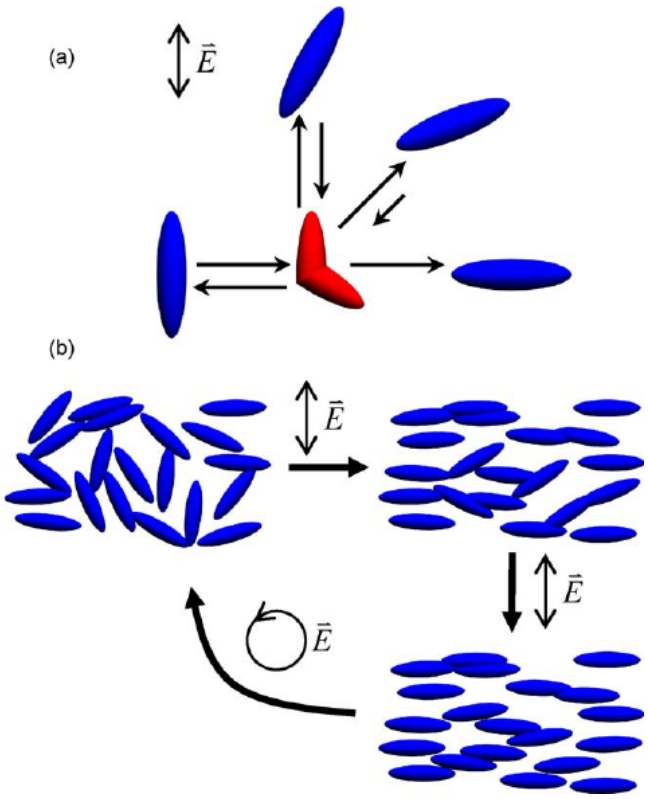

Fig. I-5 : The mechanism of statistical photo-orientation of azo molecules. (a) The molecules aligned along the polarization direction of the incident light will isomerize, and take on a new random orientation. The molecules that lie perpendicular to the polarization of light cannot absorb a photon and remain fixed. (b) An initially isotropic distribution of chromophores will become progressively aligned with polarized irradiation. Irradiation with circularly polarized light can restore isotropy [23]

Polarized irradiation will make an azo-material anisotropic and therefore optically birefringent and dicroic[24], [25]. In these systems, the physical and optical properties such as the absorption spectrum, dipole moment, refractive index and molecular conformation can be reversibly changed through the trans-cis isomerization of azobenzene. This photo-orientation can also be used to orient other materials (especially in liquid crystal systems). For instance, it has been used to selectively orient liquid crystal domains, and to create NLO materials and high density data storage[26]–[31]. Azo isomerization can also be used as switching elements for microelectronics and to photo-switch the liquid crystal phase of a material [32], [33]. The azobenzene moiety is robust and adaptable, having been incorporated into a wide variety of

different system types, including: small molecules, doped into polymeric systems, supramolecular assemblies, liquid crystals, and covalently bonded to crystalline or amorphous polymers. Although doping is an easy and convenient way to include azobenzene in a matrix of choice, it is usually found that mobility leads to aggregation and crystallization of the azo molecules, making the resultant films heterogeneous and optically cloudy. Thus, by far the most often-employed incorporation strategy is to covalently bind the azochromophore to a polymer backbone [34].

In 1995, it was discovered that exposing a thin film of azo-polymer to a light intensity (or polarization) gradient leads to spontaneous surface patterns [35], [36]. In essence, the polymer material will reversibly deform so as to minimize the amount of material exposed to the light. This phenomenon is not laser ablation, since it readily occurs at low power and the transformation is reversible. The exact mechanism of this surface holography is still unresolved, although it is clearly related to the azobenzene isomerization.

I.5. SRG Formation

In 1995, a remarkable, unusual and unexpected effect was discovered simultaneously by two independent research groups in the azo-polymer materials well below their glass transition temperature[35], [36]. Since these first two articles, more than 1000 articles have been published to characterize the phenomena, to suggest the possible mechanisms and to propose some future applications. When the material was irradiated with two coherent laser beams (which generate a sinusoidally varying light intensity or polarization pattern at the sample surface), the materials spontaneously deformed in order to generate a sinusoidal surface relief grating (SRG) in this case the first order diffraction efficiency of a low power He-Ne laser (in the wavelength that polymer is transparent) will increase excessively. This is a one-step fabrication technique. Usually SRG topological formation is monitored by AFM to distinguish

between bulk (birefringence) and surface gratings. This surface deformation is reversible and the original film thickness could be recovered upon heating the material past its glass-to-rubber transition temperature (T_g) and/or in many cases even at room temperature by impinging a single beam of laser light with the appropriate polarization. SRG has been studied on azo dye doped polymers (guest-host systems)[37], amorphous side-chain and main-chain azopolymers[38], [39], and on liquid crystalline azo-polymers[40], [41], mostly in the form of spin-coated films. Sol/gel materials[42], Langmuir-Blodgett (LB) films[43], and films assembled by ionic layer-by-layer interactions [44]–[46], single crystals [47] and more recently monomeric glasses [48] have also been used. Monomeric glasses have fast response to writing process and smaller birefringence in comparison to grafted polymers [49]. In azo dye doped systems, the chromophores are not attached to the polymer chains and their photoisomeric movements are not followed by the polymer chains and consequently the surface modulation is very weak. This surface modulation is difficult to observe with AFM.

Liu et al. were synthesized azo derivative with fluorescent group which allowed them to use fluorescence confocal microscopy for observation of molecular migration [50]. Polymer chain migration, which is thought to be responsible for the large surface relief features, however, does not appear to occur. As expected, the formation of the surface grating in the main chain polymers was much slower than the side chain polymers. This is because the polymer has a rigid backbone and the azobenzene groups are bound to the backbone at both ends, which restrict the mobility of the chromophores. However, when it is considered that these main chain polymers have very high T_gs, and relatively low absorption at the writing wavelength compared to the side chain polymers, the observation of the surface modulation is quite remarkable. The results of several research groups show that side-chain azo-polymers are the best materials for inscription of SRG. It is well-established that the surface-patterning phenomenon is strongly polarization dependent [51]. Both the efficiency of the process (as

measured by topography height) and the exact shape of structures are affected by the incident polarization state. The two s polarized writing beams produce the largest light intensity variation (the intensity recording condition). However, there is no polarization gradient of the resultant electric field and no component of resultant electric field along the grating vector direction. This configuration only produces a very low diffraction efficiency and small surface modulation for the SRG (<10 nm). Under the polarization recording conditions, the two writing beams have orthogonal polarization (s-p). The resultant electric field on the film surface has the largest variation but the light intensity is uniform over the entire irradiated area. Very small surface modulation and diffraction efficiency are obtained under this purely polarization recording condition. Under other recording conditions (p:-p, +45°: −45° and RCP: LCP), variations of both light intensity and the resultant electric field polarization on the film exist simultaneously. The SRGs formed have much larger values for the surface modulation and diffraction efficiency. It has been observed by several authors that illuminated regions of the grating correspond to pits and dark regions to peaks of the surface, except in the case of side-chain liquid crystalline polyester of low T_g where the opposite result was obtained. In essence, the topography encodes both the incident light intensity pattern and the polarization pattern[52].

I.5.1. Two beam experiment

In order to form the SRGs, it was found that irradiation with a double beam exposure of a light intensity and/or polarization gradient would lead to spontaneous large-scale motion of polymer material in the thin film, resulting in surface topographical patterning.Two beams of equal intensity with appropriate polarizations made to impinge on the surface of sample. The molecules move from high to low light intensity regions[53].

Fig.I.6 shows the typical experimental setup used for a double beam setup for inscribing SRGs, and a typical topography of a SRG.

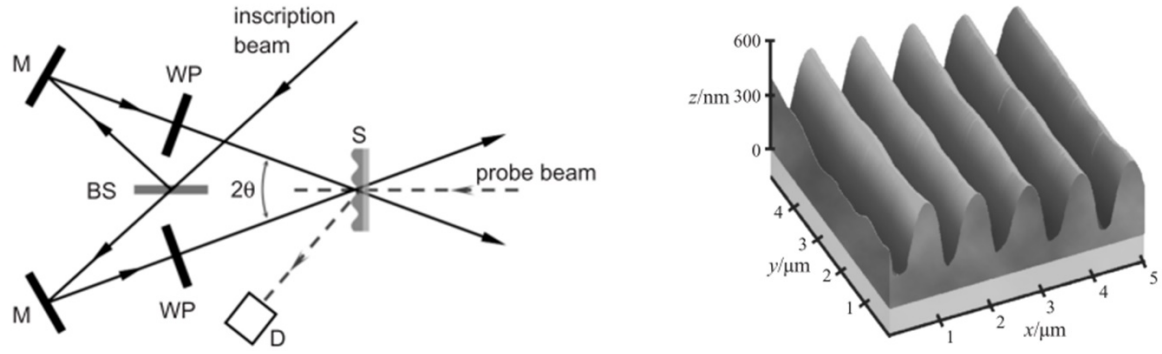

Fig. I-6 : a) Typical experimental setup for the inscription of surface relief gratings. In the diagrams, M refers to mirrors that control the incident beams, WP are polarization-controlling wave-plates, BS is a beam-splitter, and D is a detector used to measure the diffraction efficiency of a probe laser beam. b) Atomic force microscopy (AFM) image of a typical surface relief grating(SRG) inscribed on an azo-polymer film

I.5.2. Single beam deformation of azo-polymers

Following the discovery of SRG and the ability of deformation of the azo-polymer surface by the interference of two coherent beams, several research groups started to study the possibility of deformation of azo-polymer systems under illumination of a single laser beam.

A single focused laser beam surface deformation experiment was performed by Bian et al. to study the phase relation between writing beams interference pattern and SRG. The results help to a deeper understanding of the grating formation mechanism [54], [55]

The experiment demonstrated two important characteristics. First, the photoinduced surface deformation depends strongly to the input laser beam polarization direction. The maximum deformation happens along the direction of laser beam polarization. Second, the surface deformation profile along the polarization is not proportional (positively or negatively) to the laser intensity. Instead, it approximates to the second derivative of the laser intensity along the polarization direction (x-axis).

According to the migration (diffusion) model, the azo molecules have tendency to move from higher intensity region of beam (more trans-cis-trans photoisomerization) to the lower one and finally to the dark region in the direction of laser beam polarization and deform the surface of polymer film.

The single-beam experiment is particularly relevant to reveal the photoinduced lateral migration of polymer chains and to deduce the phase shift of the SRG with respect to the interference pattern since no such unambiguous assignment could be given in the grating writing experiment.

I.6. Mechanism of SRG Formation

There remains, however, much controversy surrounding the fundamental origins of all-optical surface patterning of azo thin films, and no proposed mechanism appears to provide a suitable explanation for all observations. Here we will review almost all the proposed mechanisms:

I.6.1. Isomerization pressure model

This model is based on pressure gradient induced transport deformation and the resulting viscoelastic flow to form surface gratings on the azo polymer films[56], [57]. The pressure gradients arise from the increased cis population in the bright regions, together with the cis isomer's large free volume requirement and the viscoelastic flow of the polymer is related to the velocity components by Navier–Stokes equations (Fig.I.7). The thickness h of polymeric film, its molecular mass M, its viscosity μ (proportional to M) as well as the pressure P are taken into account and lead to an expression of the temporal evolution of polymeric film thickness:

$$\frac{\P h}{\P t} \mu \frac{d^3}{\mathrm{m}} . \frac{\P^2 P}{\P \mathrm{C}^2} \mu \frac{d^3}{M} . \frac{\P^2 P}{\P \mathrm{C}^2}$$

where X represents the direction according to which the distribution of intensity or polarization takes place. The theoretical dependence of the rate of inscription (¶d/¶t) to the thickness of polymeric film (d^3) is checked in experiments [58] for low thicknesses of polymeric films.

Based on this, a relationship between the grating formation rate and intensity of the writing beams, molecular weight of the polymer and thickness of the film is derived and experimentally verified.

For thinner films, there is excellent agreement of the experimentally observed and predicted writing efficiency and film thickness. Inscription rate is found to increase linearly as a function of light intensity and is accurately accounted for by this model. The gradient of isomerization pressure model however, does not adequately account for the strong polarization dependent grating formation process. The theory predicts the highest pressure gradients for two s-polarized beams. This is in contradiction with experimental data, which demonstrate negligible diffraction efficiency for this geometry.

Sumaru et al. have developed this approach to successfully describe the evolution of the surface relief gratings over longer time periods for any initial thickness of polymer film [59], [60]. However, this model does not take into account the influence of the polarization of writing beams.

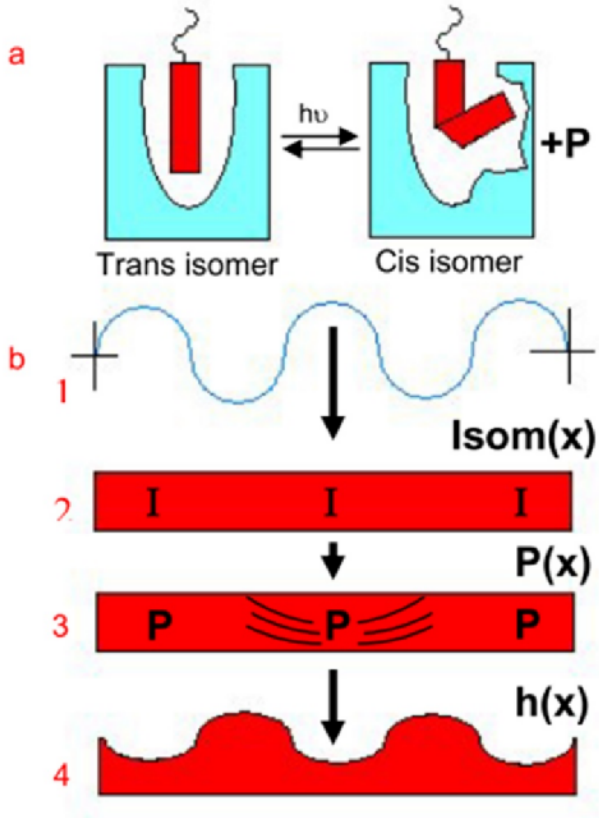

Fig. I-7 : Schematic representation of isomerization pressure model. a) Trans-cisphotoisomerization and difference in the free volume requirement for trans and cis isomers. b) Intensity modulation rise from two coherent beams interference (1) that causes more isomerization (2), more pressure (3) and finally deformation of polymer surface (4)

I.6.2. Gradient electric force mechanisms

This model has been proposed by Kumar et al. [61], [62] and is based on the interaction of the azochromophore functionalized macromolecules with the optical field induces polarization in the material in the direction of the field. Efficient trans-cis-trans photoisomerization cycling leads to a photostationary state when there is a net chromophore orientation perpendicular to the field direction. The associated decrease in the refractive index and hence the susceptibility of the material defines the direction of flow of the polymer chains. The unique aspect of the azo polymer system is that these processes occur simultaneously and the time averaged effect results in transport of the polymer chains in the field gradient direction. The process is initiated

at the film surface and continues through the bulk of the material as the polymer layers are moved, leading to high amplitude gratings [63]. The force responsible for the movement of the polymer involves a spatial variation of the susceptibility of the material and an electric field gradient (Fig.I.8).

In this case the time-averaged force would take the form:

$$\vec{f} = \left\langle \left(\vec{P}.\tilde{\nabla}\right)\vec{E} \right\rangle$$

where $P = \varepsilon_0 \chi E$ and E are the optical field induced polarization in the material and electric field amplitude of optical field, respectively. Thus, the grating inscription would be related to the spatially-varying materials susceptibility χ , the magnitude of the electric field E, and the gradient of the electric field. This naturally includes the polarization dependence observed in experiments.

In this model a photo-induced plasticization is assumed, allowing material mobility well below T_g. The force density estimated for conventional lasers is 100 N/m^3 which is two orders of magnitude smaller than that of the gravitational force (104 N/m^3), and thus is too small to be of influential importance.

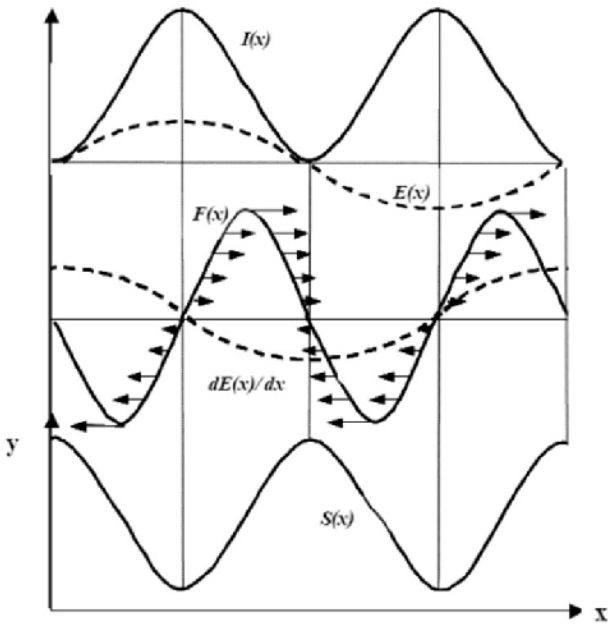

Fig. I-8 : Schematic representation of model. The intensity and surface modulations have phase difference of π

More recently Yang et al. have developed this model by adding magnetic force to have an electromagnetic force[64].This electromagnetic force is driving force for SRG formation process. They assumed that the medium is not a magnetic medium. They considered polymeric material as an incompressible viscous fluid and used Navier-stokes equation to describe the motion of material. The obtained theoretical results of the inscription rates and the expected z-component surface velocity directions are in good agreement with experimental result. Again the heart of this model is photoplasticization of polymeric material.

I.6.3. Thermal mechanisms

Models involving thermal effects appear to be the most readily proposed. Thermal gradients would be created due to the inhomogeneous illumination (light interference pattern) of the sample surface, but their magnitude and persistence time would be expected to depend strongly on material parameters, geometry, and size scale. Such mechanisms would be sensitive to the intensity of the light interference pattern, but not its polarization, counter to observations. For example, SRGs have been written using a pure polarization pattern, where the intensity of the light at the film surface is constant. Attempts to produce SRGs with absorbing chromophores other than azobenzene have not been successful, and it appears that the isomerization is necessary for the process. Experiments at high laser intensity [55] (and experiments with pulsed systems[65], which are equivalently high intensity) on the other hand show neither polarization dependence nor a strict on azobenzenechromophores. Recently Yager et al. have created a simulation, to clarify the role of thermal gradients in the SRG inscription process[66]. They showed that thermal gradients are negligible for typical modest irradiations (for the intensities of 50mW/cm^2 the temperature of sample raise about 5K)[67], and the temperature gradient achieved within the sample is on the order of 10^{-4} K, and does not appear to vary with inscription or geometric conditions. This gradient cannot lead to an appreciable spatial variation of material properties, and certainly does not explain the dependence of SRG inscription on many variables.

The pulsed irradiations are likely causing destructive sample ablation, and not mass transport.

I.6.4. Permittivity gradient model

Baldus and Zilker have proposed a mechanism for SRGs formation based on spatial variation of the permittivity of material due to the periodic alignment of the polymer side-chains caused

by intensity or polarization modulation of interfering writing beams. This gradient of permittivity under an optical electric field results in a force[68].

This force is proportional to the square of the optical electric field in the grating vector direction, and to the gradient of permittivity at any point:

$$\mathbf{f}(x) = -\frac{\varepsilon_0}{2}\mathbf{E}^2(x)\tilde{N}\varepsilon$$

Material is moved out of areas with high gradients of permittivity, and in general is moved out of areas of illumination and causes the modulations of the surface (Fig.I.9).

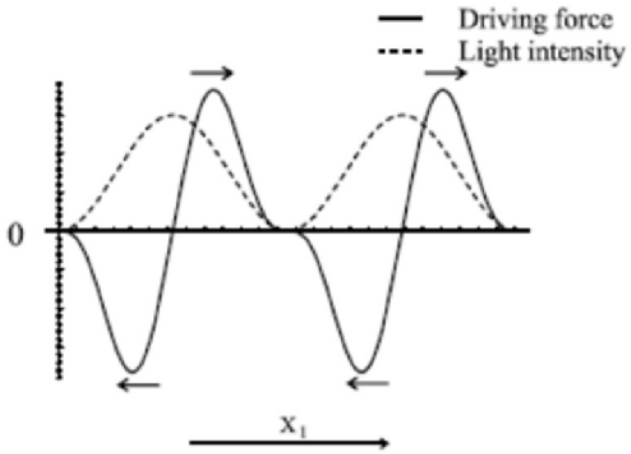

Fig. I-9 : X_1 component of force under a periodical modulation of the incident light. The material is pulled out of areas with high gradients of the permittivity (arrows denote the force direction)

In this model they assumed that the softening of the material can achieve thermally, and trans-cis cycles of the side chains, and therefore chromophore reorientation, play a negligible role.

I.6.5. Asymmetric diffusion (migration) model

Nunzi et al. have developed a model based on the anisotropic translation diffusion of azo dyes in a direction that is parallel to the polarization direction of the writing beam [69]–[71]. This translation is due to the photo-excitation and thermal re-conversion (photoinducedtrans-cis-trans isomerization cycles) of chromophores (Fig.I.10).

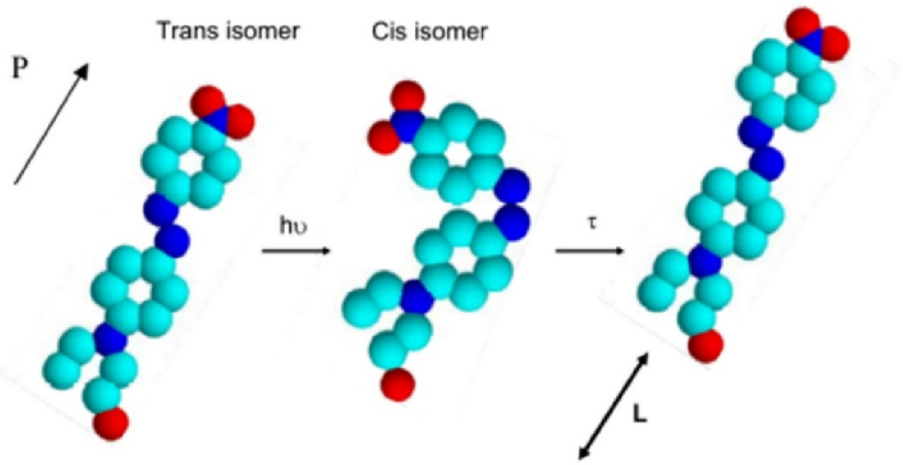

Fig. I-10 : Photoinduced worm-like motion of disperse red 1 azo molecule

The probability of undergoing a statistical random-walk is related to the probability of excitation, which in turn is related to the intensity of light and the angle between the electric field vector of the light and the chromophore dipole moment. There is thus a net flux of molecules out of areas of light and into the dark, aided by pointing the dipoles towards the dark regions through a polarization-dependent photo-alignment. Once a molecule has diffused into a dark region, there is a zero probability of it being excited back into a light region, and hence the azo molecules would be expected to congregate coincident with the interference pattern,

and produce a surface relief grating. Attached azo molecules to backbone polymer chains can act as tractors that pull the polymer material. This model explains very well the polarization dependence observed in the azo polymer films.

I.6.6. Mean-field model

Mechanisms based on electromagnetic forces seem promising, since these naturally include both the intensity and polarization state of the incident radiation. In the mean- field model, each chromophore is subject to a potential resulting from the dipoles of all other chromophores[72], [73].

Under irradiation, chromophores at any given point will be oriented perpendicular to the light polarization at that point. The mean-field that they generate will tend to align other chromophores in the same direction, and also causes an attractive force between side-by-side chromophores oriented in the same direction. Overall, this results in a net force on chromophores in illuminated areas, causing them to order and aggregate. This mechanism predicts a collection of mass in the areas of high light intensity, at the expense of areas of lower intensity.

Theoretical predictions of the polarization dependence of the periodicity and shape of the surface relief profiles have been found to agree well with the experimental results. However, the model presumes a spatially constant intensity when two orthogonally polarized beams interfere at an angle ($\theta>0$).

This treatment, based on the intrinsic mobility of the LC materials, does not account for the dip (instead of peak) inscribed in the material where the intensity is maximum, observed in the amorphous azo polymers.

I.7. Crossed gratings formation

The possibility of inscribing two sets of gratings on the same area of the polymer film was checked (Fig.I.11). On a set of SRGs of an azopolymer thin film, interfering two laser beams were irradiated to append another set of gratings. As a result, appended gratings were superposed on initial gratings and the direction of the mass transfer in the SRG formation was turned to be restricted along its wave-vector[36].In addition, multiple gratings, up to 10, have been recorded on the same spot, provided that the polarization of the writing beams was properly selected, which allowed a variety of complex patterns to be produced.

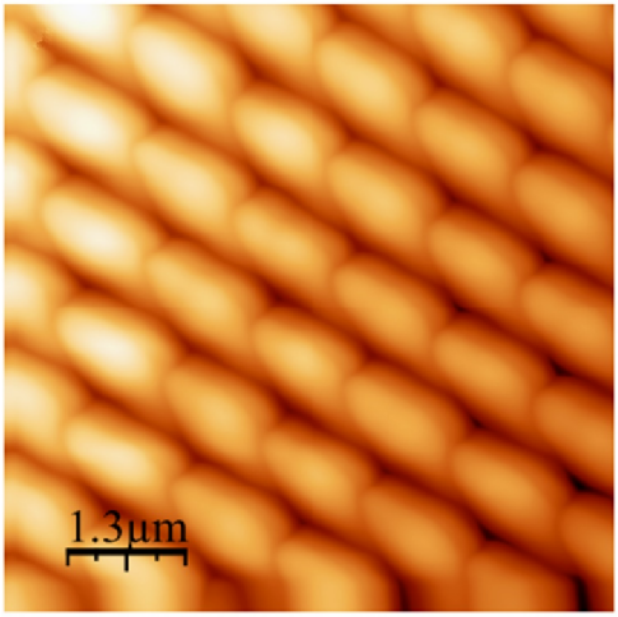

Fig. I-11 : 2D view of AFM image of two grating recorded on the same area of azopolymer film

I.8. Quasi-Crystal structures through SRG inscription

It is well-known that subtle and complex surface structures can manipulate light through physical effects such as scattering, diffraction, and interference[74], [75]. These structures can be seen on various types of minerals, insects, and birds such as opal, butterfly wings, peacock

tails, and hummingbird feathers [74]. Man- made micro/sub micrometer surface relief structures have found wide applications in various optical devices as diffraction gratings, microlense arrays, and sensors[76]. Interest on these optical surfaces still rapidly grows because of many new potential applications [75].

Structures with mesoscale features can be used as an ideal photonic bandgap (PBG) material[77]. The meso scale quasi-crystal structures have been prepared through hololithographic methods using materials such as photoresist[78] and polymer-dispersed liquid crystal[79]. Recently, the quasi-crystal patterns have also been prepared by the dual-beam multiple exposure technique using photoresist as a processing material[80]. Two-dimensional surface quasi-crystal structures can be considered a new type of the optical surface, which is characterized by the 2D long-range aperiodic order with rotational symmetry and can be used as novel diffraction gratings and so forth[81]. Fabrication of surface quasi-crystal structures on azo polymer films can be considered a new approach to further develop the surface patterning technology based on the photo-driven mass- migration scheme. Theoretically, quasi-crystal surface relief structures on azopolymer films can be inscribed by a suitable multiple exposure procedure. Therefore, to our knowledge, documentation of fabrication of quasi-crystal surface structures through the photo-driven mass-migration scheme is still lacking in the literature.

I.9. Random and Quasi-random surface structures

No surface is perfectly flat or ordered at every length scale. However, all natural and man-made surfaces show some degree of roughness. Moreover, since a rough surface will give rise to a partly random phase of the scattered electromagnetic field, a complex intensity pattern will result due to the scattered field interfering constructively or destructively as angle of scattering is altered. Such patterns are known as speckle patterns and they show rich properties that have

fascinated researchers for decades. Therefore, it is imperative to know how surface disorder may affect physical process at, or in the immediate vicinity, of the surface[82].

Due to the practical applications of waves, and the number of naturally occurring surfaces being rough, it is rather remarkable that it took several hundred years from the birth of optics, as a scientific discipline, to anyone started to consider wave scattering from rough surfaces. As far as we know today, the first such theoretical study was made at the end of the 19th century (probably in the year of 1877) by one of the greatest scientists of its time, the British physicist Lord Rayleigh [83]. He considered the scattering of light incident normally onto a sinusoidal surface. In 1913 Mandel'shtam studied how light was scattered from liquid surfaces[84]. By doing so, he became the first to consider scattering from randomly rough surfaces. This, as it turned out, should define the beginning of an active research area – wave scattering from randomly rough surfaces – which still today, almost a century later, is an active and vibrant field [85]–[87]

Disordered photonics has made significant contributions to the field of science and engineering in the recent past with potential applications ranging from imaging, random lasers to solar energy harvesting[88], [89]. Most of the natural systems in our daily life such as human tissue, blood cell, milk colloid, clouds, marble stone etc., strongly scatter light due to their structural disorder[90]. The surface phenomena such as higher brightness[89], super hydrophobicity, super lyophobicity, and super oleophobicity also stem from the structural randomness of the surface[91]. Disordered systems host interesting optical phenomena such as coherent backscattering[92], Anderson localization[93], super and hyper diffusion[94], wave focusing[95], random lasing[96], enhanced energy storage[97] and etc. Thus, fabrication of nanostructured materials for control of light-matter interactions has become particularly important for improving different phenomena involving a high degree of light scattering[98].

For example, light emitting diodes necessitate out-coupling of light with a large directivity. Development of solar cells requires the reduction of the active layer.

The usage of the random textures and the diffractive elements (both dielectric and plasmonic) are crucial in reducing the reflection, increasing the path length of light inside the cell and for optical coupling [99]. Having both random medium and diffraction features in a single element is a clear advantage in the case of solar cells. Hence, random grating elements may be useful for reducing reflection as surface element and at the same time spreading the light inside the cell due to its dual properties. This certainly enhances the light harvesting capability of the cell.

All physical phenomena in a random medium are demonstrated in arbitrary random structures that are fabricated by different methods such as removing the particles from random positions in photonic crystal[100], self-assembly of particles[96], deep reactive ion etching[101], chemical vapor deposition[102], introducing particles into polymer matrix [103], and femto-second laser focusing to create randomly distributed voids[104] and electron lithography for small area fabrication[105]. More or less all fabrication methods suffer from lack of reproducibility, control and limitations attributed to wide area fabrication. Hence, random medium is least exploited for device fabrication in spite of all its advantages. However, a fabrication strategy that results in predictable, tunable and reproducible random and quasi-random structures will open up new possibilities with which we can tailor them towards future device applications.

A variety of lithographic techniques are now available for direct processing of materials at the nanoscale[106], [107]. While the resolution of these techniques has continued to improve, the cost of their implementation and system complexity have also increased substantially. For example, traditional photolithographic nanofabrication techniques rely on costly masks[108], while electron and focused ion beam writing require expensive beam sources and elaborate

control systems[109], [110]. Similarly, sophisticated equipment is required for lithographic techniques based on scanning probes and optical tweezers[111]–[114]. Alternate strategies, involving self-assembling nanostructures, have been explored to improve the versatility and lower the fabrication costs[115], [116]. However, arbitrary direct writing cannot be performed by these methods due to the lack of mobility of these nano components. Inspired by natural biological systems[117], [118], the recent development of synthetic nanomotors has paved the way towards major advances in nanoscience[119]–[121].The nanomotors 'swim' over the surfaces for creating spatially defined complex surface patterns. This approach is made possible by developing an 'on-the-fly' strategy for manipulating the light incident on the moving nanomotors. Using such a versatile method, various nanoscale features are generated through modular nanomotor design.

Beside the mentioned methods, there are several techniques used for fabrication of disorder and ordered structures in literature, as discussed in the next sections.

I.10. Dewetting

Patterned polymer thin films find use in many applications, including in the optoelectronic, semiconductor, bio-related and medicinal industries, for which a broad range of methods have been developed to pattern polymers. "Top-down" and "bottom-up" are two strategies to generate patterns [122]–[124]. Among those bottom-up methods, the spontaneous formation of micro- and nano-patterns at the surface of soft matter induced by surface instability is a unique approach. When a liquid film on a solid surface is thick enough, the film is stablized by the effect of gravity. As soon as the liquid film is thinner than a certain thickness, namely the capillary wavelength, λ_{cap}, of the liquid, molecular forces dominate over gravitational forces and the film may dewet[125]–[128]. Controlled dewetting is then a convenient and effective

way to pattern surface on a micro/nano-meter scale without a lithographic process. Pattern generation by dewetting paves the way for low- cost, large-area, solution-processing techniques to pattern and orient organic crystals in desired locations, providing important components for organic field-effect transistors (OFETs), organic light-emitting diodes (OLEDs), and organic solar cells [123], [129].

I.10.1. Fundamental of dewetting

It is necessary to clarify the distinction among stable, metastable, and unstable films. The effective interface potential $\phi(h)$ is defined as the excess free energy per unit area necessary to bring two interfaces (solid–liquid and liquid–gas interface) from infinity to a certain distance, h. The distance h then defines the thickness of the liquid layer between them. As shown in Fig.I.12, $h \rightarrow \infty$ induces $\phi(h) \rightarrow 0$, indicating stability of a film with infinite film thickness. When $\phi(h)>0$ and the global minimum lies at infinite thickness, the film is called stable (curve [1] of Fig.I.12). If the second derivative of ϕ with respect to film thickness is negative, $\phi''(h_0)<0$, where h_0 is the initial thickness of a homogeneous film, the system is unstable (curve [2] of Fig.I.12), such that capillary waves on the film surface are spontaneously amplified under thermal annealing. The rupture mechanism is termed “spinodal dewetting” [126], [130], [131]. In curve [3], the film is unstable for small film thicknesses where $\phi''(h_0)<0$, whereas for larger film thicknesses ($\phi''(h_0)>0$), the film is metastable. In the metastable case, the system has to overcome a potential barrier in order to reach its state of lowest energy at $h=h^*$. Some kind of nuclei, e.g. dust particles or defects, are required to lower $\phi(h)$ and can therefore induce rupture of the film, a mechanism called “heterogeneous nucleation”[132], [133]. It is difficult to distinguish metastable and unstable mechanisms experimentally since both nucleation and spinodal dewetting can lead to dewetting in unstable films [131], [134], [135]. In case of unstable system, however, there is a certain wavelength λ_s, the amplitude of which grows

fastest, leading to a characteristic dewetting pattern of the liquid film [136]. The wavelength λ_s and $\phi''(h_0)$ are connected by Eq. (1):

$$\lambda_s = \left(\frac{-8\pi\gamma}{\phi''(h)} \right)^{\frac{1}{2}} \qquad (1)$$

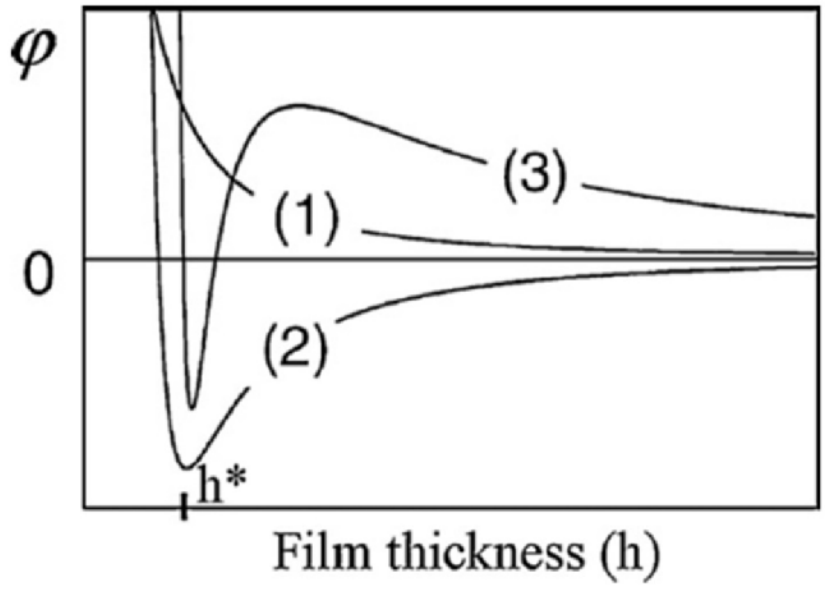

Fig. I-12 : Effective interface potential $\phi(h)$ as a function of film thickness h for stable (1), unstable (2), and metastable (3) films. Reproduced from [136] with permission.

Where, γ is the surface tension of the liquid film (with respect to air) [124]. Numerical simulations indicate that the dewetting pattern is related to the given surface tension, and there may be a cross region between the two mechanisms[137], [138]. Close to the sign reversal of $\phi''(h_0)>0$, thermal activation is sufficient to overcome the potential barrier for the nucleation of holes, a process called “thermal nucleation” or “homogeneous nucleation” representing a third dewetting mechanism[136], [139]. The characteristic feature of homogeneous nucleation is a continuous breakup of holes, whereas heterogeneous nucleation causes holes that emerge only

within a narrow time interval[140]. Thus, the hole opening is most likely to happen at locations having the smallest thickness, which can be caused by fluctuations of the film thickness or elevated regions on the substrate. A stable film, ($\phi''(h_0)>0$), may become unstable locally on an elevated heterogeneity if the local thickness decreases below the critical thickness. On a complex substrate comprising both wettable and less wettable (or unwettable) regions, holes generate at the unfavored locations and the wettability contrast drives the liquid flow from the less wettable areas to the more wettable areas, lowering the total energy.

After the hole opening (Early stage), the classical process includes hole growth (Hole growth and rim), the combination of holes to form ribbons (Intermediate stage), and the decay of ribbons into droplets (Late stage) [125], [141]. A typical hole shows a circular shape and the round shape remains stable until holes contact one another. However, fluctuations of the rim shape in a growing hole may occur [142] and the rim may subsequently become unstable and form fingers, called finger instability[125]. For films of polymer with molecular weight M greater than the molecular weight, M_e, between entanglements, the period between the fingers, λ_f, is a constant after their maturation:

$$l_f = \left(\frac{M_e g}{|S|}\right)^{1/3} \frac{h_0^{7/6}}{M^{1/2}} \qquad (2)$$

Where, S is the spreading coefficient. Eventually these fingers decay into droplets by Rayleigh instability [143], and the mean diameter D of droplets grows linearly with the initial thickness h_0 of film, $D \sim h_0$[144].

Dewetting can be understood as one possible route for the preparation of well controlled surface patterns. In addition to film instabilities driven by van der Waals forces [145], instabilities due to electrostatic forces [146], [147], elastic forces[148], acoustic instabilities[149], density fluctuations [150] and temperature gradients [151] were reported.

Methods of dewetting on polymer films worked so far are “Thermal dewetting” and “solvent vapor induced dewetting”.

I.11. Pattern generation by dewetting

The familiar morphology of a dewetted film is polygonal arranged droplets, suggested to be the result of competition between order and chaos [152]. But the arrangement is not regular on a larger scale, exhibiting irregular arranged droplets with polydispersed sizes. However, by tailoring the substrate with physical or chemical patterns, modifying the topography of the film surface, controlling the moving front of the three-phase line, and triggering the instability of film with an external field the manner and the final morphology of dewetting can be controlled to achieve the desired patterns.

I.11.1. Physical heterogeneous substrate

The presence of physical heterogeneity introduces larger differences between the time of primary hole “nucleation” and spinodalhole formation. The local film thickness is reduced over the elevation leading to the faster growth of the instability because of the stronger attractive force there. Higgins et al. [153] showed that an interfacial roughness on a scale of the order of Angstroms and with a dominant direction (a kind of nematic roughness), formed by simply rubbing the substrate, can initiate a corrugated dewetting pattern at a polymer/polymer interface (Fig.I.13(a)). Such an anisotropic spinodaldewetting at a polymer/polymer interface is probably initiated by small changes in dispersion forces due to the very small differences in film thickness (spinodaldewetting is a very sensitive function of film thickness). Similarly, a PS film on a regularly cor- rugated silicon substrate films started dewetting by the formation of holes nucleating along the peaks of the corrugations (Fig.I.13(b)) [154]. Films thicker than a critical value of 0.55Rg were seen to be stable, probably due to an increasing number of undistorted chains. Such chains do not minimize their free energy by diffusing to thicker areas

of the film. After the dewetting, PS collected in the grooves forming strips, as shown in Fig.I.13(c). If one facet of the corrugation is covered with another material (e.g., Au) forming a chemical heterogeneity on the surface, similar dewetting would also happen, but the location of resulting PS channels would be determined by the position of coated Au[155].

The PS channels no longer locate symmetrically within the grooves but tend to cover the facets covered by Au, which has more affinity to PS. Luo et al. [156] studied the dewetting of PS on a regularly striped substrate (Fig.I.13(d)–(g)). The rupture of film started at the edges of the elevated strips. The rims moved towards the center of elevated strip, forming a string which then broke into droplets because of a Rayleigh instability. Irregularly dispersed droplets formed on the bottom of grooves with same size as the elevated strips. Recently, an array of approximately 70nm PS droplets were formed on the desired regions of a 200×200 mesa or indent surface [157], where the undesired area was treated with (tridecafluoro-1,1,2,2,-tetrahydrooctyl) trichlorosilane (FDTS) and became extremely hydrophobic. Similarly, the organic light emitting materials of (8- hydroxyquinoline/poly(9-vinycarbazole) (Alq_3/PVK) and ($C_6H_5C_2H_4NH_3$)2PdI4 (PhE-PdI4/PS)) were collected in the microwells patterned on a PDMS substrate by solvent vapor annealing [158]. However, on such a square-microwells patterned PDMS substrate, the sites of hole opening may cause different kinds of dewetting patterns, such as holes that are circular, tetragon-like [159], square, octagon, or rounded octagon [160]. With an unfavorable physical heterogeneous pattern (OTS) on the silicon wafer, Zhang et al. [161]found holes formed exclusively on every small OTS particle. Of course, dewetting by a heterogeneity does not require that the patch be less wettable compared to its surroundings. More wettable patches are equally efficient since they cause an inward flow from the patch periphery to the center, thus causing rupture by an annular hole at the periphery.

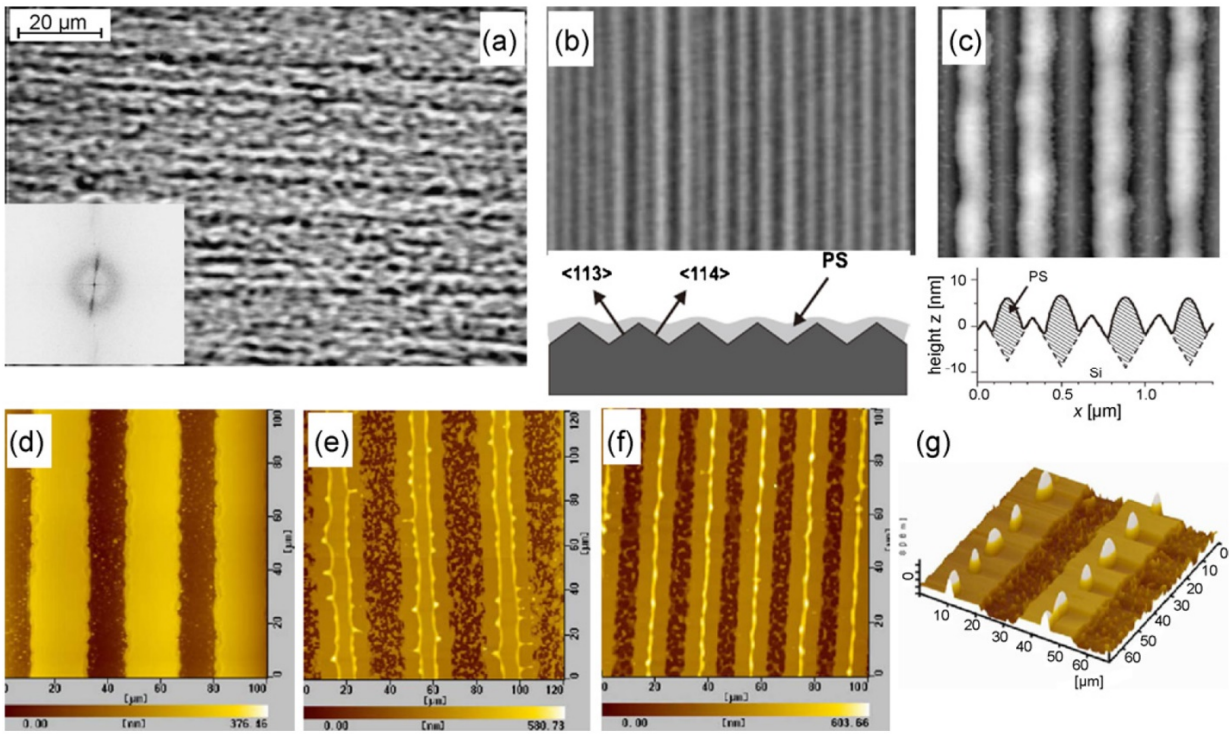

Fig. I-13 : Optical images of (a) dewetted morphology of Si/PS/PMMA sample, where the PMMA film was prepared on rubbed glass; Reproduced from [61] with permission. Copyright 2000, Nature Publishing Group. (b and c) PS film prepared on corrugated substrate before and after heating, respectively, and corresponding schematic illustration. Reproduced from [154]. AFM images of typical morphological of thin PS films on physically patterned stripes (d) after spin-casting, and annealed at 167◦C for (e) 2min, (f) 8min, (g) 3h, respectively. Reproduced from[162]

I.11.2. Chemical heterogeneous substrate

Obviously, a chemical heterogeneous substrate would drive material to specific areas exclusively, forming a pattern [163]. Since Krausch[164] found that mixture of PS and brominated PS phase separated following the chemical pattern on the substrate and the observation that phase separation of the similar system of PS/PSxBrS1−x and PS/PVP can also copy the pattern on substrate [165], considerable attention has been given to the influence of chemical heterogeneous substrate on the film structure [166]. Recent science and technology permit the creation of various chemical patterns [165], [167]. Some methods such as microphase separation of block copolymers[168], technologies based on atomic force microscopy[169], and so on can even create patterns on the nanometer scale. These make it possible to study dewetting on chemically patterned substrate on various scales [170], [171].

I.11.3. Pattern generated by topographic structure on film surface

The Navier–Stokes equation governs the stability and spatio-temporal evolution of a thin film on a rough surface. If the film–substrate interface is homogeneous and the free surface of thin film is not homogeneous, but exhibits topographic structures, dewetting occurs different.

Placing a PDMS mold on the surface of a PS film and then heating above T_g of PS, the PS chains are activated and climbed up the confining walls, thinning the film due to the capillary force between the stamp and the film. To a certain extent, dewetting of PS film happens under the physical confinement of PDMS mold, also termed confined dewetting lithography [171]–[173]. It is found that the dewetting is observed only when the wavelength of the capillary wave for the residual film is smaller than the pattern size, which indicates that the mold walls block the propagation of the capillary wave. Otherwise, the capillary wave would be blocked by the PDMS mold, and no droplets and thus no ordered pattern would appear. So, it's a pity that the nano-scaled pattern on a film surface fabricated by techniques such as nano-imprinting cannot be treated further to form nano-scaled droplets. Using a multi-layered structure, Yoon et al. [173] fabricated micropatterns with both topographical and chemical contrasts. Selective partial layer inversion in the imprinted areas resulted in top PS and bottom P4VP layers on the Si substrate, while the rest of the areas remained with the top P4VP and bottom PS layer. Combining this dewetting-mediated method with flexographic roll-to-plate transfer technique, arrays of silver lines of 20μm width, 40μm pitch, and 170nm thickness were fabricated over an area of 25.4mm×93mm in a single transfer step[174]. By removing the PDMS mold before the rupture of the PS film, an ordered disturbance can be preserved on the film surface, but the film/substrate interface kept homogeneous. When a film with a topographic structure is dewetted, either of two different phenomena may be observed, depending on the excess surface energy ΔF of the system[175]–[177]. When ΔF is less than a critical value (i.e., the disturbance amplitude is under a critical value), the PS film will flatten and finally become stable. If the

size of the disturbance amplitude is larger than the critical value, ordered PS liquid droplets form by further dewetting (Fig.I.14(a)–(d)) [178]. In an opposite way, imprinting PDMS mold into PS film (make sure that PDMS contacts the substrate under PS film), arranged defects were introduced to the film. These selected locations then broke up, leading to hole or line opening [179]. Ingeniously, on imbedding arigiflex mold with relief structures into a liquid film simply by a roller, the liquid film beneath the convex structures thinned, leading to spontaneous dewetting[180].

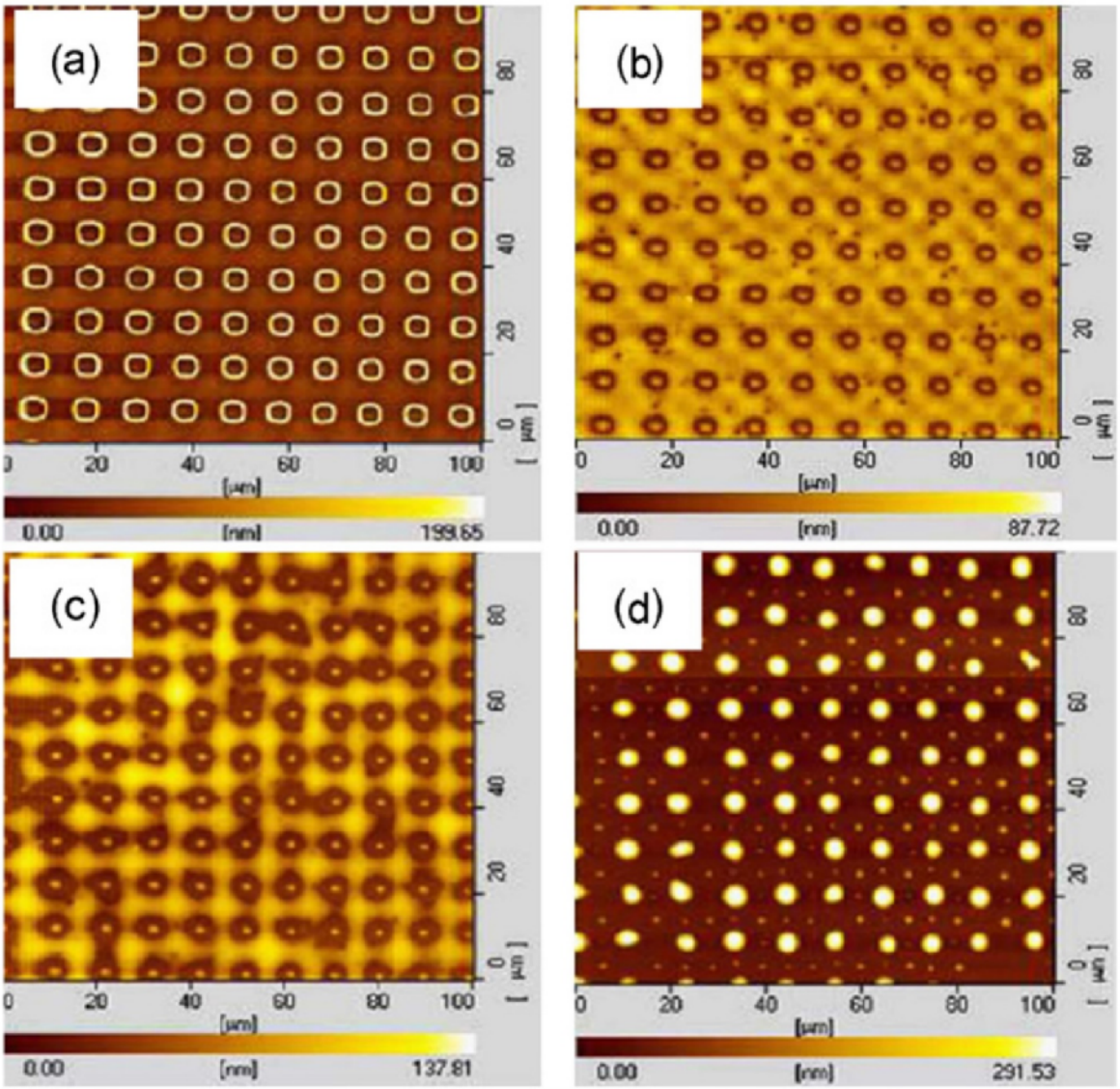

Fig. I-14 : AFM images of (a) the PS film after removing the PDMS; and (b) 180◦C for 1.5min; (c) 180◦C for 11h; (d) 180◦C for 104h[181].

The advantage of this process is that careful control of mold geometries and process parameters yields highly reproducible, large-area patterns with a high productivity. Of course, the necessary condition for the method is that the spreading coefficient of spin-coated liquid be negative.

However, formation of nanostructures via the dewetting method for a photoinduced material as azopolymer has not been suggested in the literature. For such materials, due to the presence of highly photoactive azobenzene derivative, illumination by a polarized laser light shows the possibility of a further growth and reshaping of the structures.

The possibility to provide a photoinduced reshaping opens a way to the fundamental study of size-dependent scaling laws of optical properties, photoinduced reshaping efficiency and possible nanoreactor or nanoresonator behaviors at nanometer scales.

I.12. Colloidal Polymeric Particles

Polymeric particles are used in a diverse array of applications including drug delivery[182], advanced materials [183], personalcare [184], and medical imaging [185]. They also are used in fundamental studies in fields such as microfluidics [186] and nanotechnology[187].

Over the last few decades the preparation of dispersions containing spherical particles with a narrow distribution of particles has been extensively developed and now a wide range of sizes with defined surface properties have become available [188]–[190]. These materials have found wide application as model colloidal particles for fundamental studies of the behaviour of colloidal dispersions. The spherical geometry of the particles and their monodispersity has

enabled excellent correlations to be made between experiment and theory. A subject of considerable interest is the behaviour of axisymmetric colloidal particles such as ellipsoids, in particular, their scattering, rheological, coagulation properties etc., since many theories already exist for such systems. Thus, particle shape is a critical parameter that can significantly influence particle function. The vast potential of shape, however, has not been fully explored due to difficulties in creating polymer particles with controlled shapes. Several reports exist on fabrication of polymeric particles with nonspherical geometries. These approaches make use of self-assembly [191], [192], photolithography[193], nonwetting template molding[194], microfluidics[195], [196], and stretching of spherical particles [197], [198]. Collectively, these methods have produced particles of several distinct shapes. Some of these methods provide advantages such as scalability, high throughput, and precise control over particle shape. However, they also suffer from drawbacks including cost, particle size limitations, low throughput, and limited ability to sculpt particles in three dimensions.

Accordingly, simple, versatile, inexpensive, and high-throughput methods of fabricating nonspherical particles still remain a bottleneck of future discoveries in a diverse array of fields.

In the polymer colloid field there have been a few reports of non- spherical particles of regular shape, although Owens [199] reported that cross-linking by divinyl benzene in the formation of polystyrene particles produced "potato-like" particles and Vanderhoff et al. [199] carried out extensive work using cross- linking and swelling procedures to produce particles of various shapes described as egg-like, ice-cream cone-like, popcorn-like multiplets etc. An electron microscope characterization of ellipsoidal polymer particles was reported by Keville et al. [200] in 1986, but no details of the preparation were given. In a publication Nagy and Keller [201] described a method of preparing ellipsoidal polystyrene particles with a predetermined axial ratio. More recently, a method using a cross-linked poly(dimethylsiloxane) matrix has been described by Klein et al. [202] to produce ellipsoidal poly- methylmethacrylate particles.

Currently, the main strategy to impart shape-changing abilities to colloidal particles is to utilize stimuli responsive polymers such as azopolymers.

Incorporating azo polymers into colloidal particles can combine interesting properties of azo polymers and colloidal particles. Recently, it has been reported by us that, through gradual hydrophobic aggregation, uniform colloidal spheres can be constructed from amphiphilic random azo copolymers or azo homopolymers with polydispersity in the molecular weight[203]–[205]. The colloidal spheres are formed through gradual hydrophobic aggregation of the polymeric chains in tetrahydrofuran (THF)-H2Odispersion media, which is induced by continuously increasing the water content in the media[205]. The colloids exhibit some interesting properties such as photoinduced dichroism18 and photoinduced elongation upon Ar+ laser beam irradiation(Fig.I.15) [204].

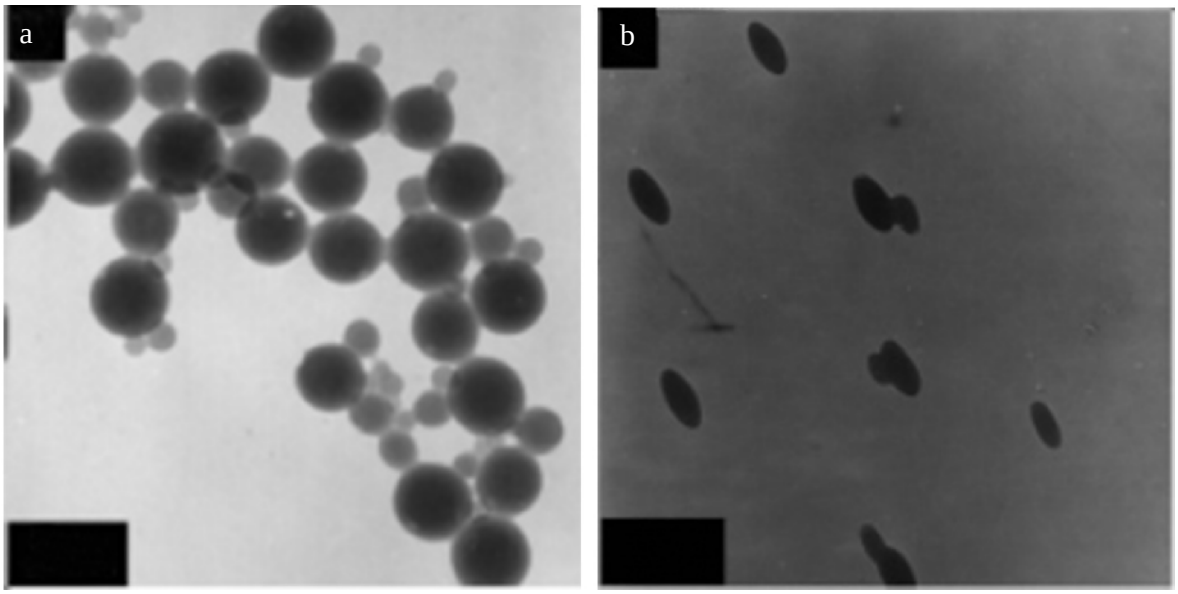

Fig. I-15 : Typical TEM images of the colloidal spheres, a) before and, b) after being irradiated by the linearly polarized Ar+ laser beam

Nunziet al[206] studied colloidal azopolymernanospheres assembled on a glass substrate exposed to a single collimated laser beam. The combination of photo-fluidic elongation of the

spherical colloids and lightinduced self-organization of the azopolymer film allows the quasi-instantaneous growth of a large amplitude surface relief grating. Pre-structuration of the sample with the nanosphere assembly supports faster creation of the spontaneous pattern. Confinement into the nanospheres provides exceptionally large modulation amplitude of the spontaneous relief. The method is amenable to any kind of photoactive azo-materials. Also, photoinduced deformation of the individual nanospheres under white light illumination was demonstrated by Nunzi[207].

Despite all efforts, fabrication of new exotic shapes for polymeric particles is still a subject at large.

I.13. Soft Lithography

The ability to generate small structures is central to modern science and technology. There are many opportunities that might be realized by making new types of small structures, or by downsizing existing structures[208]. The lithography has been emerged as a widely used and standard technique for micro and nano structure fabrication. Significant number of strategies have been used in this technique such as photo-lithography, nano imprint lithography, electron beam lithography and soft lithography[209].

Soft lithography, however, extends the possibilities of conventional photolithography. Unlike photolithography, soft lithography can process a wide range of elastomeric materials, i.e. mechanically soft materials. This is why the term “soft” is used. For instance, soft lithography is well suited for polymers, gels, and organic monolayers. PDMS, however, has been the most widely used material for the applications of soft lithography because of its useful properties including low cost, biocompatibility, low toxicity, chemical inertness, versatile surface

chemistry insulating, as well as mechanical flexibility and durability, the PDMS can also be easily manipulated and doing PDMS device can require only few equipment[208].

I.14. Conclusion

In summary, we introduced some natural and optical self-organized pattern formation. Also, we reviewed SRG formation mechanisms in azo-polymers and their applications. Interference of two coherent laser beams has been used to writing surface relief grating on azo-polymer films. Formation and development of SRG depend on the material characteristics and experimental details. Several mechanisms were proposed to explain the origin of this phenomenon. Fabrication of surface quasi-crystal structures on azo polymer films through multiple SRG inscription is considered. The idea of one beam manipulation of azo-materials was developed. Single laser deforms the surface of azo-polymer materials with the material diffusion in the direction of input beam polarization. Through such deformation, fabrication of Random and Quasi-random surface structures on the surface of azopolymer thin films are deliberated. Next, Dewetting, as a new approach to surface structuring of azopolymer thin films, is introduced and pattern formation via controlled dewetting is suggested. In the end, Azo-colloids spheres have been introduced and their deformation by a single laser beam is presented in liturature.

In the next chapter we will present a azopolymer materials, solvents, optical setups, equipments, nanoparticles and experimental methods used in this study, for sturcture formation on azo-polymer films. We will also discuss the synthesis process of new azoparticles.

Chapter II:
Materials and Methods

II.1. Introduction

In this chapter we will present the azopolymer materials used during this study, along with their characteristics. The experimental method for thin film preparation and characterization will be introduced. Different optical setups for the surface deformation of thin films will be described. PDMS replication of surface structures through soft lithography will be shown. A list of used solvent in the dewetting process will be given. The experimental equipments and microscops employed during this project will be presented. Also, the synthesis process of the new group of azoparticles will be described.

II.2. Azo-polymers

In this work a series of new azo copolymers for light induced phenomena was used. The chromophoric monomers were derivatives of azobenzene containing heterocyclic sulfonamide moieties. The monomers of the methylacrylate type contained aliphatic spacers of different length between chromophoric and methylacrylic groups. These monomers were polymerized in order to obtain homopolymers and copolymerized with butyl 2-methylacrylate (MB) and 2-ethylhexyl acrylate (AI) to get copolymers containing various percentages of chromophoric units.

The structures of copolymers that used in this work are presented in figure II-1.

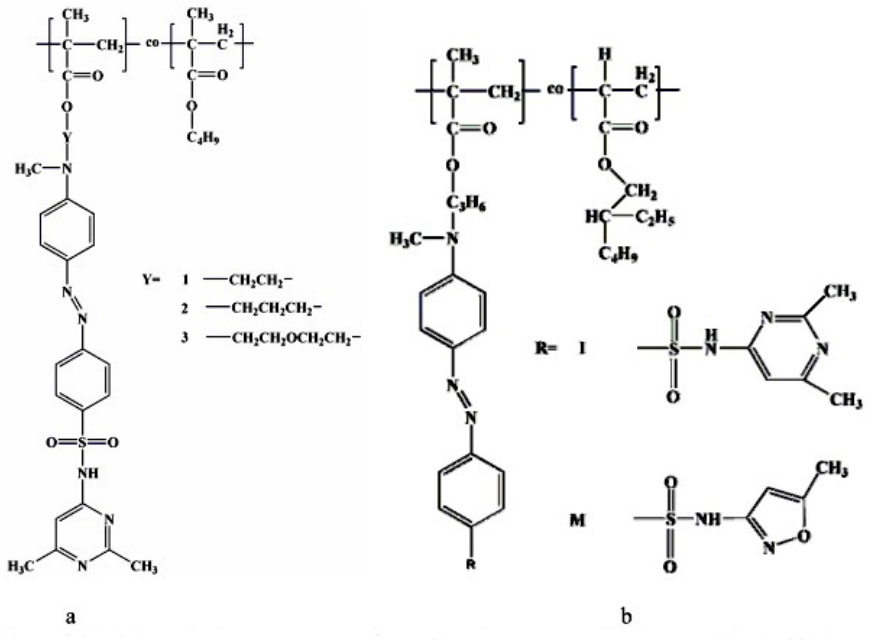

Fig. 0-1 : Chemical structures of copolymers: a) MBYI and b) AI2I&M copolymer series

Another series of azopolymers was used for random and Gaussian surface structuring. The first material is a chiral azopolymer 1 (figure II-2.a) which was synthesized by polymerization of

three-component mixture of azobenzene group containing N-[4-[(E)-[4-[bis(2-hydroxyethyl) amino] phenyl] azo]phenyl]sulfonylbenzamide, chiral 2,3-O-benzylidene-D-threitol and isophorone-diisocyanate (molar ratio of azobenzene derivative, chiraldiol and diisocyanatein that mixture was 1:1:2).

The second chiral azopolymer 2 (figure II-2b) was synthesized by radical copolymerization of equimolar mixture of photoisomerizableazobenzenegroup containing 2-[4-[(E)-[4 (acetylsulfamoyl)phenyl]azo]-N-methyl-anilino]ethyl 2-methylprop-2-enoate and chiral 2-methyl-N-[(1S)-1-phenylethyl]prop-2-enamide.

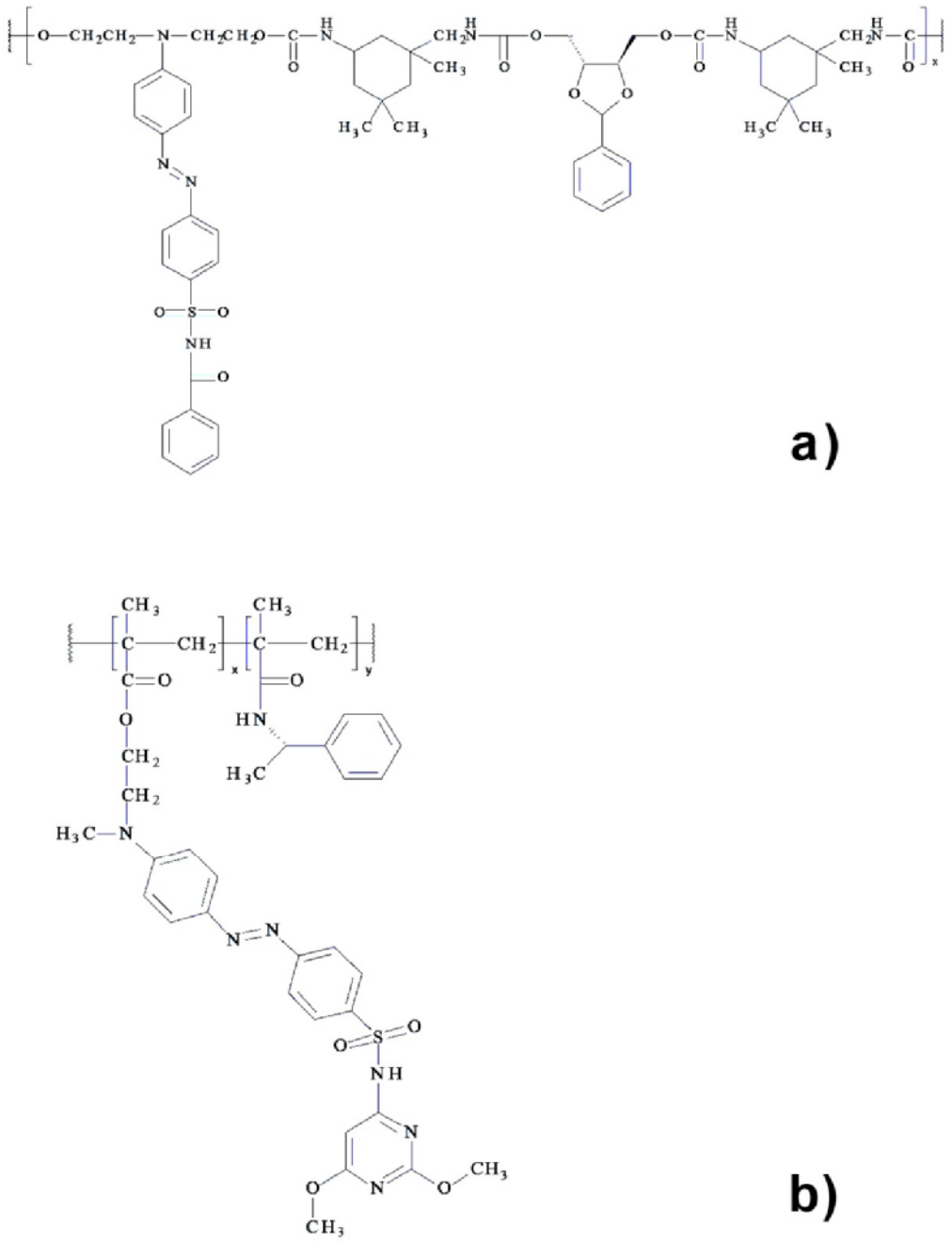

Fig. 0-2 : (a) Chemical structure of chiral azopolymer1, b) Chemical structure of chiral azopolymer 2

II.2.1. Characteristics of the monomers and polymers

Mean molecular weight, M_W, of polymers has been determined by GPC using Waters 917 columns, RIDK-102 detector and APEX ver. 3.1 recorder. A mobile phase was γ-butyrolactone and molecular weight referes to polystyrene standards. A Mettler Toledo DSC has been used for glass transition temperature (T_g) determination of polymers with scanning of 20K/min. Table II-1 shows glass transition temperature and Mean molecular weight of the polymers.

Table 0-1: Characteristics of the polymers

Azopolymer	M_W (g/mol)	T_g(°C)
MB2I	15800	71.1
MB3I	16500	71.5
AI2I	16250	57.5
Azopolymer (a)	18400	88
Azopolymer (b)	14700	77

II.3. Thin film preparation

II.3.1. Spin coating

Spin coating is a procedure used to deposit uniform thin films to flat substrates. Usually a small amount of coating material is applied on the center of the substrate, which is either spinning at low speed or not spinning at all. The substrate is then rotated at high speed in order to spread the coating material by centrifugal force. A machine used for spin coating is called a spin coater, or simply spinner.

Thin films were prepared by dissolving azopolymer in THF (50 mg in 1 ml of THF) and spin-coated on a pre-cleaned glass substrate. Prepared films were let inoven overnight at temperature over polymers' glass transition temperature to remove any residual solvent and also forobtaining films whose surface morphology appears featureless or isnot dominated by pinholes and other surface defects

II.3.2. Determination of Film Thickness

The Dektak is a profilometer for measuring step heights or trench depths on a surface. This is a surface contact measurement technique where a very low force stylus is dragged across a surface. The display range of the data is 200 A to 655,000 A (65.5 um) with a vertical resolution of ~ 5 A. The lateral resolution is limited by the tip shape. A video camera with variable magnification allows for manual placement of the stylus and the system is programmed for scan length and speed. Data leveling is done in the software and printouts with cursor locations and step heights are provided. The data can also be saved to a PC for further analysis.

The film thickness was determined by a Dektak Profilometer and was around 550_600 nm.

II.4. Solvents

All the solvents used in the study were of highest available purity from Merck. The selected employed solvents are listed in Table II-2.

Table 0-2 : Selected solvents

Solvents	***ε***	***Boiling point***
Acetic Acid	6.20	118
Carbon Tetrachlorid	2.24	76.8
Diethyl ether	4.627	34.5
Ethyl acetate	6.25	101.1
n-Heptane	1.92	98
n_Hexane	1.98	69
Pentane	1.84	36.1
1,4-Dioxane	2.21	101.1
Cyclohexane	2.02	80.74
Benzene	2.27	80.1
Toluene	2.38	111
Chloroform	4.81	61.15
Tetrahydrofuran (THF)	7.58	66
Dichloromethane	8.9	39.6
O-Xylen	2.57	144
Aniline	6.7	184.1
Pyridine	12.3	115.2
Triethylamine	2.4	88.9
Hydrogen Peroxide	84.2	150.2
Diethyl Glycol	31.8	246
2-Butanon	18.6	79.6
DMF	38.25	153
DMSO	47	189
1-Butanol	17.8	117.7
Ethanol	24.6	78.5
Methanol	32.6	64.6
2-Propanol	18.3	82.4

Octane	2.0	125.1

II.5. Dewetting

Dewetting of the thin films were done via the solvent droplet induced method. A droplet of solvent was dropped on the surface of the film with a LabnetBioPette- Plus Autoclavable, Adjustable VolumePipettes, Multi-Channel- and let dry at room temperature.

II.6. Optical setups

II.6.1. Single Beam Laser Setup

The λ= 473 nm laser beam of a horizontally linearly polarizedDPSS laser is used to excite the azo polymer absorption close to its absorption maximum. Polarization state of the laser beam is controlled using half- and quarter-wave plates. Sample is set perpendicular to the incident laser beam. The size of the collimated laser beam impinging onto the polymer sample is controlled with a Kepler-type afocal system and a pinhole (Fig II-3).

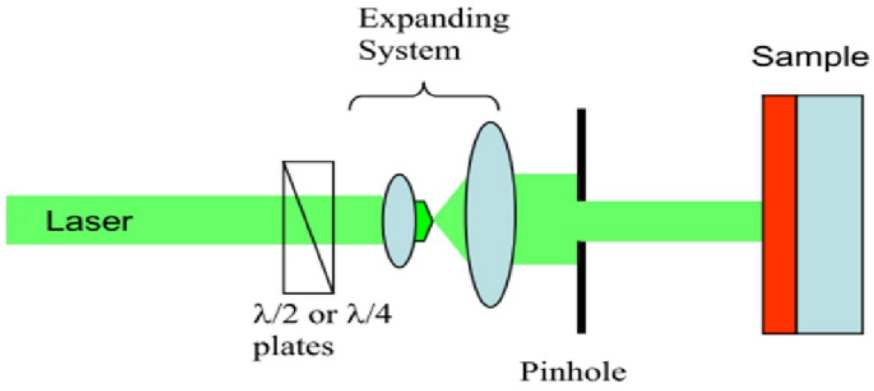

Fig. 0-3 : Experimental single beam setup for spontaneous patterning on azo polymer surface

II.6.2. Double beam set up

Optical set up for double beam exposure was done using a horizontally linearly polarized beam of a DPSS laser operating at a wavelength of λ = 473 nm.The beam was spatially filtered, collimated and then split by a beam splitter (BS), givingtwo beams of equal intensity. The two beams, after reflecting from a mirror, are recombine to form an interference pattern and were incident on the sample stage (Fig II-4).

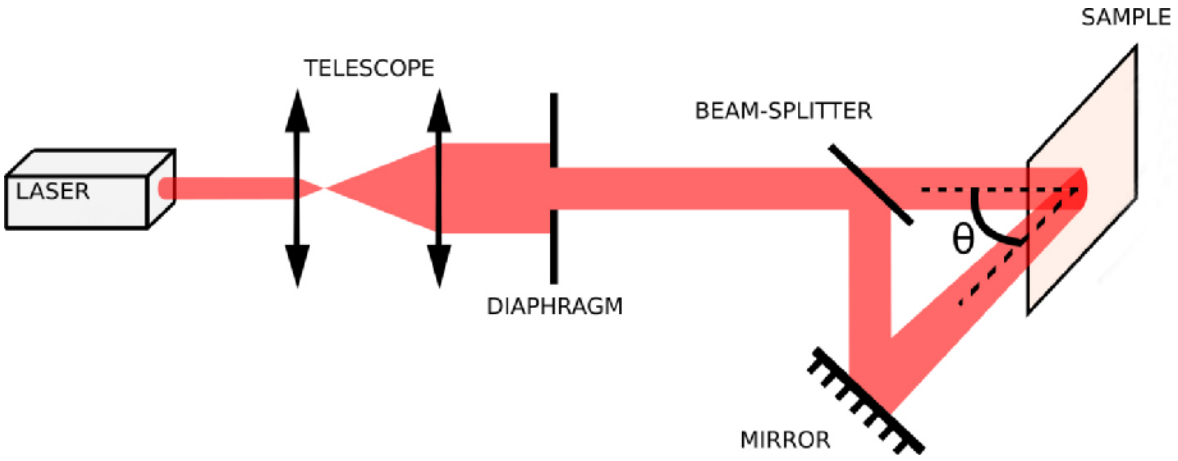

Fig. 0-4 : Experimental double beam setup for SRG formation on azo polymer surface

II.6.3. White light setup

An incoherent white lightfrom a xenon lamp (Hamamtsu, C2177-01) was used to initiate thephotoinduced mass transport in the film. The size of the beam is controlled with a selection of lens system (Fig II-5).

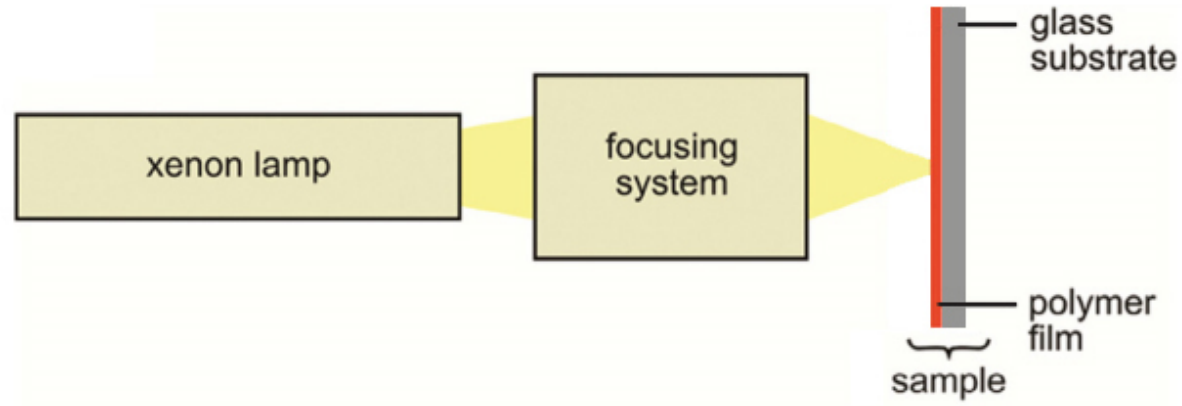

Fig. 0-5 : Experimental setup of the white light illumination of the sample in the experiment

II.6.4. Optical setup for diffraction pattern measurement

A circularly polarized laser (He-Ne, 632.8nm) is used to illuminate the PDMS sample. The PDMS replica of the azo's SRG is stretched horizontally and/or vertically by a system of clamps fixed to two linear translation stages. The diffraction pattern of the sample was formed on a sheet of paper, placed 4.0 cm from the sample, and acting as a diffuser. In order to prevent the image from saturating, the central spot from laser was masked via a black dot. Pictures of the diffraction patterns are captured by a Canon camera (EOS 550d and Canon ultrasonic objective 28-80mm), for every millimeter of stretching and recorded with different exposure times (Fig II-6).

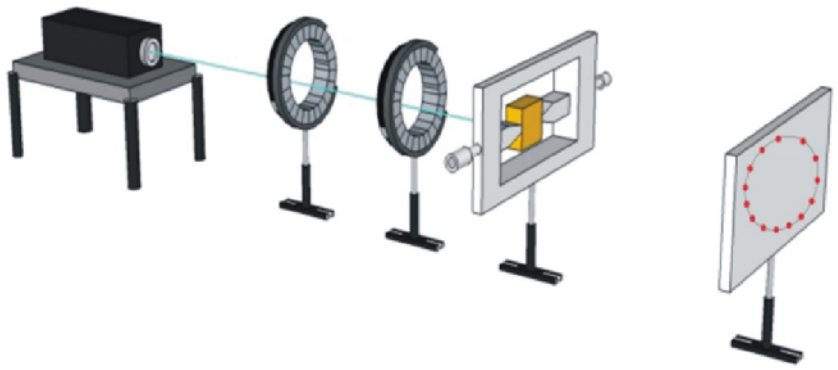

Fig. 0-6 : Optical setup used to observe diffraction pattern

II.7. Inscription of 2D quasi-crystal pattern via surface relief gratings

The inscription of the 2D quasi-crystal pattern is done by irradiation of azo polymer thinfilm with an interference pattern given by polarized laser beams. It leads to a reversibleand controlled topographic modification of the polymer film surface, which results in theinduction of a surface relief grating, in conjunction with the light's interference pattern. 22 Theprocess occurs readily at room temperature (well below the T_g of the amorphous polymersused) and it is believed that a large-scale photo-driven migration of polymer chains occurs during the SRG formation.

In a surface relief grating experiment, two beams are intersected at an angle θ at the sample surface, giving rise to an SRG with period:

$$L = \frac{l}{2\sin q}$$

Where, λ is the wavelength of the inscription light.

Microscopic surface relief gratings were inscribed onto the polymer films using a horizontally linearly polarized beam of a DPSS laser operating at a wavelength of λ = 473 nm.The beam was spatially filtered, collimated and then split by a beam splitter (BS), givingtwo beams of equal intensity. The two beams, after reflecting from a mirror, are recombinedto form an interference pattern and were incident on the sample stage. The exposure timefor each gratings was 5-10 minutes with a laser power of 0.7 W cm^{-2}. However, the highernumbers of gratings (for 16-fold and 32-fold quasi-crystal structures) needed a higher exposure time to reach the sufficient efficiency. After each irradiation, the sample is rotated, bya calculated angle depending of the complexity of the surface structure required, and a newexposure is repeated on the same spot. The degree of rotation depends on the number ofmultiple exposures done on the sample. For 2, 4, 8, 16 exposures the degree of rotation is90, 45, 22.5, 11.25 degrees, respectively.

II.8. Topography study of surface structures

II.8.1. Atomic force microscopy (AFM)

The thin film topography was studied with an atomic-force microscope (AFM). AFM is one kind of scanning probe microscopes (SPM). SPMs are designed to measure local properties, such as height, friction, magnetism, with a probe. To acquire an image, the SPM raster-scans the probe over a small area of the sample, measuring the local property simultaneously.

Direct measurements of topographic characteristics, surface morphology and photoinduced modifications of the and surface structure of the thin films and PDMS were conducted using an atomic force microscope AFM (Nano-Observer scientec, Veeco Instruments Inc) in contact and tapping mode, respectively.

II.8.2. Scanning electron microscope (SEM)

The scanning electron microscope (SEM) uses a focused beam of high-energy electrons to generate a variety of signals at the surface of solid specimens. The signals that derive from electron-sample interactions reveal information about the sample including external morphology (texture), chemical composition, and crystalline structure and orientation of materials making up the sample. In most applications, data are collected over a selected area of the surface of the sample, and a 2-dimensional image is generated that displays spatial variations in these properties.

Characterization of the particles was done using a scanning electronic microscope, SEM - JOEL 6301F, which was operated with an accelerating voltage of 3 kV.

II.9. PDMS replica of azo gratings

The Polydimethylsiloxane (PDMS) prepolymer was purchased from Momentive (RTV 615). PDMS is a polymeric organosilicon compound. It is optically transparent and does not allows aqueous solvents to infiltrate and swell the material. The shear modulus of PDMS is typically in the range of 100 kPa to 3 MPa, rendering the material flexible. The PDMS prepolymer was prepared by mixing the elastomer base and curing agent in a proper ratio (10:1, wt/wt). The mechanical properties of the elastomer depend on this ratio. A 10x10x2 mm 3D printed frame was placed on top of the thin film with the SRG and the prepolymer was poured into the frame and dried at room temperature for 2 days. The dried PDMS layer was removed from the thin film afterwards.

II.10. Extinction measurements

The extinction measurements of the pattern replica were done with a collimated halogen lamp (SCHOTT KL1500 electronic halogene lamp 15V/150W) covering the spectrum from 400 nm to 800 nm, transmitted through the sample. The light is collected with a fiber and a collimating lens and sent to a spectrometer (Edmund optics,Te Cooled CCD Spectrometer 64814, Model N0 BTC112E, Serial Number: 101127304).

II.11. Nanoparticles

Spherical citrate-stabilized silver nanoparticles, with an average diameter of 60 nm were purchased from Sigma-Aldrich (Sigma-Aldrich, Merck KGaA).An OD1 (i.e. 4 pM) 60nm silver nanosphere droplet was deposited on a coverslip and the PDMS replica of the azo-SRG was pressed against it for a few seconds. Then the PDMSSRG was removed and let dry for a couple of hours.

II.12. Synthesis of azoparticles

The particles composed of the azo polymer and PMMA are fabricated through microphase separation. These particles were obtained through slow volatilizing of chloroform from azopolymer/PMMA/chloroform droplets dispersed in aqueous solution of poly(vinyl alcohol). Azopolymer and PMMA, each with the concentration of 20mg, were dissolved in 2ml of chloroform. 1 ml of obtained solution was added carefully into the bottom of aqueous solution of poly(vinyl alcohol) (2,5 wt%, 30 ml), under moderate stirring, to promote the dispersion of the organic solution into microdroplets. Afterwards, the stirring speed was increased up to ca. 450rpm to disperse the organic phase. In order for the evaporation of the chloroform to be

slow, the stirring was continued for 24 hours. Subsequently, the obtained suspension was centrifuged and washed with water several times.

II.13. Conclusion

In summary, this chapter contains the materials and the methods used in this study. Different types of azopolymer materials are introduced as a subject of surface structuring. Several optical setups are employed during these processes and the resulted topographies are studied by microcops (AFM, SEM). Obtained surface structures are replicated by the soft lithography method on a transparent elastomeric material (PDMS) for further studies. Also, a new group of azopolymeric particles are synthesized.

In the next chapter, a more detailed description of the obtained structures and their characteristics and possible applications will be given.

Chapter III:
Results and Discussion

III.1. Introduction

Complex and engineered surface structures can manipulate light through physical effects such as scattering, diffraction and interference. These optical surfaces present a growing interest due to many new potential applications in photonics. Among all these surface structures, 2D quasi-crystal structure presents a type of unconventional crystallographic structure possessing a long-range aperiodic order and a rotational symmetry. Quasi-crystal structures layed out on surface of polymer thin films can be considered as a new type of optical surfaces and could be used as novel diffraction gratings. Fabrication of surface quasi-crystal structures on azo polymer films can be considered as a new approach to further development of the surface patterning technology based on the photo driven mass migration scheme. Surface-relief gratings (SRGs) can be inscribed on azo polymer films upon irradiation with an interfering laser beams with a wavelength in the absorption band of the azo polymer, at temperatures well below the glass transition temperatures (Tg) of the polymers.

However, azopolymer surfaces are not transparent and are not chemically inert. Here we propose to adapt the duplication of the photoinduced azopolymer surface-relief gratings through a soft lithographic approach, to the case of the quasi-crystal in order to create a transparent, stretchable and chemically inert surface, with tunable and ordered nanocavities for single nano-objects deposition.

III.1.1. Formation of quasi-crystal on azopolymer films

We create nano-cavities on an azopolymer film by superimposing multiple sinusoidal phase grating patterns with different directions. The different grating patterns do not interfere with each other and simply add-up. Adding multiple sinusoidal grating tends to smooth the surface and consequently diminish the diffraction efficiency. It is possible to inscribe one-dimensional (1D) line gratings (Fig.III.1-1a) with the varying period, by changing θ of the interference angle between the beams.

$$\Lambda = \frac{\lambda}{2\sin\theta} \qquad \text{(III.1)}$$

Following, the second illumination step was added after rotating the samples around the surface's normal at 90◦, with respect to the writing beam. Such an inscription procedure 3resulted in a 2D cross grating with the same period Λ in both principal directions (Fig.III.1-1c). A successive overwriting of multiple 1D interference patterns give rise to 2D SRGs with controlled geometries. Writing four SRGs by rotating the sample four times at 45◦ results in an interesting flower like structure seen Fig.III-1.1e. Continuing overwriting eight and sixteen SRGs on the same spot by rotating the film at 22.5° and 11.25°, respectively, successively results in a set of complex structures seen in Fig.III.1-1g,i.

a

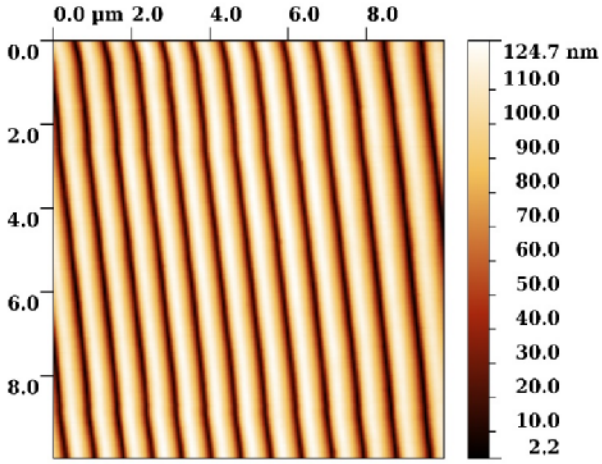
0.0 µm 2.0 4.0 6.0 8.0
0.0
2.0
4.0
6.0
8.0
124.7 nm
110.0
100.0
90.0
80.0
70.0
60.0
50.0
40.0
30.0
20.0
10.0
2.2

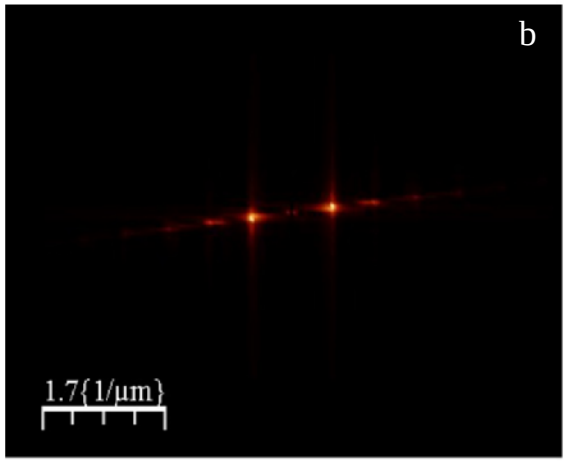
b
1.7{1/µm}

c

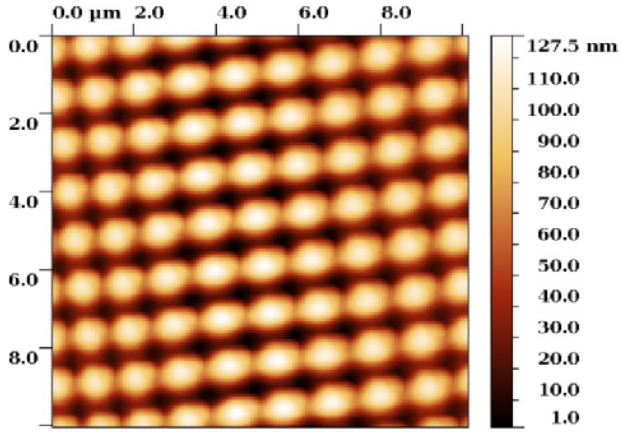
0.0 µm 2.0 4.0 6.0 8.0
0.0
2.0
4.0
6.0
8.0
127.5 nm
110.0
100.0
90.0
80.0
70.0
60.0
50.0
40.0
30.0
20.0
10.0
1.0

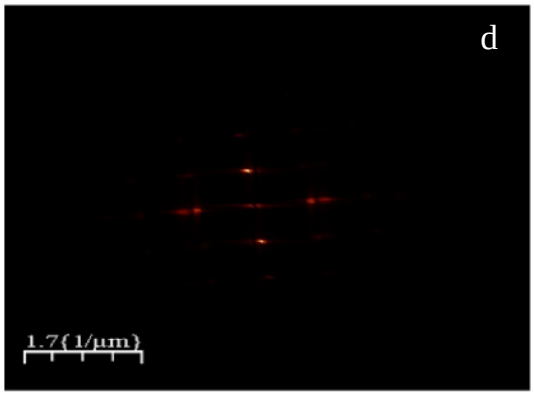
d
1.7{1/µm}

e

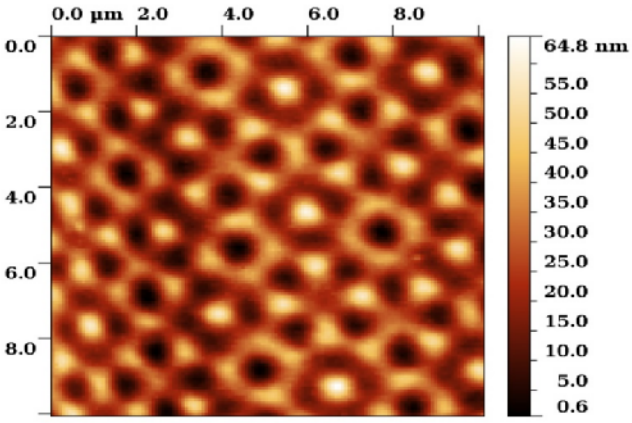
0.0 µm 2.0 4.0 6.0 8.0
0.0
2.0
4.0
6.0
8.0
64.8 nm
55.0
50.0
45.0
40.0
35.0
30.0
25.0
20.0
15.0
10.0
5.0
0.6

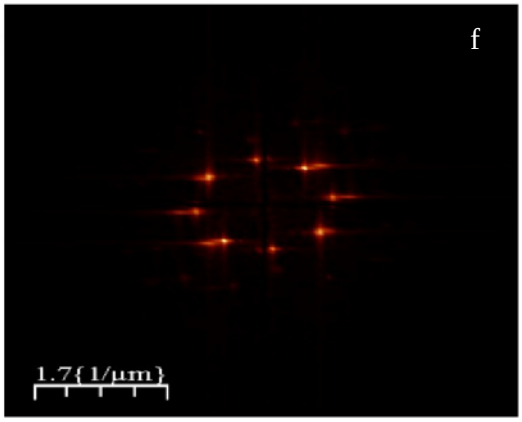
f
1.7{1/µm}

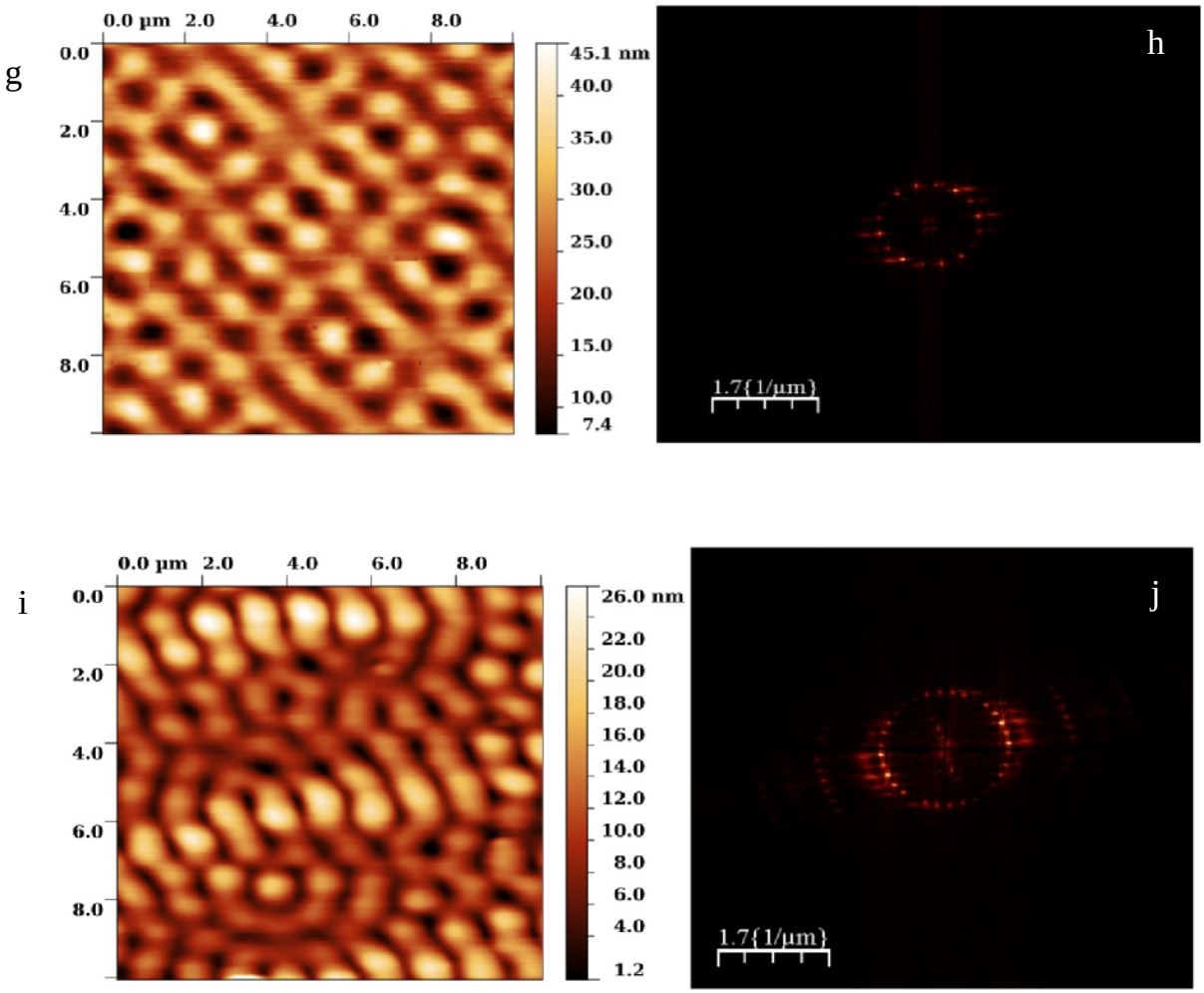

Fig. III.1-1 : a) AFM measurement of a 1D Grating c) AFM measurements ofa 2 superimposed gratings e) AFM measurement of a 8-fold quasi-crystalstructure g) AFM measurement of a 16-fold quasi-crystalstructurei) AFM measurements of a 32-fold quasi-crystal structureb,d,f,h,j) FFT of AFM measurements a,c,e,g and i, respectively

III.1.2. PDMS replica of azo gratings

As mentioned in Chapter II, PDMS replicas of gratings were done through soft lithography. The PDMS prepolymer was prepared by mixing the elastomer base and curing agent in a proper ratio (10:1, wt/wt). A 10x10x2 mm 3D printed frame was placed on top of the thin film with the SRG and the prepolymer was poured into the frame and dried at room temperature for 2 days. The dried PDMS layer was removed from the thin film afterwards.

III.1.3. AFM measurements on PDMS replica of azopolymer SRG

The AFM measurement of the PDMS replica of a 4, 6 and 8-fold quasi-crystal structure, (similar to the samples presented on fig.III.1-1) is shown on fig.III.1-2. The PDMS surface is a fairly good negative reproduction of the initial SRG, as suggested by the four, six and eight spots pattern on the FFT of the AFM images.

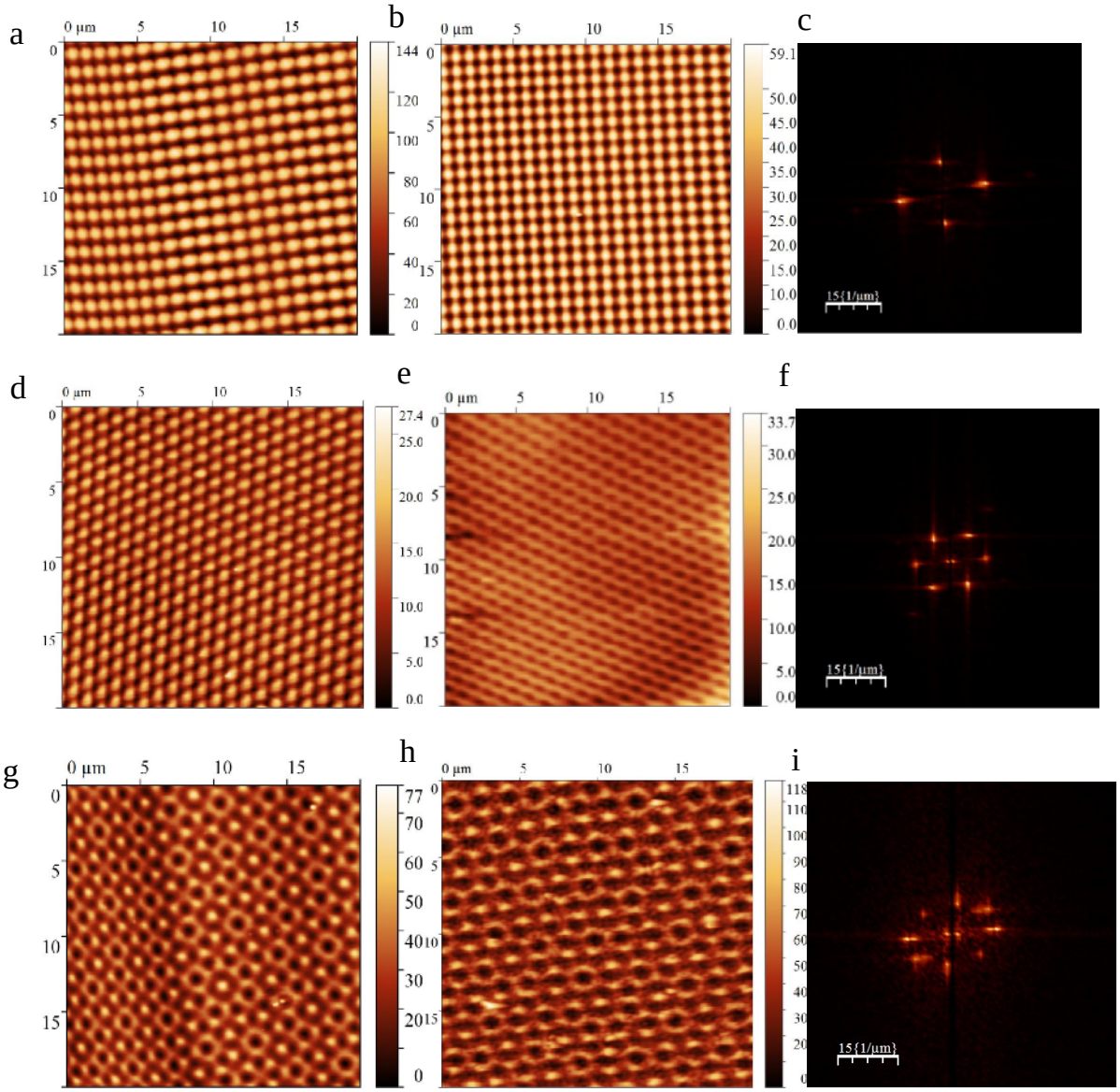

Fig. III.1-2 : a) AFM image of the surface of an azopolymer4-fold SRG. b) PDMS replica of the same sample. c) FFT of AFM measurements of PDMS replica (4-fold SRG) d) AFM image of the surface of an azopolymer 6-fold SRG. e) PDMS replica of the same sample. f) FFT of AFM measurements of PDMS replica (6-fold SRG). g)

AFM image of the surface of an azopolymer 8-fold SRG. h) PDMS replica of the same sample. i) FFT of AFM measurements of PDMS replica (8-fold SRG)

III.1.4. Modification of the diffraction pattern while stretching the PDMS quasi-crystal

As pointed out, the PDMS replicas of the surface structures are stretchable. Fig.III.1-3a presents the evolution of the diffraction pattern of a 8-fold quasi-crystal PDMS replica under different horizontal stretching distance.

Reduction of the distance of the horizontal spots from the center indicates a decrement in the pitch (a compression) for the sinusoidal gratings perpendicular to the stretching direction. On the contrary, the increase in the distance for the vertical spots indicates an increment (an elongation) for the sinusoidal gratings colinear to the stretching direction. It is important to note that these transparent and stretchable quasi-crystal samples could also have interesting applications in beam steering. These elongations and compressions are linear up to six millimeters of stretch, as shown on fig.III.1-3c. From these measurements, we can say that a stretch at the macroscopic scale of 1mm leads, in microscopic scale, to a compression of 116 nm of the pitch of the sinusoidal gratings perpendicular to the stretching direction and an elongation of 56 nm for the pitch of the sinusoidal gratings along the stretching direction. Nonetheless, these evolutions concern only one sinusoidal component of SRG but doesn't give direct access to the progress of the dimension of the nanocavities during the stretching of the PDMS (Refer to Chapter IV for simulations and measurements).

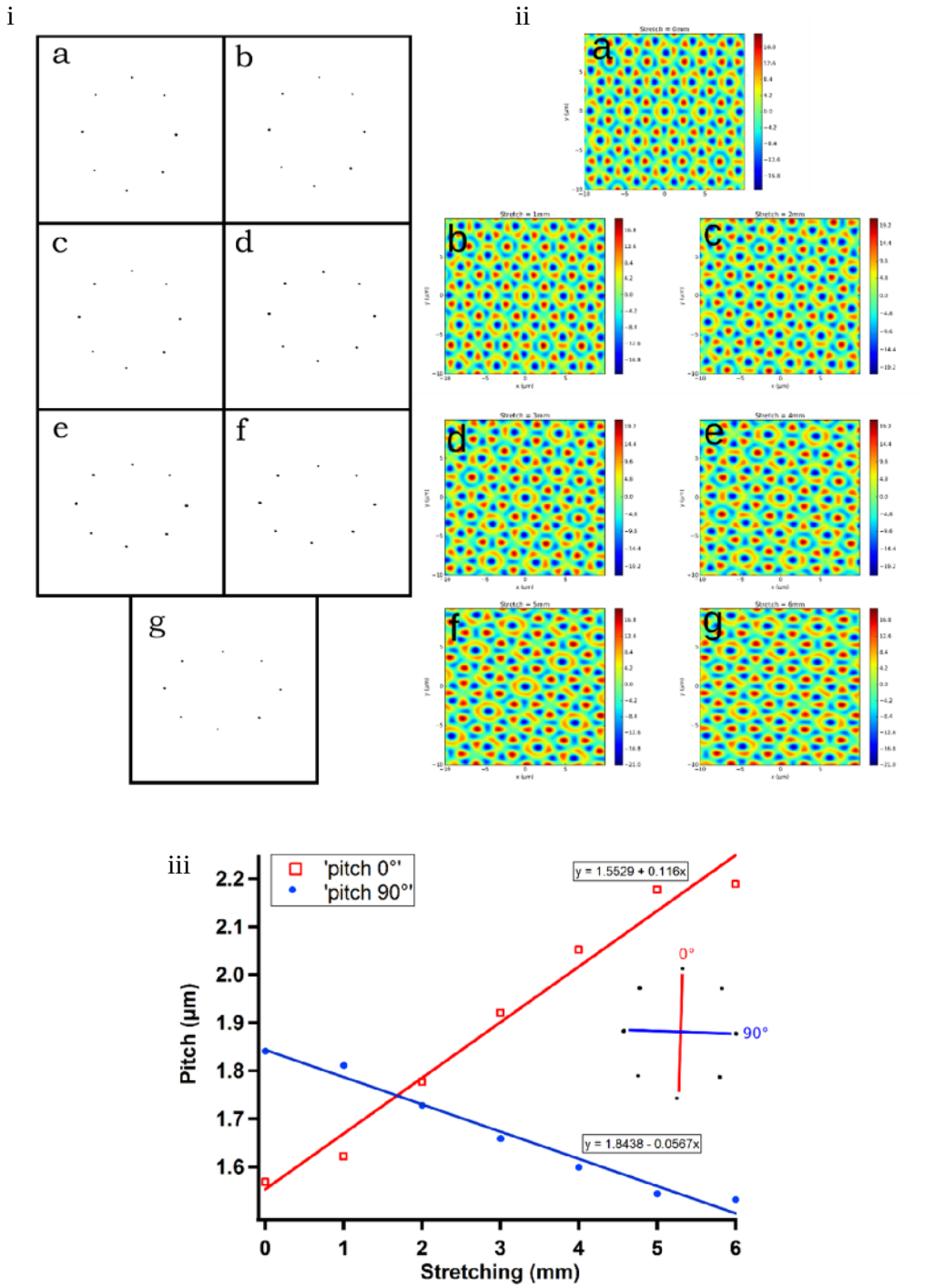

Fig. III.1-3 : i) Evolution of 8-fold PDMS SRG diffraction patternwith stretching. a) no stretching b-g) stretching 1 mm to 6mm. ii) Evolution of the 8-folds quasi-crystal SRG on PDMSwith a) 0mm, b) 1mm, c) 2mm, d) 3mm, e) 4mm, f) 5mm and g)6mm of stretching. iii) Evolution of the pitch for 4 gratings. 0° and 22.5°gratings are oriented following the direction of elongation, 90°and 112.5° gratings are oriented perpendicularly. The line fitgives an elongation of 116 nm and a compression of 56 nm per1mm of stretch

III.1.5. Single nanoparticle deposition on PDMS quasi-crystal

As a proof of concept, we show in the fig.III.1-4 that a single nanoparticle can easily be deposited into the nanocavities formed on the PDMS surface. Direct nanoparticle deposition on a coverslip usually leads to the so-called coffee-ring effect that creates uncontrolled aggregation of the nanoparticle. Here, the nanoparticle is naturally trappedinside the cavity during the evaporation of the solvent, as shown for example for a large number of particle by B. Reinhold et al. with the appropriate concentration of nanoparticle, we can ensure that, statistically, there is less than one particle per cavities. Since the PDMS is transparent, the presented PDMS SRG sample is a very effective platform for conducting optical measurement of a single particle. Through several deposition step, it would also possible to deposit different kind of nanoparticles inside the same nanocavities; for instance, such as silver and gold nanoparticle, in order to study the plasmonic response of heterodimer. Moreover, since the sample is strechable, it is also possible to deposit elongated nanoparticle such as nanorod in the stretched nanocavities.

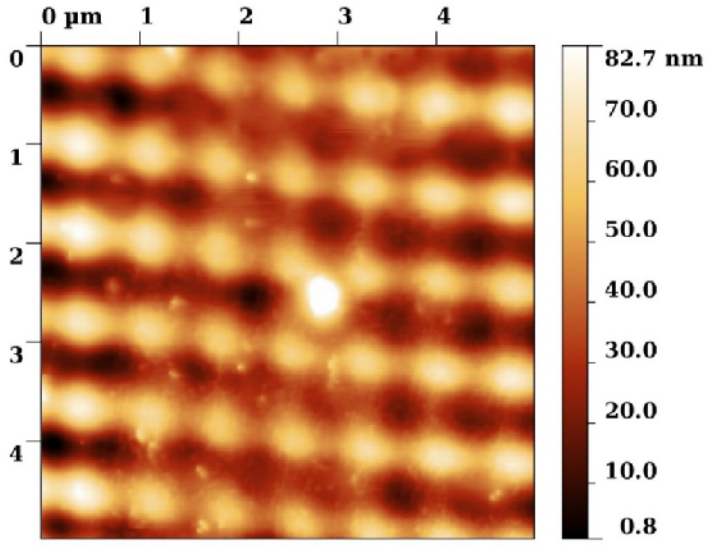

Fig. III.1-4 : AFM measurement showing a 60nm silver nanosphere deposited in one of thecavities of a 4-fold PDMS SRG

III.1.6. Conclusion

We have presented the fabrication of surface quasi-crystal structures on azopolymer films and its replication through soft lithography on a transparent elastomer (PDMS). The quasi-crystal structures were prepared simply through a multistep light irradiation via an interference pattern of laser beam without additional manipulation. The printed patterns on PDMS showed the same patterns as the masters and the same relief depths as the stamps. The light diffracted by the PDMS stamp was used to observe the deformation of the surface as a function of its stretching. The PDMS SRGs were used as a tailored surface for the deposition of single nanoparticle in nanocavities.

III.2. Introduction

Disordered photonics has experienced a burst of activity in the last two decades. Fabrication of nanostructured materials for control of light-matter interactions has become particularly important for improving different phenomena involving a high degree of light scattering. Quasi-random or Gaussian random structures have been proposed as good candidates for energy harvesting.

Here, we propose a new method to generate a 2D quasi Gaussian surface and a quasi-random periodic surface (quasi-random gratings) based on molecular nano-motor lithography, where the nanoscale movements of molecules, acting as nano-motors, is fueled by the laser light. This movement can induce self-organized randomly dispersed nanopatterns on the surface of a thin film. The nanomotors are azobenzene molecules. Azobenzene derivatives are one of the most frequently studied class of switchable compounds. The azobenzene functionality exhibits a *cis-trans* isomerization. The thermodynamically stable trans isomer can be converted to the cis isomer by a light stimulus, whose wavelength is in the absorption band of azobenzene, with a back isomerization induced by a thermal relaxation. Engineering azopolymer materials can lead to a photoisomerization induced by light, to create self-induced patterns on the surface of thin films. One example of such induced patterns is the production of self-organized structures, leading to gratings on the surface of side-chain azobenzenegraphted copolymer DR1 thin films. This study was the first experimental result of photoinduced spontaneous structure of azopolymer, generated with a single beam. As such, the use of azopolymer is a good choice for the fabrication of random nanostructured materials, for the purpose of controlled light-matter interactions, particularly for the improvement of high light scattering through different phenomena involving in the process. Through this process, different self-structured surface patterns were observed, in particular with epoxy-based azopolymers, acrylic polymer bearing the photoresponsive moieties as side chains of the polymeric backbone or 4VP(OH-DMA) [12], but none have ever been used for light management in photonics.

III.2.1. Quasi Gaussian surface

The first experiment is done by illumination of the azopolymer 1 (Chapter.II). Fig.III.2-1a presents the surface topography of azopolymer1, obtained with an atomic force microscope (AFM). Topography of the first sample is a quasi-random pattern. Illumination by a laser light induces a spontaneous self-structured surface pattern with spontaneous created cells, with diameters in the range of nanometer scale, giving a granular aspect.

The cell size has an average perimeter in the order of 2.3 mm. Fig.III.2-1b gives the Fourier transform of the surface. The lattice has a Fourier energy concentrated into a well-defined circular range of k-vectors with a radius value, around 15.2 mm^{-1}.

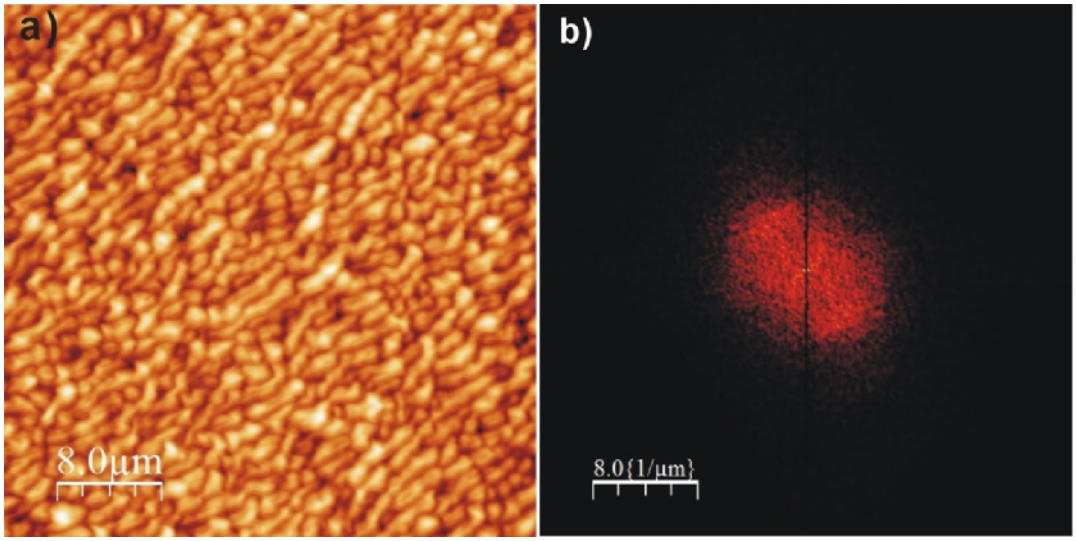

Fig. III.2-1 : a) Surface pattern of the azopolymer 1 measured with an AFM in the contact mode, b) Fourier transform of the surface pattern.

A histogram of data given by a statistical roughness analysis, calculated from the topographic measurements acquired by the AFM, is shown in fig.III.2-2a. Fit of a Gaussian curve to the roughness histogram gives an excellent match, and the measured average height is 265 ± 10 nm. The granular pattern has a very small structuration anisotropy, confirmed by the symmetry

of Fourier transform. While the laser polarization was linear during the illumination, no specific correlation of the polarization with the direction of the pattern is observed.

The RMS roughness (s) is 82 ± 2 nm. In fig.III.2-2b, the correlation function of surface heights' is also quite close to a Gaussian curve. We measured the lateral correlation length considering a Gaussian fit (defined as the e^{-1} half-width of the correlation) and obtained a value of x = 510 ± 10 nm. The ratio s/x is 0.16. With this small ratio, slopes of the surface roughness are small. This result is confirmed by the Kurtosis parameter (K), which is a dimensionless quantity giving a measurement of the sharpness of the height distribution function. We found K = 2.7, close to the value 3, for a Gaussian height distribution.

This low ratio of the surface roughness implies that if we consider a ray-tracing, following the geometrical optics, multiple scattering or shadowing effects will be attenuated and will be insignificant at small angles of light scattering (referred to the normal axis). Second order reflections can take place only for high angles of incidence.

The surface can be described, in details, with a height–height correlation function (HHCF), H(r) (fig.III.2-2c).The measured surface is explained in terms of scaling exponents. The HHCF data reaches a saturation height, which can be related to the roughness of the image as well as the average grain size, by utilizing the Hurst function given by the following equation (Eq.III-2):

$$H(r) = 2\sigma^2 \left\{1 - \exp\left(-\left(\frac{r}{\xi}\right)^{2\alpha}\right)\right\} \qquad \text{(III-2)}$$

Where, α is the Hurst parameter (or surface roughness exponent), σ is the surface roughness and ξ is the correlation length. The surface morphology is completely characterized by these

parameters. The curve reaches a plateau and the Hurst parameter (a) or surface roughness exponent influences the slope of the function before it reaches the saturation height. The surface roughness is a measure of changes in height across the surface of sample. The correlation length influences the saturation height, which is defined as the largest distance in which the height is still correlated. The surface roughness exponent, α, allows the determination of the fractal dimension and the frequency of height fluctuations. The fractal dimension, D_f, corresponds to the changes in surface morphology, which occur due to the effects of the photoinduced surface patterning. The surface roughness is linked to the fractal dimension, D_f, of the random surface by $D_f = D - \alpha$, where D is the Euclidean dimension of the surface, (D=3) that defines the geometry of the sample. We fitted the Hurst function, plotted in the figure 3c, to the calculated HHCF data to obtain the values of parameters in Equation (III-2).

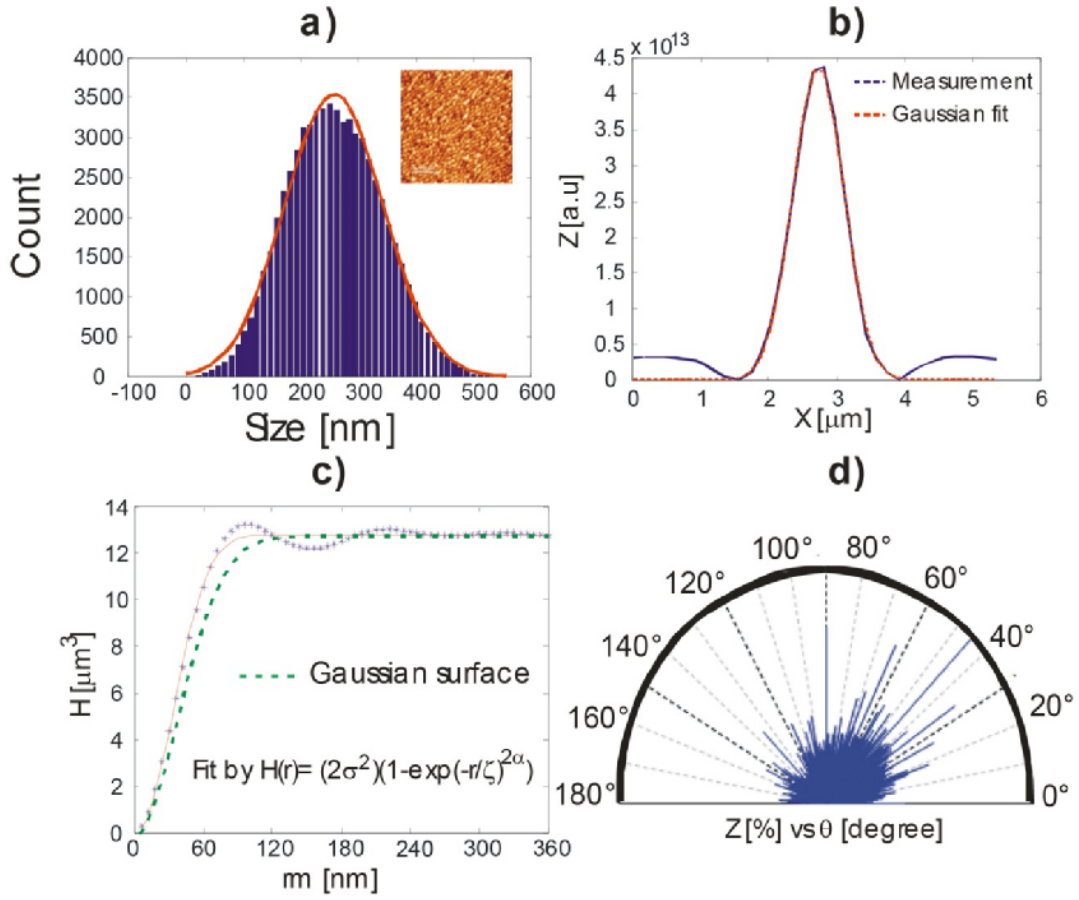

Fig. III.2-2 : a) Histogram of the surface RMS roughness of the azopolymer 1 and its fit with a Gaussian curve, b) auto-correlation function of the pattern surface and comparison with a pure Gaussian surface (red), c) height–height correlation function (HHCF) and fit, d) directionality of the light emission from the surface.

The fit shows a great agreement with a model of a Gaussian surface. The surface roughness exponent, a, obtained from fitting the HHCF data of the AFM surface is 0.92. The Hurst parameter, a, is close to 1, meaning that the surface is smooth. The fractal dimension, D_f, is 2.08.

The directionality of the emission in fig.III.2-2d gives a broadband range of angles. The emission isotropy for this random surface is 52.6 %. This effect is mainly due to the low value of the roughness angles and the smoothness of the surface, as it was measured with the Hurst parameter and the ratio s/x. This directionality leads to an emission of light into all directions

of a hemisphere, with almost constant radiance, and consequently can be considered as quasi Lambertian.

III.2.2. Quasi random grating surface

The second experiment is done with azopolymer 2 (Chapter.II). Fig.III.2-3a gives the topographical measurement of the surface after laser irradiation. The surface is spontaneously organized into sub-zones, oriented with different angles, and a periodic structure giving the aspects of quasi random periodic structuration. Two different types of subzones, where a periodic structure appears, are present. Each of these subzones contains a periodic structure with a pitch, defined as the distance between two maxima, of 0.51 ± 0.2 µm, in the descending direction, or 0.35 ± 0.2 µm, in the ascending direction. The subzones have an average length of 7.8 ± 0.3 µm, with a maximum width of 1.6 ± 0.2 µm. These zones inside the whole pattern appear to be superposed. Some parts of the sample show an overlapping between the randomly arranged sub-zones of gratings, where the periodic structures are photoinduced.

Self-organization of the thin film surface in multi gratings is the result of a mass transport due to *cis-trans* photoisomerization, as the light illuminates the surface. In our experiment, the light illumination is by a single Gaussian laser beam, without any structuration of light. The long side chain of the second azopolymer, with high T_g, limits the process of molecular mass transport on the surface, in order to induce a large periodic structure by increasing the local viscosity. Another possible involved phenomenon could be the free volume size in the proximity of the azobenzene chromophore leading opto-mechanical movements. The calculated molar volume of sulfabenzamide azo derivative with Gaussian09 package, present in azopolymer 1, is 293 cm^3/mol. While, this value for sulfadimethoxine azo derivative present in azopolymer 2 is distinctly lower, 263 cm^3/mol (the molar volumes were calculated for *trans* isomers of model compounds). The lower molar volume of photoisomerizable azobenzene derivative present in azopolymer 2 provides more free volume available for *trans-cis-trans*

isomerization process. This may explain the higher photoisomerization and thermal relaxation rates observed for azopolymer 2, favouring grating patterns compare to azopolymer 1.Recently, we have presented results showing that, in the same condition for an azopolymer with a lower T_g, the self-organization takes place with features with a length of 300 ± 20 nm, revealing by the superposition of photoinduced periodic sub-structures [18].

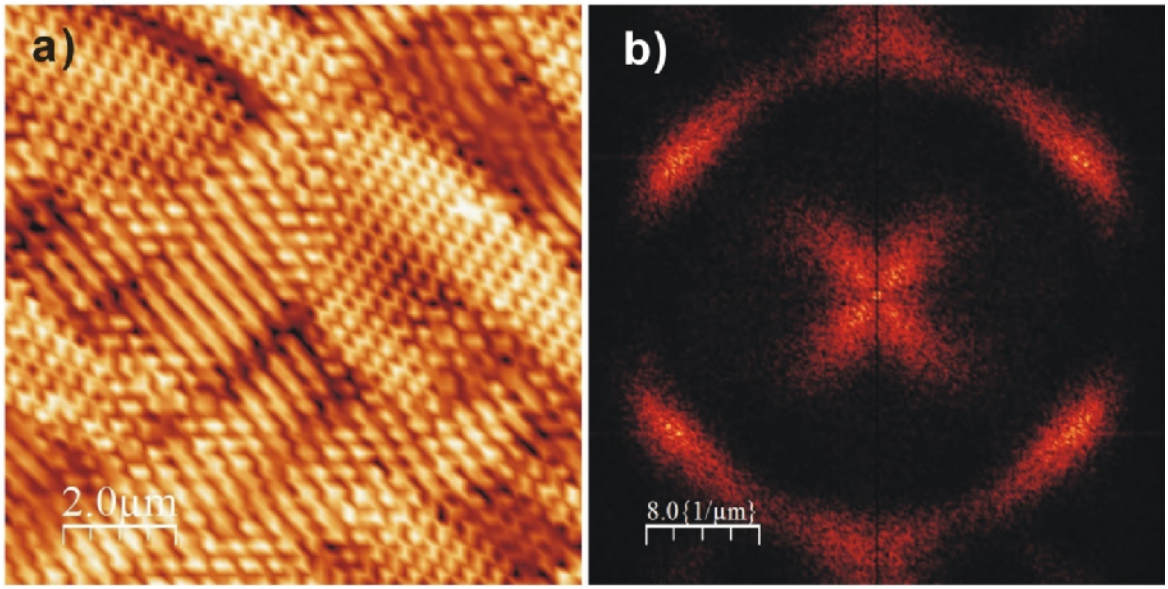

Fig. III.2-3 : a) Surface pattern of the azopolymer 2 measured with an AFM in the contact mode, b) Fourier transform of the surface pattern.

The quasi random grating structuration is confirmed by Fourier transform of the surface pattern. Fig.III.2-3b exhibits the Fourier spectrum of the AFM measurements. The Fourier spectrum is confined to a circular range of k vectors, where the largest k-space distribution is due to the small structures confined in the multi gratings. The low k-values in the central part of the Fourier space are due to the multi gratings, layered in two different directions. We measured a maximal k-vector value of 17.2 μm^{-1}, larger than the measured values obtained with quasi random nanostructures on silicon materials. The width of the k-vector ring is 4.5

mm^{-1}. Large k-vectors are a valuable property for light trapping applications. Indeed, the exit angle, θ_e, of light diffracted by a grating surface is given by:

$$\sin \theta_e = q\lambda_r k_m \quad \text{(III-3)}$$

Where, q is the diffraction order, λ_r is the reading wavelength and k_m is the maximal value of k-vector in the Fourier transform of the surface pattern. If the exit angle, θ_e, is greater than 90°, the light cannot emerge from the surface and is trapped inside the thin film. With a value of k_m = 17.2 mm^{-1}, wavelengths as small as 360 nm do not exit the surface and are trapped inside the thin film, creating quasi-guided mode. This trapping effect is experimentally tested in section 3.2.3.

Consequently, we can say that the surface presented in fig.III.2-3a offers an interesting trade-off between periodic and random domains: the diffraction efficiency presents simultaneously a concentration of light into very high and very low orders.

A histogram of roughness analysis data, obtained by measurement with AFM, is shown in fig.III.2-4a. The fit of the roughness can be done with two Gaussian curves and the histogram is in good agreement with these two curves.

The measured RMS roughness of the whole sample is s = 20.6 nm. We distinguish an average roughness height of 62.5 nm and 91 nm for the first and the second average height, respectively, given by the two roughness statistics fitted by a Gaussian curve.

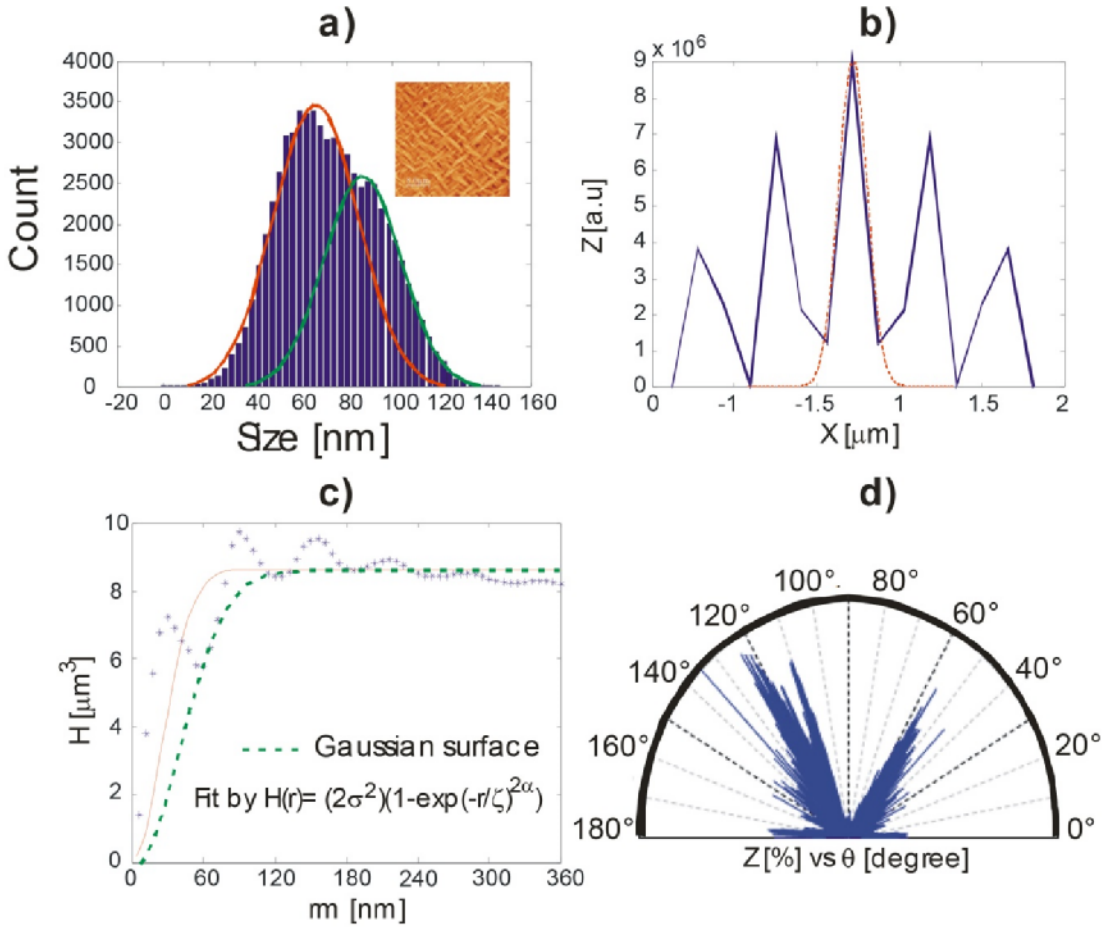

Fig. III.2-4 : a) Histogram of the surface RMS roughness of the azopolymer 2 and its fit with a Gaussian curve, b) auto-correlation function of the pattern surface and comparison with a pure Gaussian surface (red), c) height–height correlation function (HHCF) and fit, d) directionality of the light emission from the surface.

The correlation function of surface heights (fig.III.2-4b) gives a lateral correlation length of x = 98 ± 10 nm. This correlation function is not Gaussian. The different peaks are explained by periodicity of the pattern and we find the same correlation length in the other oscillations.

The ratio s/x is 0.21. With this ratio, a large proportion of the surface becomes shadowed, due to the topology for high angles of incidence of light. Any valleys on the surface start to be involved in multiple scattering events. So a part of primary reflections on the surface roughness give rise to secondary ones.

The height fluctuations occur at different length scale. The Hurst parameter corresponds to the frequency of height fluctuations. The surface roughness exponent parameter obtained from the

fitting of the AFM scan is $a = 0.63$, far from the value $a = 1$, indicating a rough surface. Fig.III.2-4d shows the light directionality of the quasi-random gratings on the surface. We calculated an isotropy of 18.3 % in the emission of light from the surface. The directionality of the emission covers mostly four directions of the space. This anisotropic emission is due to the large random variation of micrometer length gratings on the surface, associated with a nano-patterning with a honeycomb form inside the gratings. However close to the surface the directionality of the emission is almost in the surface plane, allowing the reduction of the thickness of the trapping film. The surface texture model can be thought as the superposition of emission from gratings formed by slits, separated from one another with different distances.

III.2.3. Quasi guided modes into the thin film

In order to test the validity of light coupling through quasi-guided modes into the thin film, we have created four additional grating structures next to the quasi-random grating surface (fig.III.2-5a). First, the central pattern corresponding to quasi random gratings is spontaneously created by illuminating the azopolymer 2 with a single beam. Afterwards, four gratings are made with a laser interferences pattern, illuminating the sample through a pinhole. The sample was rotated in order to inscribe the 4 gratings, one by one, at the cardinal points, close to the central quasi random grating surface. The laser interferences pattern is obtained by separating the beam from a linearly polarized laser beam via a beam splitter and recombining them with two mirrors.

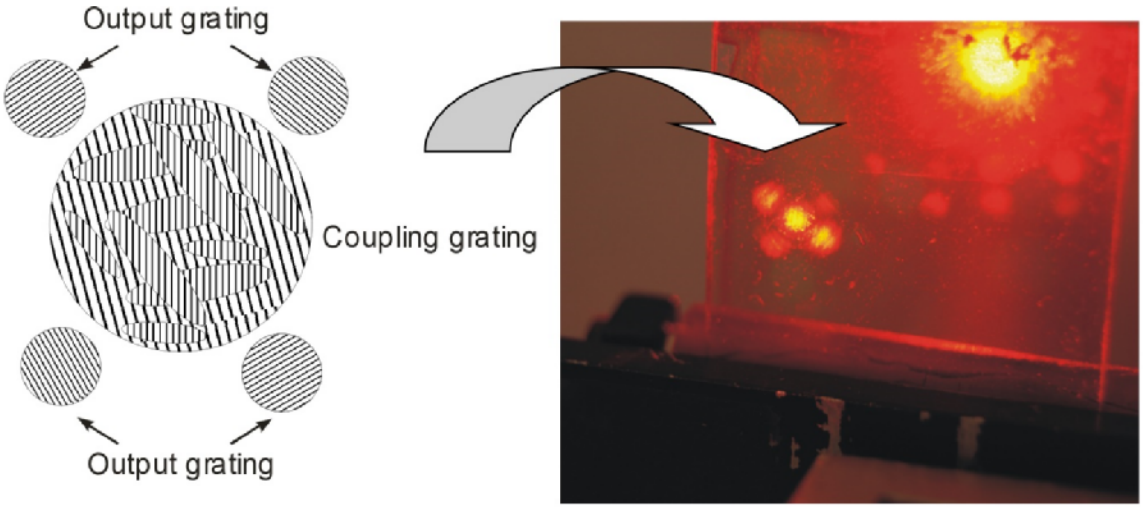

Fig. III.2-5 : Four gratings were inscribed in the cardinal direction in order to show the mode coupling of the light in all the directions and the outcoupling light by the 4 gratings. The picture on the right shows that light (He-Ne laser) injected on the quasi random grating surface (coupling grating) is outcoupled by the output gratings. This confirms the existence of quasi guided modes into the thin film.

The positions of these four gratings match the positions of the diffracted spots given by the Fourier transform of the surface pattern (fig.III.2-3b). The pitch of these four gratings, measured from AFM images is $\Lambda = 0.9 \pm 0.05$ µm with an amplitude of 100 ± 10 nm. After inscription of these gratings, a He-Ne Laser is used to illuminate the central quasi-random grating pattern of the surface. We used a He-Ne laser in order to avoid possible photoinduced changes applied on the surface by the laser.

As it can be seen on fig.III.2-5b, the central pattern diffracts the incoming light with such big angles that a part of the incoming light cannot directly exit the film. However, the trapped light can excite the quasi-guided modes into the thin film. The guided energy is then outcoupled by the 4 satellite gratings. The variation of light intensity in the four gratings is due to amplitude inhomogeneities in the central pattern, affecting the total repartition of the extracted light into the four gratings. Tilting the sample, with respect to the incident angle, is important and can also affect the extracted light. The intensity of the light coming from the gratings can be

controlled through changing the incident angle. In addition to applications for light harvesting, the quasi random-grating surface can also be seen as a four beam splitter for thin films.

III.2.4. Light trapping efficiency measurements

Due to the surface relief features, the surface-patterned azopolymer films can be used directly as a soft lithographic master to cast molds. We replicated the photoinduced surface of the chiral azopolymers 1 and 2 on a widely used elastomeric material, (poly(dimethylsiloxane (PDMS)). This material has a low interfacial free energy. The PDMS sample is largely transparent, since it has an optical absorption of 0.04 % and a transmission above 95 % in the visible region of the spectrum. The printed replicas showed the same random structures as the masters, along with the same relief depths. Fig.III.2-6a shows the photographic images of the stamps. Brilliant and iridescent colors, resulting from the diffraction of the surface gratings, can be observed for the replica of the quasi-random grating surface (sample A on fig.III.2-6a).

Taking the plane PDMS surface as a reference, we measured the light extinction, induced by the patterned surface, for both materials. We found an increase of the light extinction ratio of 28% and 41% for the quasi Gaussian surface and quasi-random grating surface, respectively (fig.III.2-6b). This light extinction is homogeneous over the visible spectrum, which is a valuable property for light harvesting. Since no absorption can occur inside the PDMS material, this extinction is due to light scattered by the random surface (for both surface) and light trapped into the thin film (only for the quasi random grating surface).

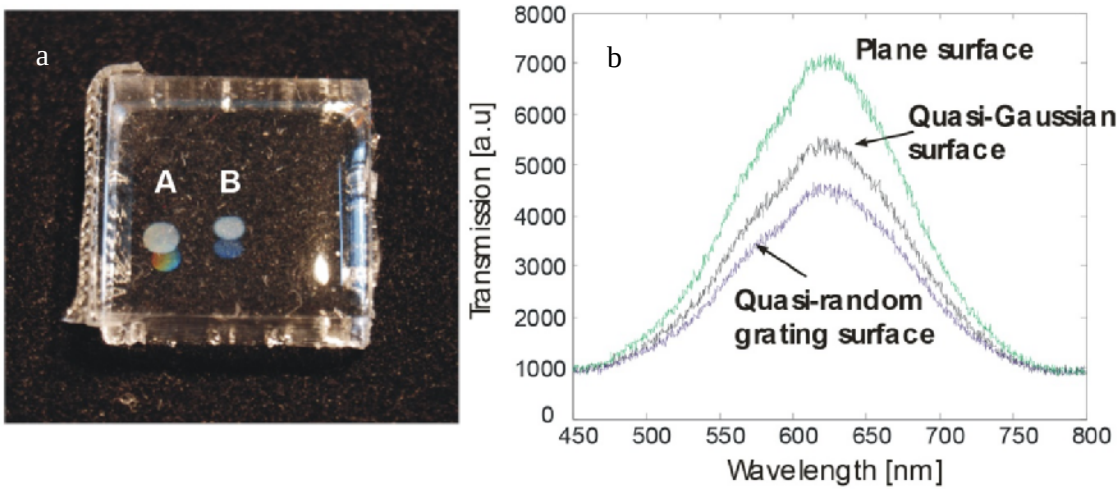

Fig. III.2-6 : a) Replica modeling of the surface pattern of the azopolymer 1 and azopolymer 2 on an elastomeric material A and B respectively (A is the quasi-random grating surface). b) Transmission spectrum of the elastomeric surface with quasi-random gratings, a Gaussian surface and comparison with the reference plane surface.

Consequently, here light extinction has to been understood in the more general concept of light harvesting. Therefore, from the measurement we can say that the quasi-random grating surface is 20 % more efficient, for light harvesting, than the quasi Gaussian surface. This effect is due to the random gratings associated with honey-comb structures inside the small gratings. We are similar or quasi better than the obtained results with photonics crystal. Let's stress out again that in the quasi random grating structure, we combine the role of random surface with the one of multi gratings to observe a large concentration of energy in higher orders, approaching the Lambertian limit. This replicated patterned surface can generate a good light trap.

III.2.5. Conclusion

We have presented a simple and cost effective way to prepare a quasi Gaussian surface and a quasi random grating surface using a self-photoinduced process on two chiral azopolymer thin films. The quasi random grating surface has the same advantages as the quasi Gaussian surface for light scattering but, as it was experimentally shown, additionally, it allows an induction of an isotropic mode coupling of light into the thin film, increasing its efficiency by 20% for light harvesting.

III.3. Introduction

Considering the importance of surface modification and the numerous applications of azopolymer thin films, this azopolymer and its relating compounds have been the subject of studies for investigating the surface deformation through laser illumination. However, the method chosen to create the initial patterns on the surface of azopolymerthin film here is solvent-droplet-induced dewetting.

Here, we experimentally showed a simple bottom-up approach to produce doughnut shaped nanostructures on the surface of azopolymer thin films by the choice of solvent-droplet-induced-dewetting method and incoherent unpolarized light illumination. Also, Due to the presence of highly photoactive azobenzene derivative in the material, illumination of these nanostructures by a polarized laser light shows the possibility of further growth and reshaping of structures.

III.3.1. Dewetting

Thin films were prepared by dissolving azopolymer in THF (50 mg in 1 ml of THF) and spin-coated on a pre-cleaned glass substrate. Prepared films were let in oven overnight at 80ºC to remove any residual solvent and also for obtaining films whose surface morphology appears featureless or is not dominated by pinholes and other surface defects. A 0.3 ml droplet of selected solvents was dropped on the thin film surface.

We tested all common solvents mentioned in chapter 2 (Table.II-2) such as hexane, cyclohexane, toluene, chloroform, dichloromethane, dimethyl sulfoxide (DMSO), 1-4 dioxane and aceton.

Upon contact with solvent droplet, the glass transition temperature of the polymer decreases below the room temperature due to absorption of the solvent into the polymer matrix, increasing the free volume of the polymer and resulting in an enhancement of the polymer molecule mobility. These molecules are now able to reorganize freely which in turn leads to the rupture and dewetting of the thin film (hole formation). For solvents with high solubility of azopolymer, penetration of solvent in polymer matrix is high, and the resulted mobility and movement of polymeric chains result in a chaotic structure, after the evaporation of the solvent droplet, as can be seen in Figs.III.3-1a-d.

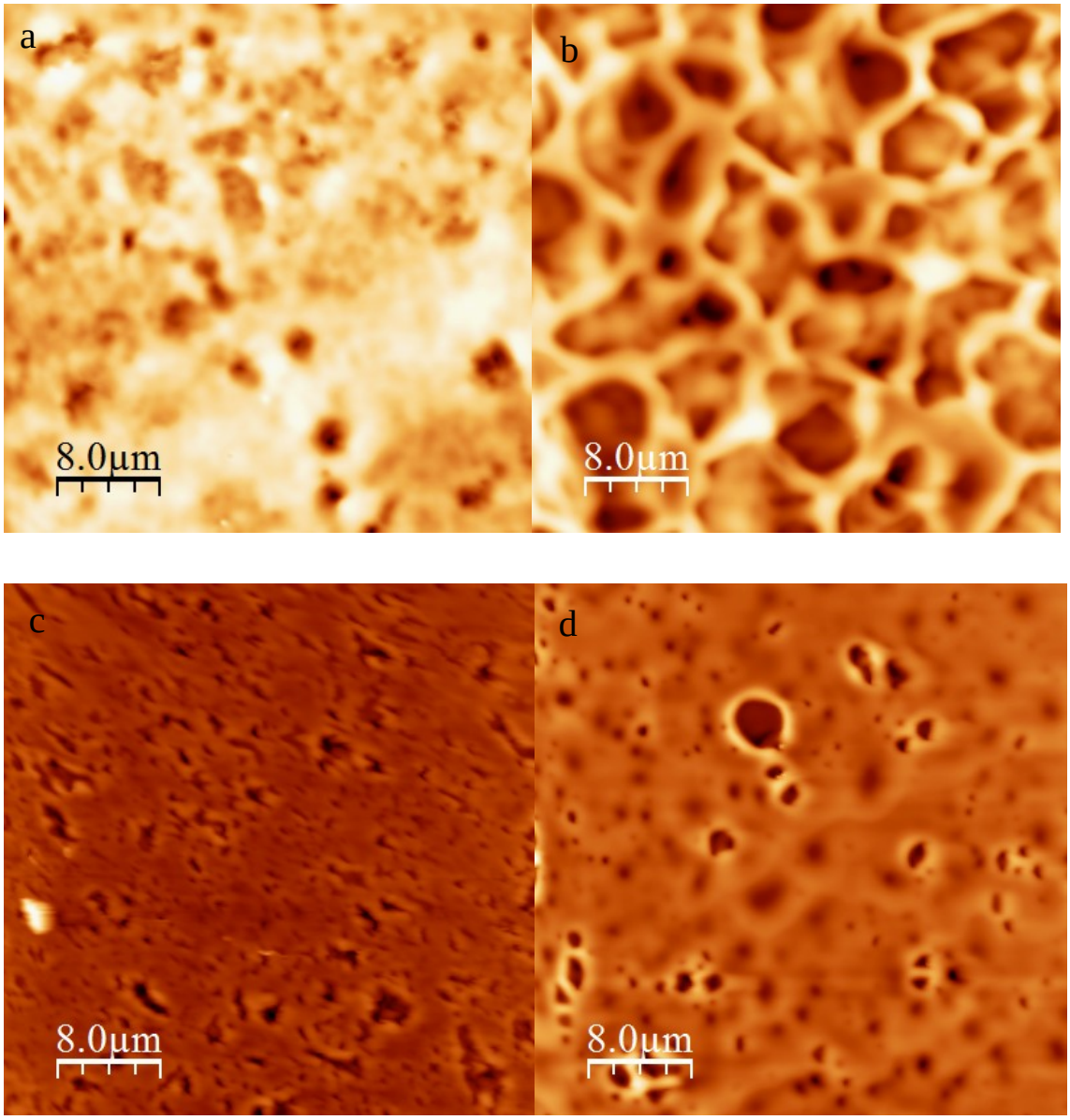

Fig. III.3-1 : a) Dewetted surface of the azo polymer film via Ethyl amin, b) 2-Propanol, c) Butanol, d) Chloroform

III.3.2. Solvent Droplet Induced Dewetting via the Selected Solvent

Based on the purpose of the study and the need for a controlled structure, finally n-Heptan was chosen for the optimal pattern on the surface in term of available structures. In a first experiment, a 0.3 µl droplet of the selected solvent (n-Heptan) was dropped off on the surface of the azopolymer thin film. A droplet of this volume covers an area of approximately 50mm^2

on the surface. n-Heptan has a medium boiling point of 98˚C and an evaporation rate of 2.80 (Butyl acetat:1). Owing to the low solubility of azopolymer in the solvent (n-Heptan), dewetted films appear completely flat and undisturbed to the naked eye and does not exhibit any changes in the absorption spectra (Fig.III.3-2).

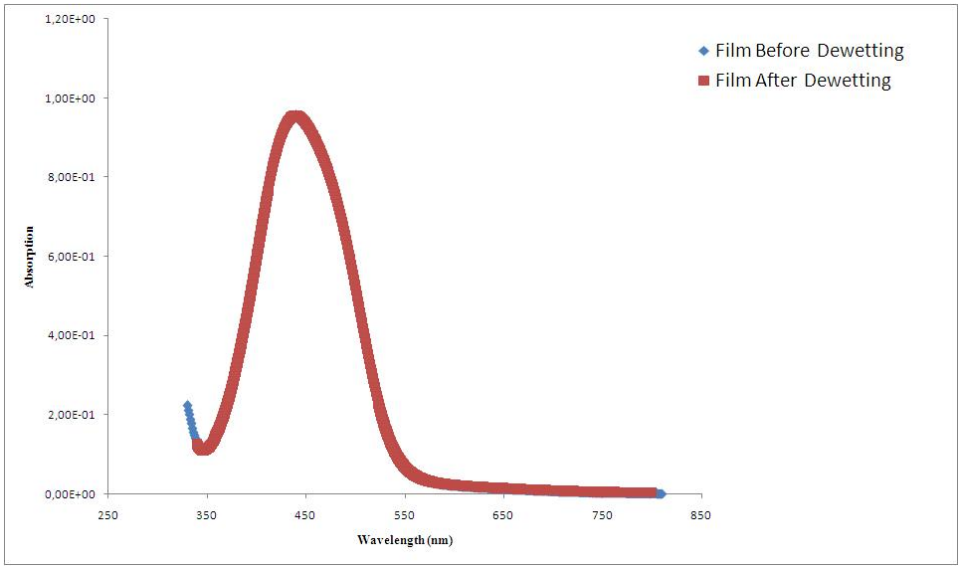

Fig. III.3-2 : Absorption spectra of azopolymer film before and after dewetting

A small quantity of solvent entering in the azopolymer thin film is not sufficient to induce enough chain mobility. The glassy state is maintained and because the polymer is neither removed nor evaporated, the dissolved polymer can only be redistributed. The hole formation is due to migration of the polymer from the center of the hole to the perimeter during solvent evaporation. The thin film topography was studied with an atomic-force microscope (AFM, Veeco Instruments Inc) in the contact mode (Fig.III.3-3a,b)

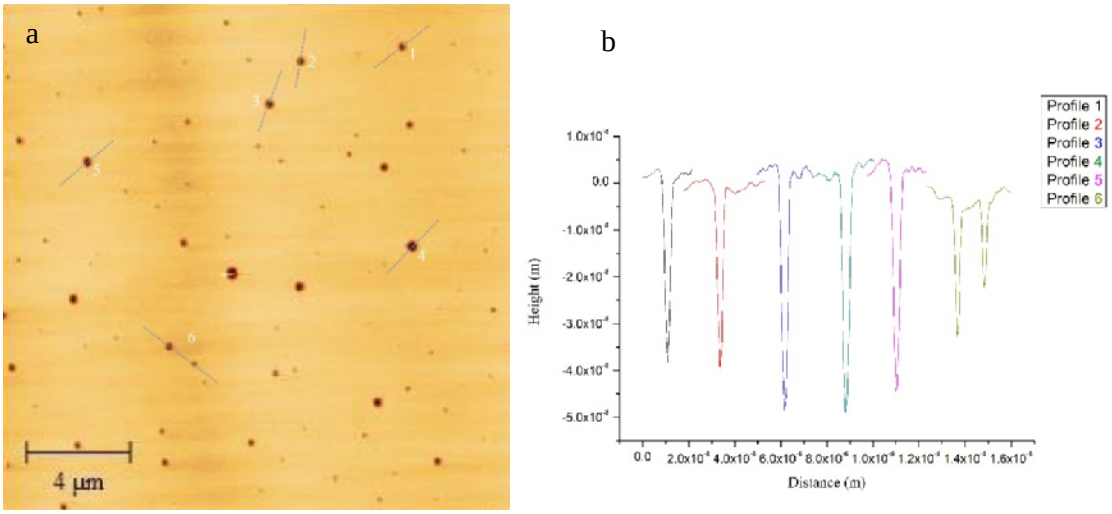

Fig. III.3-3 : a) typical topographyof azopolymer film dewetted with n-Heptan, b) corresponding height cross-section shown by the lines

The location of holes appears randomly but can be controlled with initial changes of the film topography or by dewetting on already prepared patterned surfaces as we demonstrate later.

The mean length scale of the period between nearest nano-holes created by solvent-droplet-induced dewetting on the surface of azopolymer thin film was calculated via statistical processing of obtained AFM image (Fig.III.3-5a). We found an average value λ_f of 2.5 ± 0.1 µm (Fig.III.3-4) which is in good agreement with the theoretical results of 2.17 µm, given by Eq.III-4:

$$l_f = \left(\frac{M_e \gamma_s}{|S|}\right)^{1/3} \frac{h_0^{7/6}}{M^{1/2}} \qquad \text{(III-4)}$$

With M is the PMMA polymer weight, h_o the film thickness (600nm), M_e the molecular weight between entanglements (7000 Da), |S| the spreading coefficient (70 MPa) and γ_s the PMMA surface tension (42 mJ/m^2). We consider in the calculation that PMMA has the largest matrix of material so the material was considered as pure PMMA in a simple model.

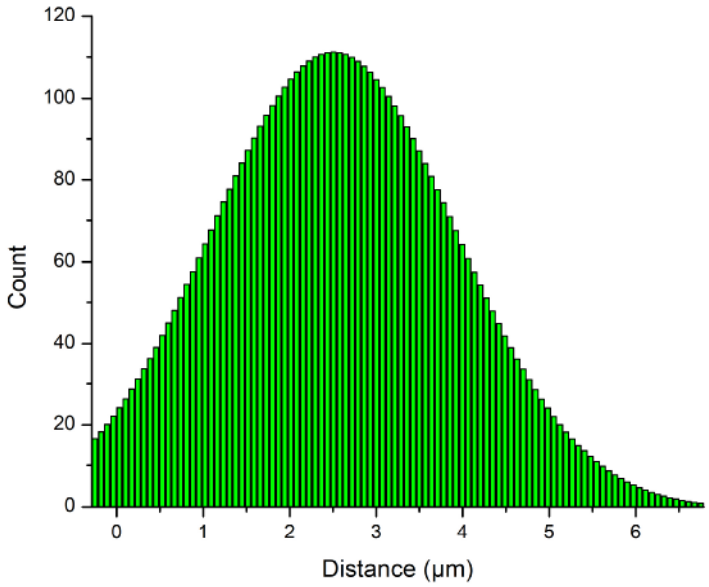

Fig. III.3-4 : Distribution of the distance between nearest neighboring nano-holes

III.3.3. White Light Illumination of Surface Structures

Multiple *trans*−*cis*−*trans*photo-isomerization cycles of chromophores in azopolymer induce a mechanical stress and deformations. Studies have recently showed that a well-organized pattern on the surface of an azopolymer film can be formed by the use of an incoherent light source. Incoherent light can indifferently propel the photo-patterning process, in comparison with a laser illumination. Using this technique, it is possible to modify the holes and their surrounding areas formed on the surface evenly and to induce a polymer growth due to a mass transport.

The incoherent white light, from a xenon lamp (Hamamtsu, C2177-01) with the effective power of 180 mW/cm^2, was used as an initiating source for a photo-induced mass transport in the film (White light setup – Chapter.II). To prove the ability of photo-induced nanostructuring, a detailed AFM scan of the film, before and after illumination, was done. Numerous randomly placed doughnut shaped nanostructures were clearly distinguished on the

film. AFM images show exclusively doughnut shaped nanostructures with diameters varying from 150 nm to 500 nm. Using this typical film topography one can benefit from this variation of diameters in any possible applications requiring a simultaneous utilization of similar nano-objects with different sizes and depths (Fig.III.3-5).

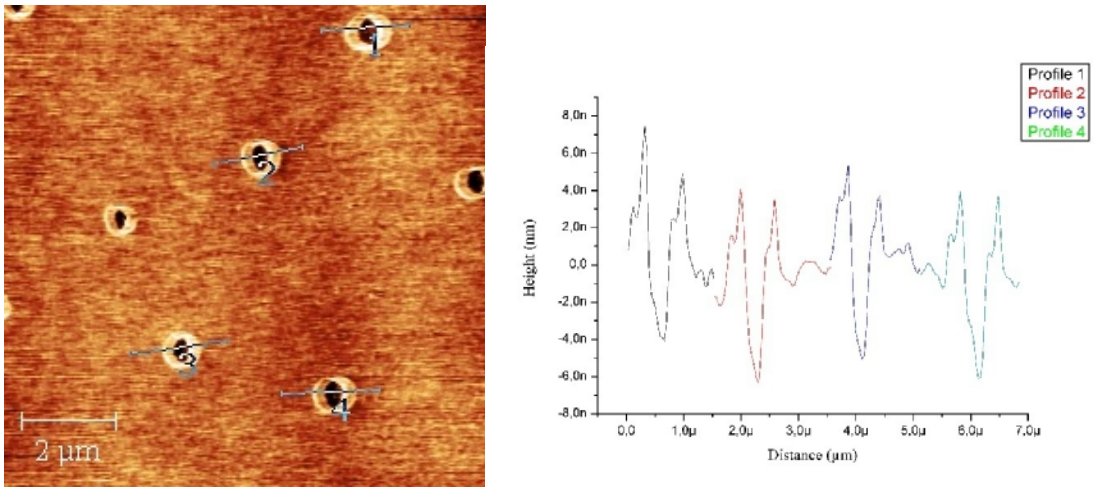

Fig. III.3-5 : a) Topographical images of the azopolymer film after the white light illumination, b) corresponding height cross-section shown by the lines

The illumination time for the sample was 30 min. During this time the force (F) needed to exert an elastic deformation on the nano-object is derived from the Hertz theory (Eq.III-5), which considers the contact deformation of elastic spheres under normal loads in absence of adhesion and fraction:

$$F = \frac{4}{3} G D_0^{0.5} \Delta D^{1.5} \qquad \text{(III-5)}$$

Where, G is the elastic modulus of PMMA (1.8 - 3.1), $\Delta D = D_0 - D$, the deformation where D_0 and D are the initial and final radius of the structure, respectively. Considering the same 1 GPa low bound, an elastic force of 22 µN was acting on the holes to produce a nano-doughnut. The volume of the doughnuts after illumination grows to reach as average amount of 0.134

μm^3, which results from a growth rate of 0.0032 μm^3, considering the 30 minutes of illumination time to reach the saturation point.

The average distance between the nearest nano-doughnuts is of 2.5 µm and is greater than their own diameters. This feature of the film makes it possible to work with nano-doughnuts in applications as isolated objects.

III.3.4. Polarized Light Illumination of Surface Structures

Beside the wide range of possible geometrical sizes during fabrication, azopolymernano-doughnuts exhibit a property of flexible reshaping under illumination.

To irradiate by a polarized light, the samples were placed in a single beam setup (single beam setup - Chapter II). A quarter/half wave plate was used to control and change the polarization and direction of the polarization of the laser beam.

The average diameter of the doughnuts is determined from peak-to-peak distances. A detailed analysis (using software WSxM and origin) shows that the average diameter of the photoinduced doughnuts is typically 350 ± 50 nm. The distribution of holes depths on the surface after dewetting seems almost constant (30 ± 10 nm).

The initial surface modification with holes acts as a mask for the photofluidization of these nanostructures. The optical manipulation of polymer structures was done by varying the polarization and irradiation time, allowing an exceptional control of structural features.

Samples were set perpendicular to the incident laser and illuminated by different polarizations (vertical, horizontal and circular polarizations) for a defined amount of time. It is seen that the initial symmetry of the nano-doughnut changes with illumination, depending on the direction of polarization and duration of irradiation.

III.3.4.1. Linear Polarization (Horizontal polarization)

When the initial symmetrical doughnuts are irradiated with a linearly polarized light (horizontal polarization), the symmetry of these structures is modified. Nano-doughnuts shapes are changed into two semi-rings with a central hole (Fig.III.3-6).

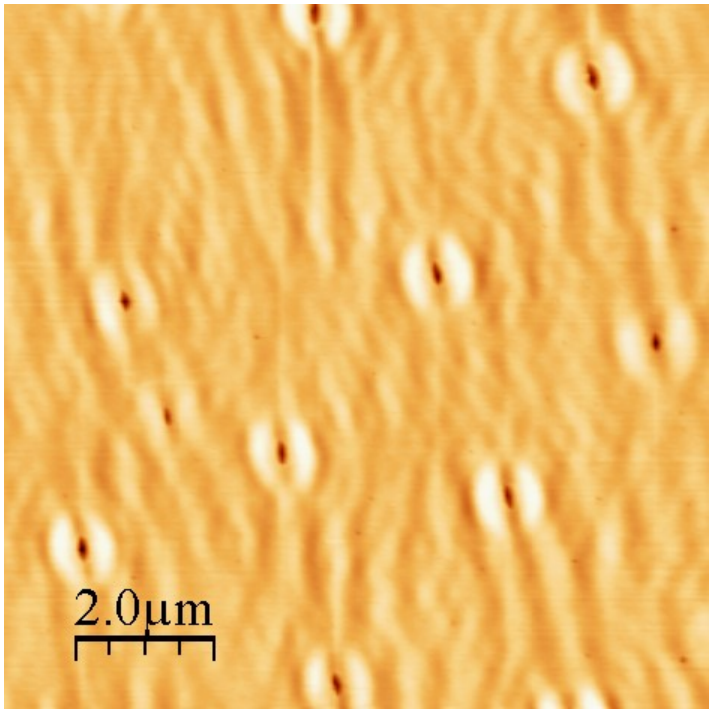

Fig. III.3-6 : Topographical images of the azopolymer film after the laser illumination (Horizontal polarization)

Under illumination the *cis-trans*photo-isomerization cycle of azopolymers gives rise to a light induced mass transport parallel to the light polarization. The molecules under irradiation are aligned perpendicularly to the incident polarization. This effect unravels the rim around the central hole. The variation of the two axial components (x or y) is not similar. The molecules along the x-axis move along the polarization direction, while the two semi-rings perpendicular to the polarization's direction build up. As a result, two poles of the doughnuts rim are voided and the two semi circles grew (Fig.III.3-7).

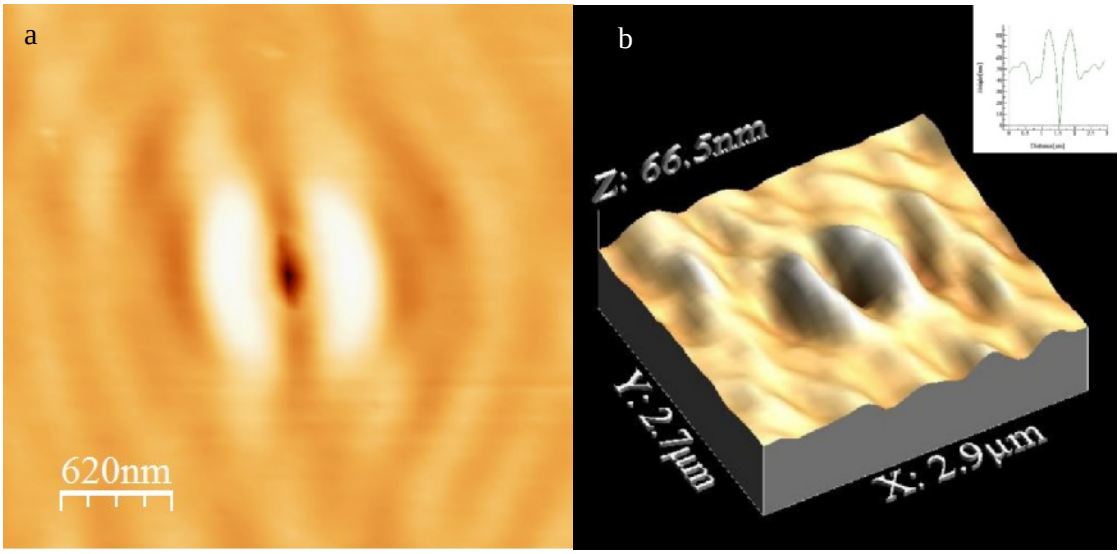

Fig. III.3-7 : a) Typical large scale topography obtained by AFM, b) Three-dimensional AFM image of nanostructures formed on surface of azopolymer film under laser radiation and corresponding height cross-section.

Such structures resemble a nano-cavity made with two semi-circular mirrors. An interesting application could be the possibility of creating cavities with nano-particles embedded in the center or be used to aggregate nano-particles along the rim.

When the illuminating time is increased (up to 10 min), changes in the shapes are even more severe. The rectangular shape of the initial nano-doughnut reaches an average length of 850 nm and a width of 450 nm (Fig.III.3-8a-c). These structures are current subject of interest in the field of surface plasmon behavior with rectangular hole arrays.

a

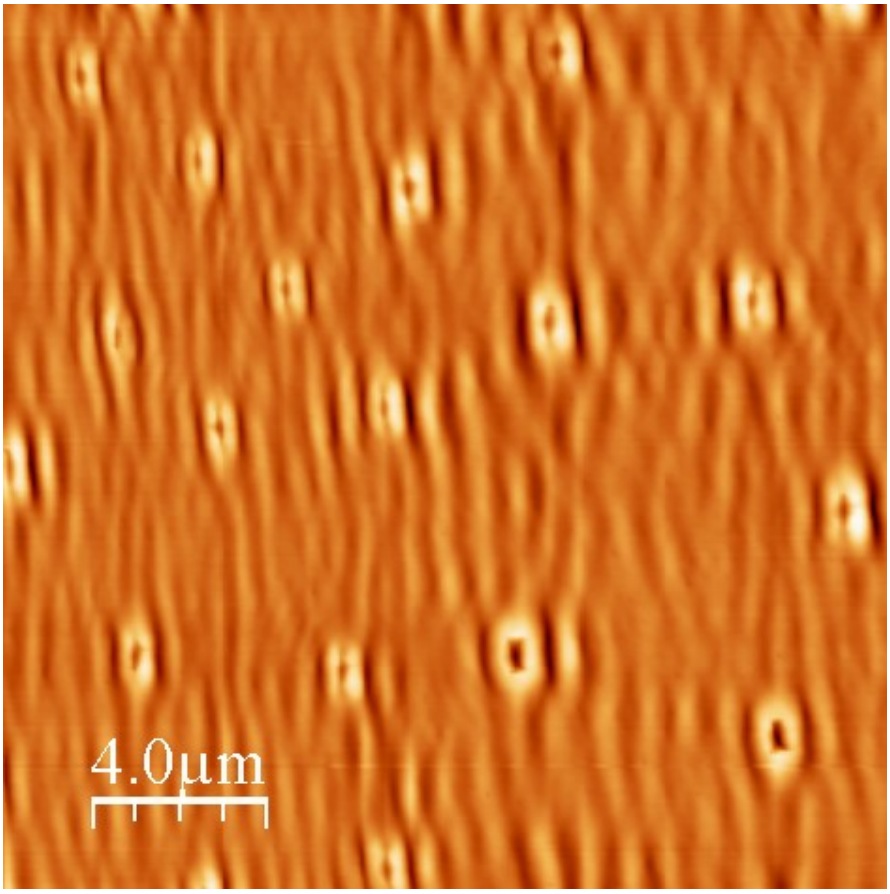

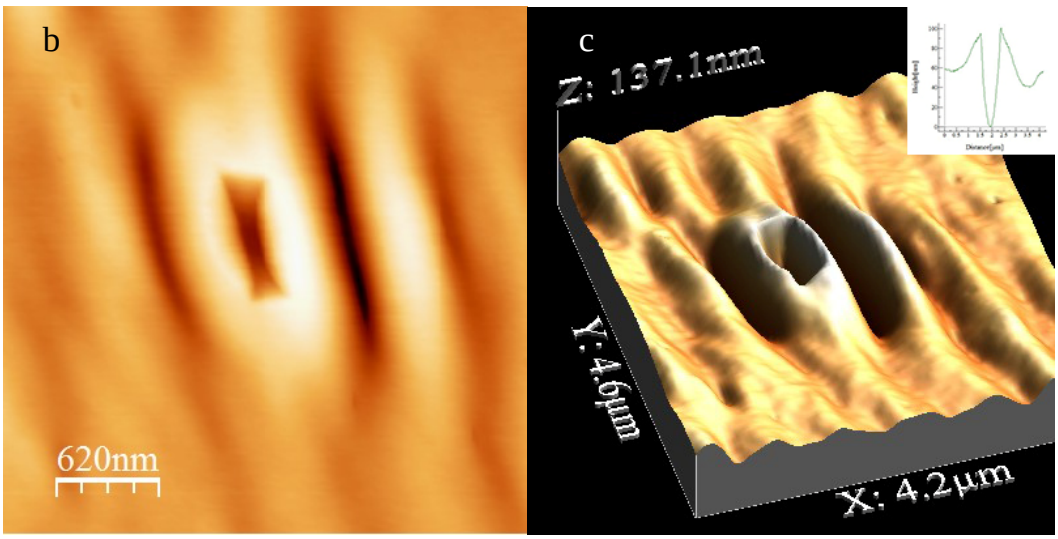

Fig. III.3-8 : a) Topographical images of the azopolymer film after the laser illumination (Horizontal polarization) up to 10mins, b) Typical large scale topography obtained by AFM, c) Three-dimensional AFM image of nanostructures formed on surface of azopolymer film under laser radiation and corresponding height cross-section.

A further increasing of the irradiation time results in surface relief grating (SRG) formation and the formed SRG overcomes the nanostructures on the surface.

III.3.4.2. Combination of Two Linear Polarizations (Horizontal and Vertical)

Interestingly, if we continue the photo-reconfiguration by illuminating the holes with a linearly polarized light, the changes also occur along the vertical direction as well as the lateral direction. So, a further irradiation with a vertically polarized light (vertical polarization) after an irradiation with a laterally polarized light (horizontal polarization) onto doughnuts leads to a transformation of a circular hole into a square hole with an average diameter of 450 – 500 nm, as shown in the Fig.III.3-9a-c.

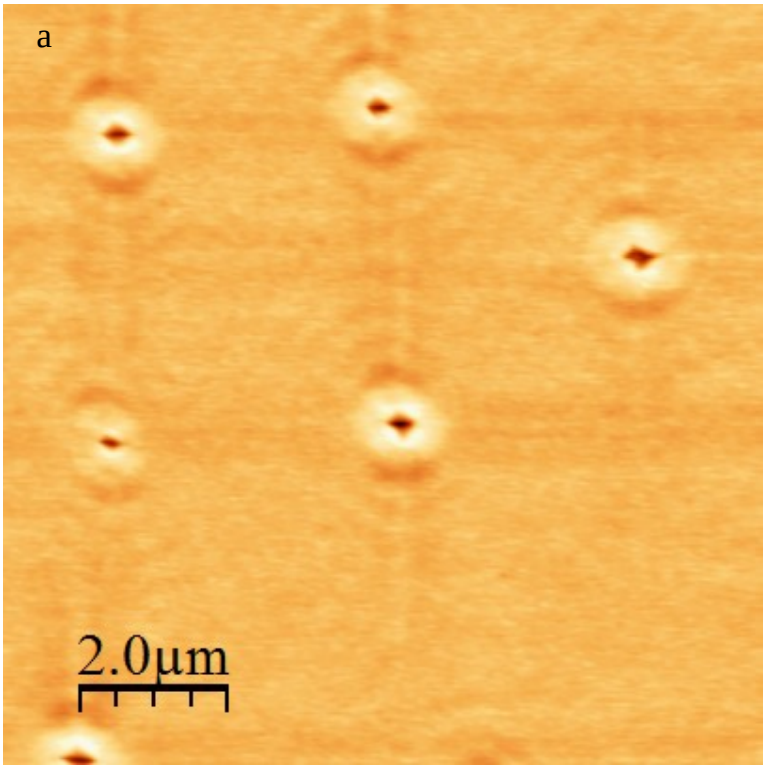

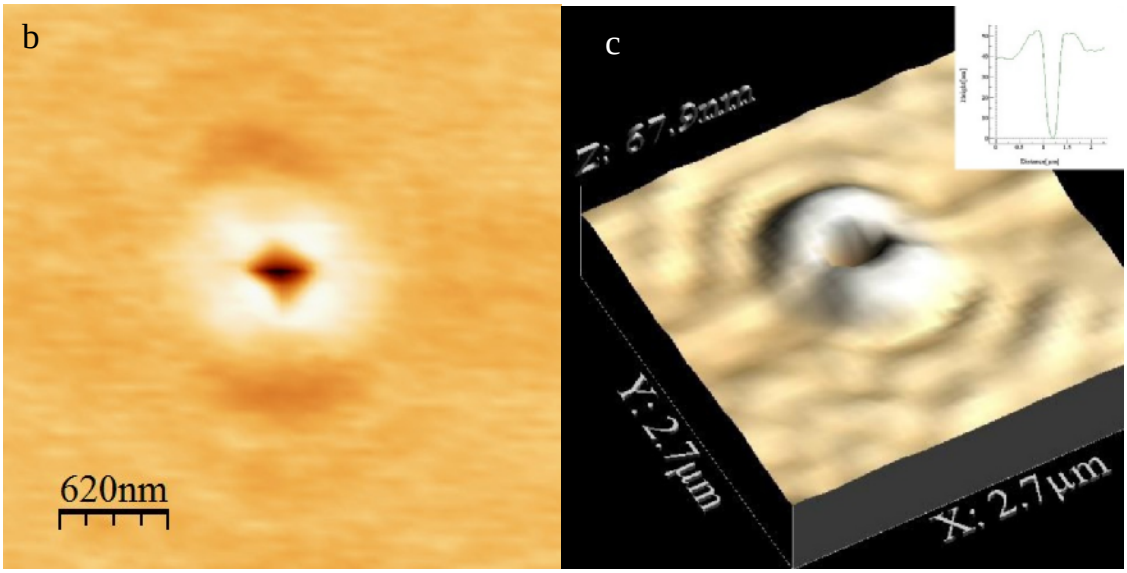

Fig. III.3-9 : a) Topographical images of the azopolymer film after the laser illumination (Horizontal nad vertical polarization), b) Typical large scale topography obtained by AFM, c) Three-dimensional AFM image of nanostructures formed on surface of Azopolymer film under laser radiation and corresponding height cross-section.

III.3.4.3. Circular Polarization

Moreover, changing the polarization of the incident light to circular polarization, via a quarter wave plate, leads to growth nano-doughnuts. The average height of nano-doughnuts are about 15 nm, but measurements on structures created via circular polarization of light shows that the typical depth of these structures range between 40 – 110 nm. The measured heights for rims of these objects above the film surface vary from 15 – 25 nm. All the informations mentioned above lead to the classification of these structures as nano-well (Fig.III.3-10a-c).

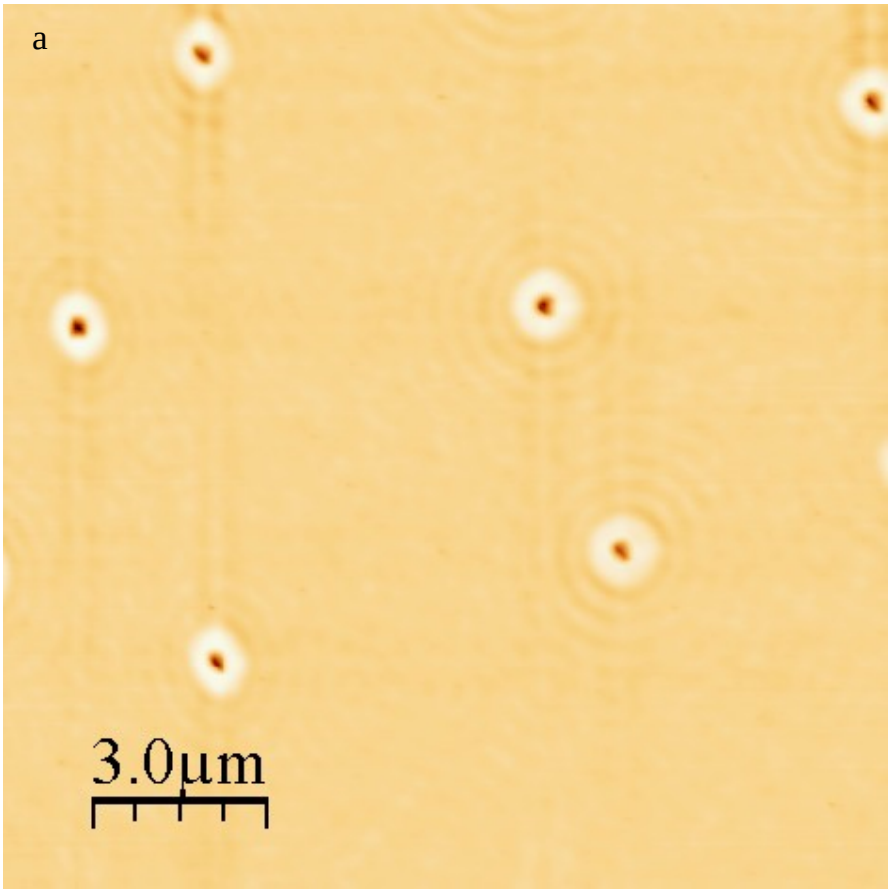

Fig III.3-10 : a) Topographical images of the azopolymer film after the laser illumination (Circular polarization), b) Typical large scale topography obtained by AFM, c) Three-dimensional AFM image of nanostructures formed on surface of Azopolymer film under laser radiation and corresponding height cross-section.

Detailed analysis show that, not only the structures change their shapes during illumination, but also due the mass transport of the azopolymer a change in diameter and depth is also observed. The average diameter of the nanostructures varies in a range from 215 nm to 320 nm. Furthermore, the average depth of the initial structures formed after white light illumination grows from 12 nm to an average amount of 35 nm (Fig.III.3-11a-d).

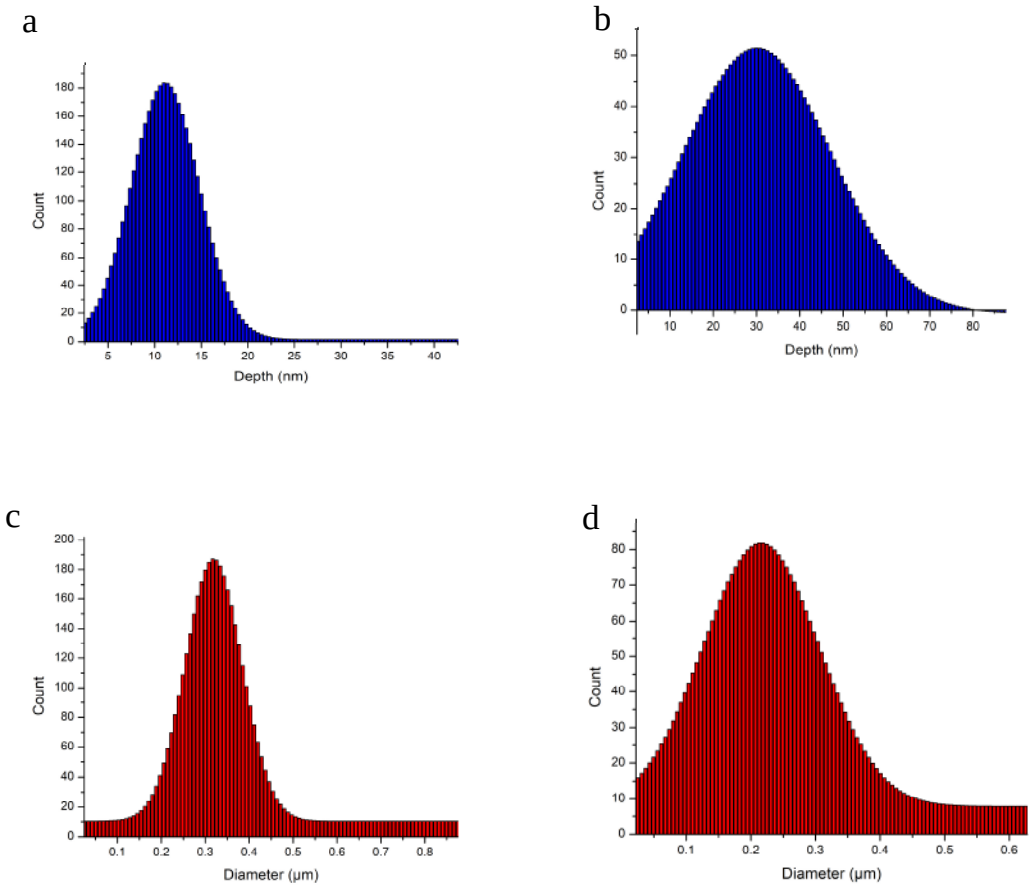

Fig. III.3-11 : Distribution of depth, of nano-structures a) before and b) after laser illumination, Distribution of diameter of nanostructures c) before and d) after laser irradiation

The study reveals a facile way to produce easily reproducible and controllable surface structures. Moreover, the great possibility of using light to dynamically photo-induce a

mechanical change of the azopolymer structures presents a significant advantage as functional materials.

Changing the irradiation wavelength in the azopolymer absorption band or far from it can switch the behavior of doughnut-shaped nanostructures and leads to a flexibility of reshaping initial surface modifications to stable transparent nano-objects, thus covering a wide range of opportunity of applications. Such nanostructures are of great interest in application fields of sensors, nano-plasmonics, plasmonic solar cells, nanoparticle trapping, photochemistry, nano-rectors etc. Also, Smart nano-doughnuts with controlled volumes can be exploited as chemical reactors for photo-catalytic and enzyme reaction. Conveniently, all the surface modifications can be reversibly changed to come back to the initial state by heating the sample above the glass transition temperature.

III.3.5. Controlled Dewetting

As mentioned, dewetting provides a simple, powerful technique for patterning nanoparticles, small molecules, and polymers. Due to the complexity of the dewetting process it seems impossible to control well-defined hole/droplet formation. However, by using a pre-patterned substrate, we are able to direct ordered hole formation during the dewetting process.

Unlike the previous research on controlled dewetting, in which the substrates were patterned through conventional lithography, microcontact printing (μCP) and vapor deposition methods, azopolymer films can be patterned readily via an optical patterning.

In this stage, the azopolymer films were illuminated through a double beam exposure experiment. The sinusoidal light interference pattern at the sample surface leads to a sinusoidal surface patterning, i.e., a surface relief grating (SRG). We applied the solvent-droplet-induced-dewetting method to this surface expecting a modification of the surface in the place where the

solvent is confined. The surface is then illuminated with a white light to produce a change of the initial surface pattern. The result is visible in the Fig.III.3-12a where the nano-doughnuts are arranged on the edge of the stripe at regular distances decorating the grating with sub-structures. We point out that the sizes of the nanostructures are smaller than the previously obtained nanostructures on a flat surface, due to the limited space for growth and confinement of the solvent.

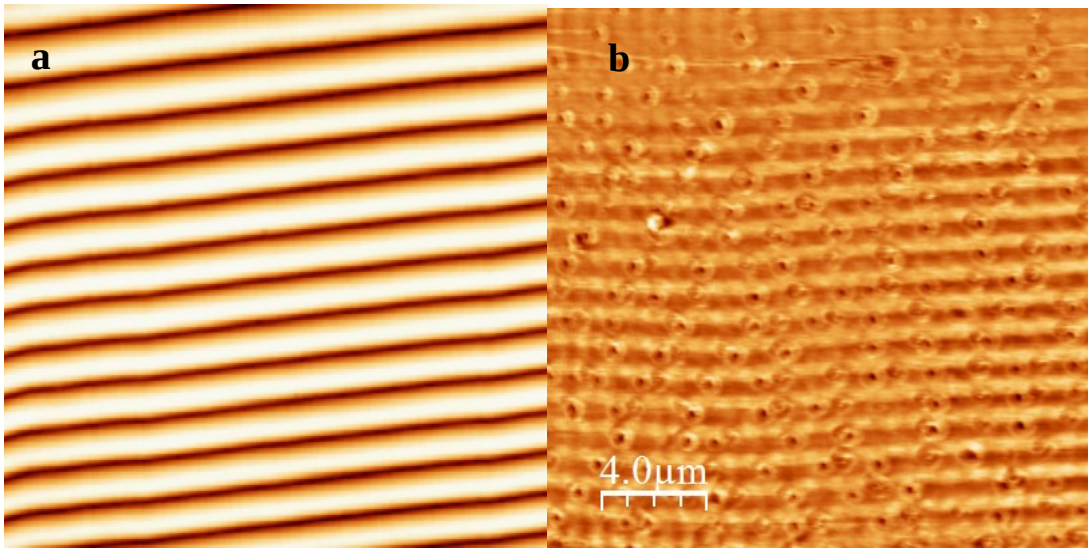

Fig III.3-12 : a) AFM image of a 1D grating,b) Dewetted structures on a 1D templated film

We continued in this direction, based on results demonstrating that azo compounds have proven to allow the inscription of multiple superimposed relief gratings providing more complex structures (Fig.III.3-13c). These gratings were considered as the template for a further dewetting process. The solvent droplet follows the pattern of the film in the regular nano-cavities. On these regularly patterned SRGs, we observed a spontaneous alignment of holes at the center of the trenches (Fig.III.3-13d). Applying solvent on the two superimposed 1D gratings leads to the formation of a 2D array of ordered holes transformed in nano-doughnuts on the surface of the film.

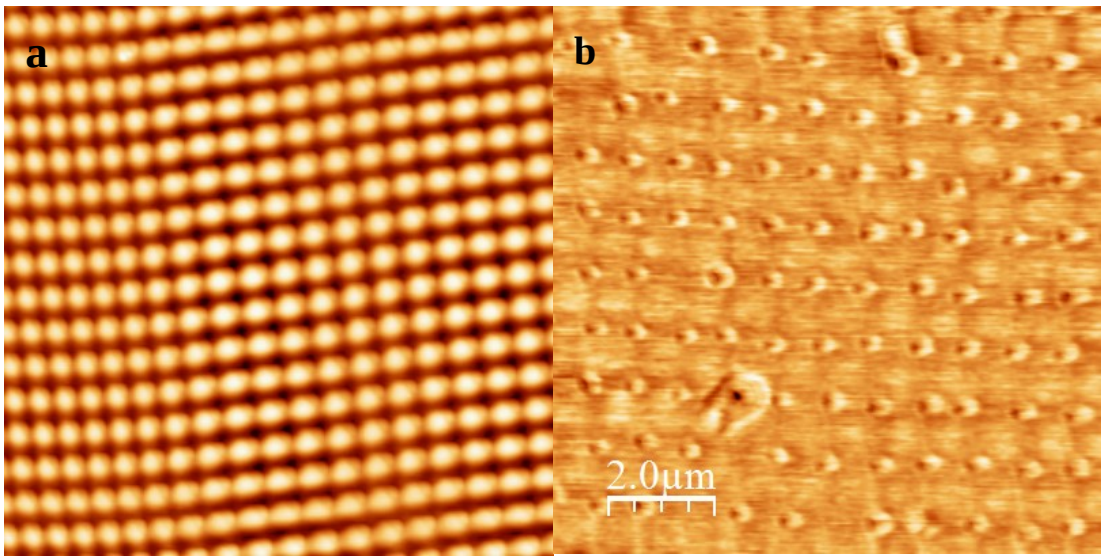

Fig III.3-13 : a) AFM image of a 2D gratings,b) Dewetted structures on a 2D templated film

III.3.6. Conclusion

We have demonstrated a route to fabricate the ordered nano-patterns from dewetting. These results present an exciting opportunity for manipulating structures and properties of an azopolymer thin film on nanometer scale. The technique chosen for this purpose is dewetting of azopolymer thin film via a solvent-droplet induced method. The produced nanostructures can be classified as nano-doughnuts, consisting of a hole and a surrounding ring. Furthermore, due to the presence of highly photoactive azobenzene derivative in the material, illumination of these nanostructures by a polarized laser light shows the possibility of a further growth and reshaping.

III.4. Introduction

As mentioned in Chapter I, Polymeric particles are used in a diverse array of applications. In this regard, particle shape is a critical parameter that can significantly influence particle function. However, due to difficulties in fabrication of polymeric particles with controlled shapes, this parameter has not been fully explored.

Here, a new and excited group of colloidal azopolymer particles, composed of PMMA and azopolymer with specific ratio, were synthesized (Chapter.II). For different ratios of PMMA and azopolymer, the particles obtained by the same procedure show different phase-separated structures.

III.4.1. Characterization of new Azo particles

Characterization of the particles was done using a scanning electronic microscope, SEM - JOEL 6301F, which was operated with an accelerating voltage of 3 kV. The morphology of the polymeric particles synthesized by emulsion polymerization is spherical, since the interfacial tension between particles and surrounding medium can be minimized due to the spherical shape. However, the newly synthesized azospheres resemble a buckyball or a soccer ball (Fig.III.4-1). But rather than being hollow they consist of a PMMA core surrounded by fragments of azopolymer.

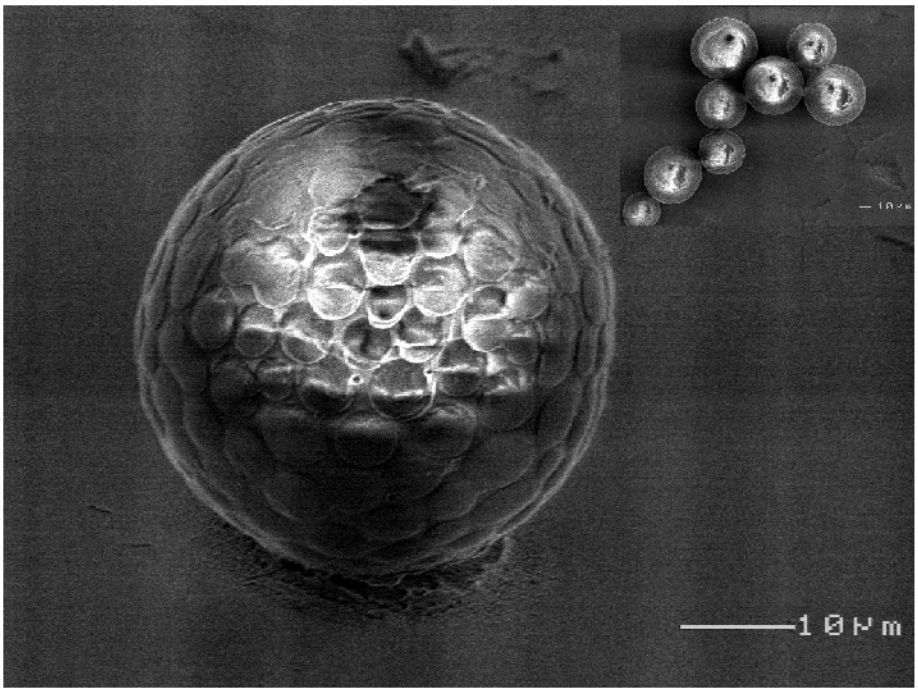

Fig. III.4-1 : SEM images of the new buckyballazopolymer particles

Based on the analysis from the SEM images, the average size of the spheres covers a wide range from 16 to 90 µm. The average diameter of the spheres used in this study is 35 µm (Fig.III.4-2).

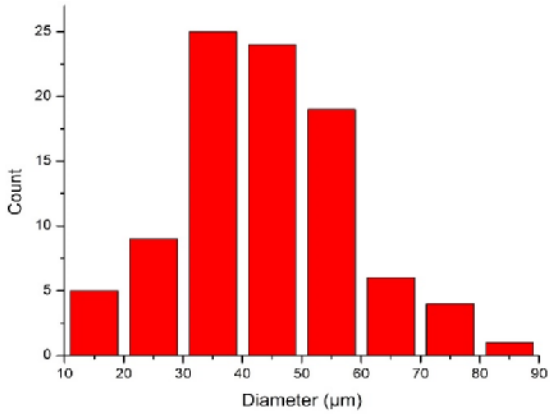

Fig. III.4-2 : Diameter distribution of the azo spheres

Fragments of azo polymer covering the core are circular in shape, which given the fact that they cover a spherical core, can't coat the whole surface, thus it possesses some porosity. Porosity or void fraction is a measure of the void (i.e. "empty") spaces in a material, and is a fraction of the volume of voids over the total volume, between 0 and 1, or as a percentage between 0 and 100%.

$$P = \frac{V_{void}}{V_{total}} \times 100 \qquad \text{(III-6)}$$

Based on measurement from the images, the fragments cover about 83±4% of the surface, meaning the surfaces of the spheres possess an average 17±4% porosity.

III.4.2. Laser irradiation of azo particles

Due to directional photofluidization of azoplymers, compartmentalized layer of azopolymer can be light manipulated to obtain unique shapes, which can hardly be obtained by other methods. To investigate this possibility, the azospheres were subjected to laser irradiation.

III.4.2.1. Laser irradiation of azo particles via linear polarization

Upon laser illumination by a linear polarization, cis_trans photoisomerzation occur at each fragment of azopolymer on the surface of the core PMMA. The photofluidazation of azopolymer as a consequence of this isoremazion results in a mass transport of azopolymers, in direction of the polarization of the laser. The photo-deformation occurs at each fragment of azopolymer surrounding the core PMMA, resulting in a very unique shape for the initial spheres. This deformation reaches a saturation point in 15 minutes. At the end of 15 minutes irradiation time, the final particles look like a porcupine (Sample1 - Fig.III.4-3a).

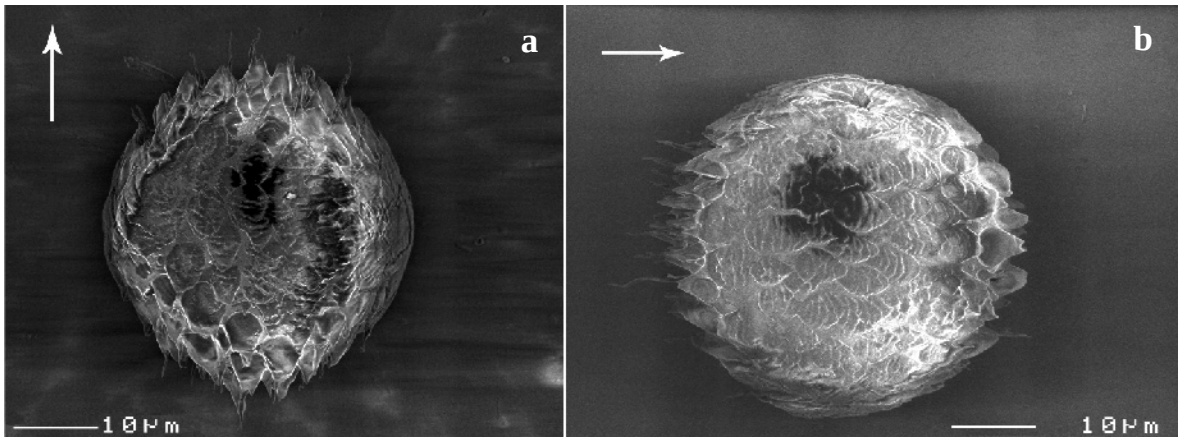

Fig. III.4-3 : a)Azopolymer particles after illumination with a vertically polarized laser light, b) Azopolymer particles after illumination with a horizontally polarized laser light

It seems as each fragment is in a struggle between its limitation to being bound to the core and its desire to move along the polarization's direction. Unable to break free of the core PMMA, the azopolymers in the fragments start stretching in the direction of polarization and become spikes.

As it has been pointed out frequently in the literature, photofluidazation of azopolymer is a polarization dependent phenomenon. To observe the validity of such dependency for these particles, direction of the polarization of laser beam was altered to vertical polarization, using a

half wave plate. The samples subjected to this polarization exhibit the same behavior, but in the vertical direction (Sample2 - Fig.III.4-3b). The flashes on the images indicate the direction of the polarization. Furthermore, mass transport of azos under laser irradiation, along with stretching of the azo fragments, result in inscription of gratings on the particles. Mean pitch value for these gratings is about 1.5±0.2μm.

The resulted porcupine particles are a set of new and exotic shaped particles, opening new doors for study of the phenomena of SRG formation and the basic understanding of the light-matter interaction.

III.4.2.2. Laser irradiation of azo particles via circular polarization

Following the further possibilities of surface deformations and new shapes using light, the polarization of the laser was changed to circular polarization, via a quarter wave plate. Initially spherical particles were illuminated by circular polarization for 15 minutes (Sample3). The final structure of the particles is shown in Fig.III.4-4. These particles resemble a sea pineapple. Under illumination with a circular polarization, there isn't any preferred direction of the movement for azoplymers. However, through the cis-trans isomerization and movement of the azopolymers, certain bump shapes are visible on the particles, which results in the particles resembling a seed or sea pineapple.

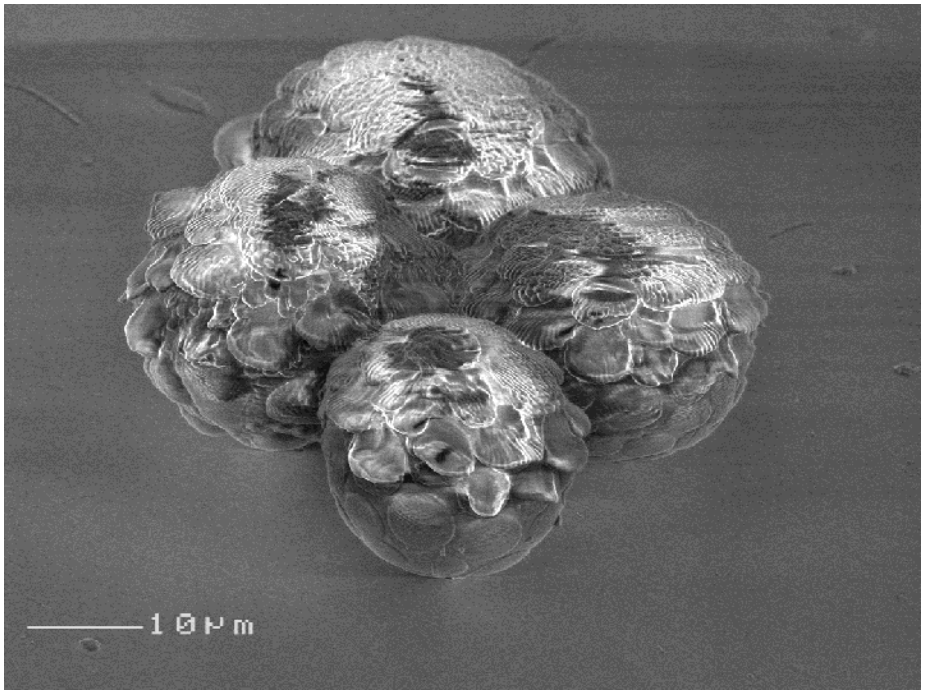

Fig. III.4-4 : Azopolymer particles after illumination with a circular polarized laser light

Such particles were recently synthesized through a complicated three step process. The seed or sea pineapple shaped particles have been used as templates for the synthesis of porous inorganic particles and production of dye-doped nanospheres.

Unlike the mentioned process, our particles, using laser illumination, were obtained faster and with less effort.

III.4.3. Double beam exposure of azo particles

As mentioned in literature countless times, inscription of gratings in the surface if azopolymer thin films are done not only by a single beam experiment, but also through an interference pattern of a double beam exposure. Following the tradition of SRG inscription, a sample of these azopolymer particles were subjected to an interference pattern (double beam setup – Chapter II). As can be seen from Fig.III.4-5a-c, upon exposure to the interference pattern, a grating is inscribed on fragments of azopolymer on the particles, during the first 5 minutes of

irradiation (Fig.III.4-5a). Continuing illuminating the sample up to 10 minutes, the grating on the fragments become more dominant and the movement and stretching of the azopolymers start (Fig.III.4-5b). After 15 minutes of irradiation, the particles are similar to the particles exposed to the single linearly polarized beam, spiked like a porcupine, with inscribed gratings on the fragments (Fig.III.4-5c).

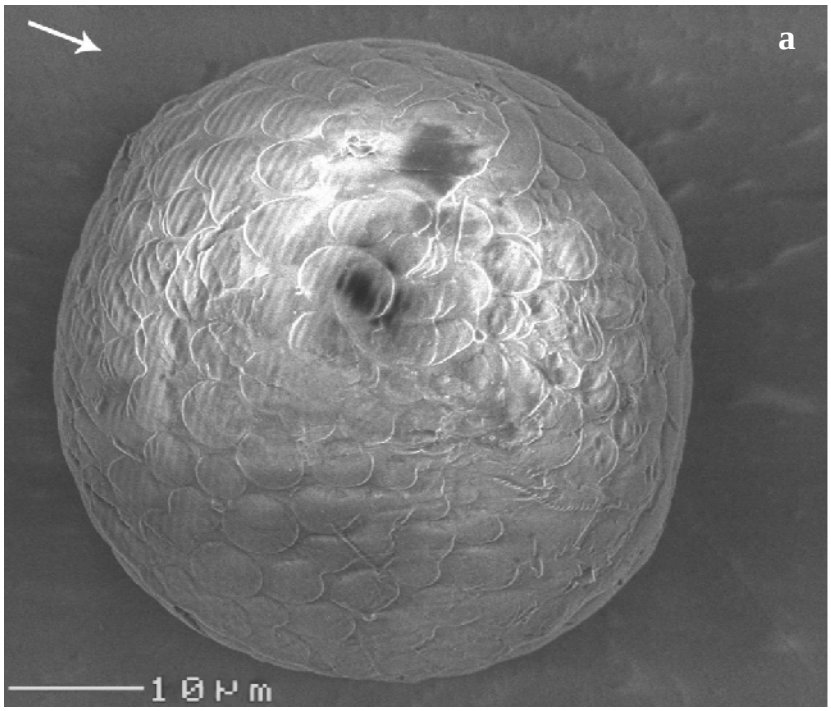

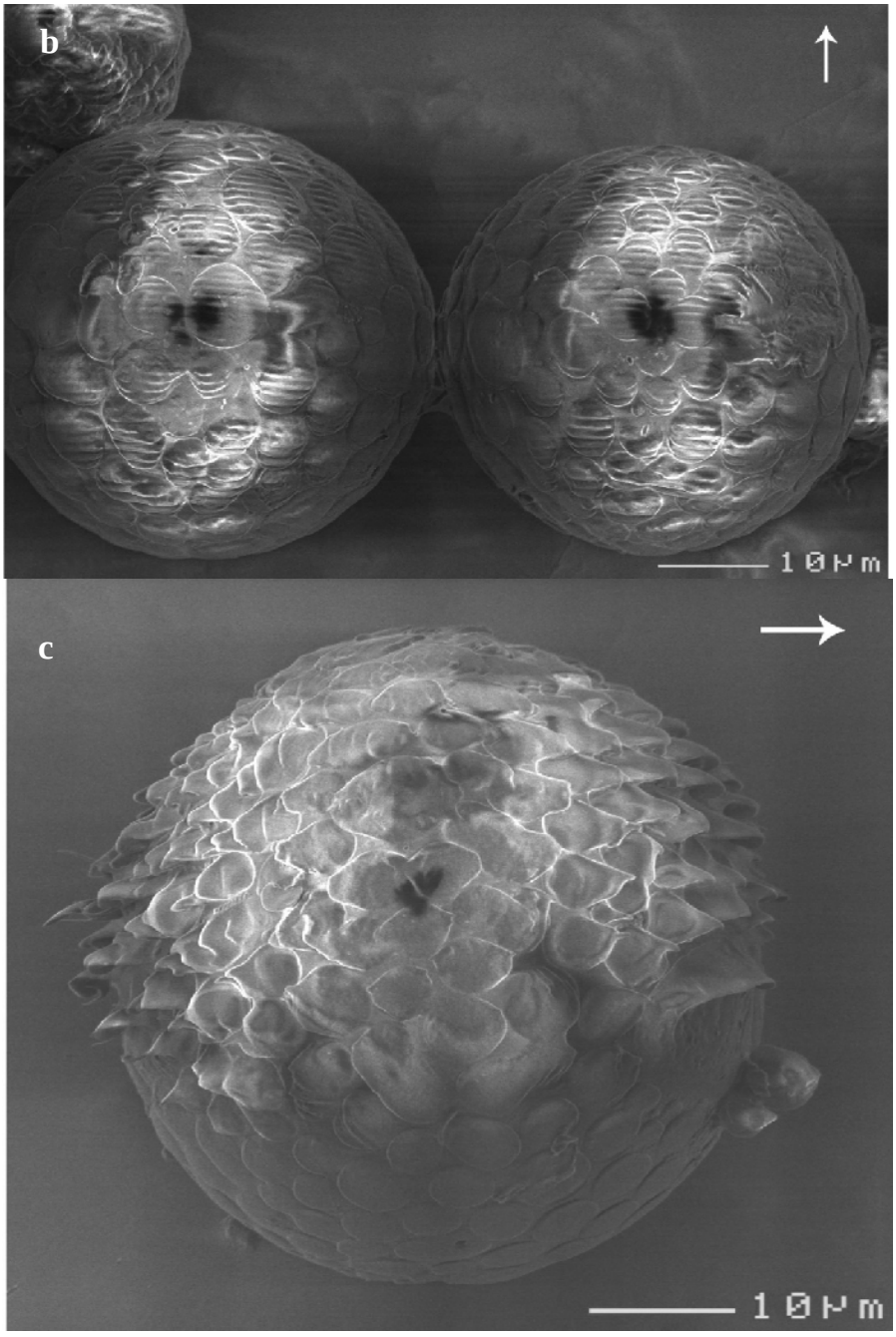

Fig. III.4-5 : a) Azopolymer particles after illumination with an interference pattern of laser light (5mins), b) Azopolymer particles after illumination with an interference pattern of laser light (10mins), c) continuing irradiation of particles for 15mins.

Pitch value for the gratings on these azo fragments are about 1.3±0.1µm, which is in agreement with the degree of the interference pattern (θ=10°). Studying the deformation process of

azopolymer fragments under single and double beam exposure is fascinating and could open a window and provide a new insight to the origin and mechanism of SRG gratings.

III.4.4. Reversibility of particles' shapes under irradiation

One of the biggest advantages of azo incorporated polymers has been their reversibility. For years researchers working with these compounds in SRG formation and photo deformation have been using methods such as circular polarization and unpolarized light to reverse the effects applied to the surface and redo the effects again and again. Given the fact that our particles are consist of a layer of azopolymer shell, there should be a degree of reversibility for the induced shapes on the particles.

To test this theory, one of the samples, already subjected to linear polarization (Sample1 - with porcupine particles, Fig.III.4-6a) were irradiated by a beam of circular polarization for 15 minutes. Due to the random directional movement of the azopolymers under such illumination, the spikes on the porcupine particles retreat and change the porcupine shape particles into sea pineapple particles (Fig.III.4-6b). Again; given the nature of the azopolymers, we should be able to reapply the changes on the particles through a directional polarization. Hence, the same sample (sample1), now with pineapple particles, was again irradiated with a horizontally linear polarized laser beam. Once more we witness the formation of porcupine particles as a result (Fig.III.4-6c). Again, the flashes on the images indicate the direction of the polarization of the laser beam.

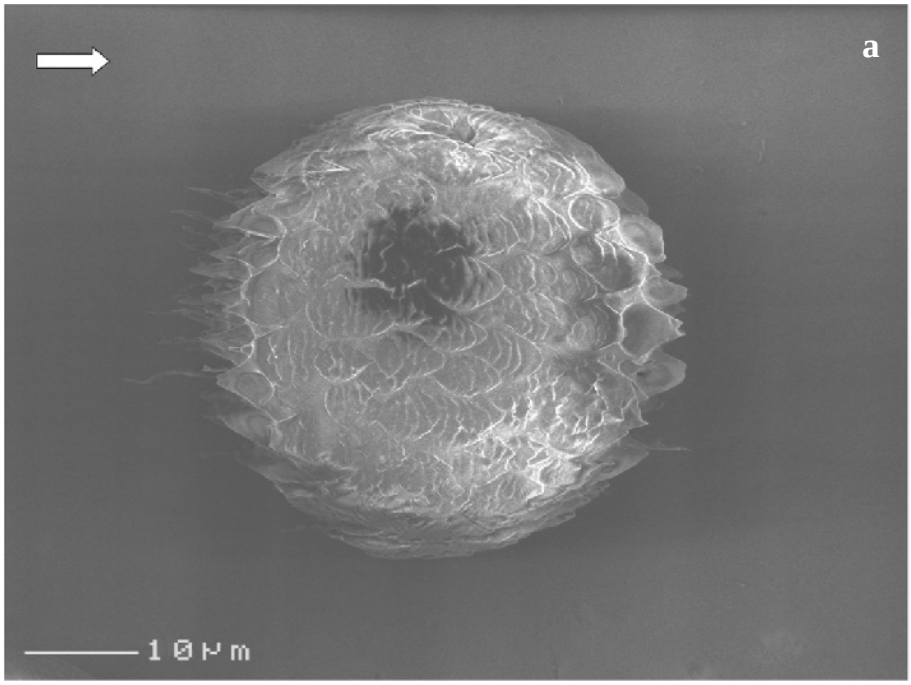
a
10μm

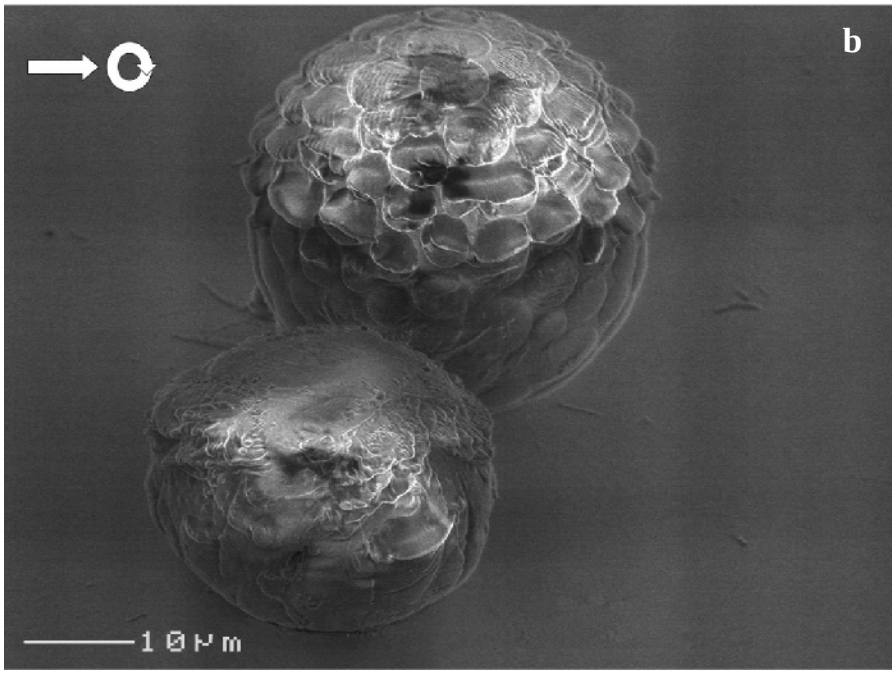
b
10μm

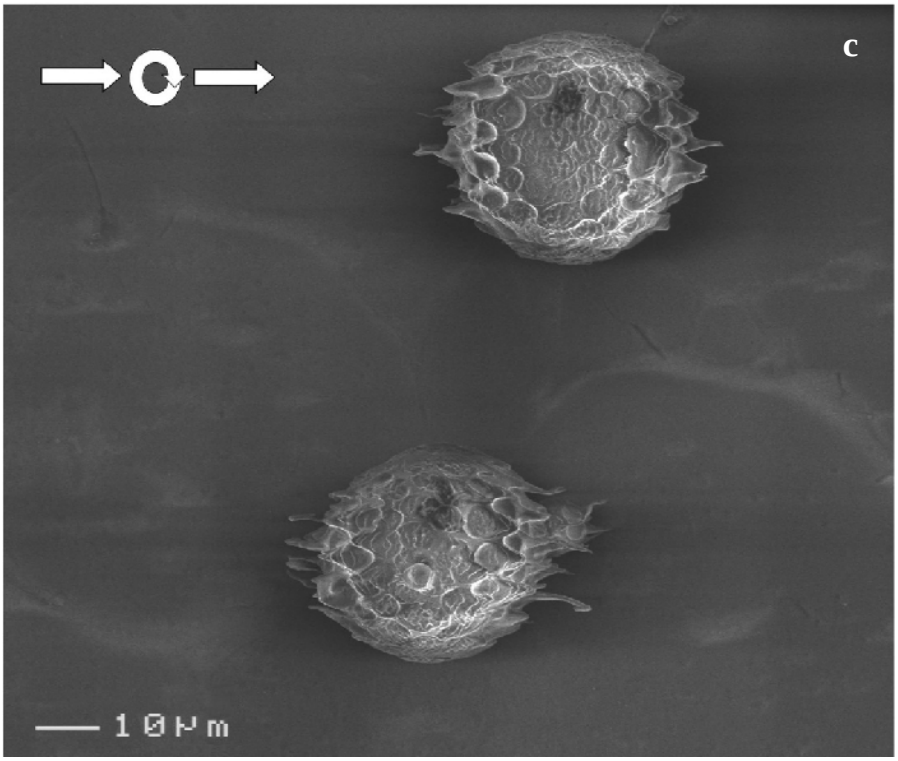

Fig. III.4-6 : a) Azopolymer particles after illumination with a horizontally polarized laser light, b) Azopolymer particles after illumination with a circular polarized laser light followed by a linear polarized irradiation, c) Azopolymer particles after illumination with a linear polarization followed by irradiation with a linear and circular polarization, successively

III.4.5. Stretching of azo particles under irradiation

Beside the unique and exotic shape of these particles under laser illumination, stretching of the azo fragments effect not only the shape of their particles, but also their coverage area. Evaluations from the images show that, for a typical size buckyball particles (with a diameter of 35μm), azo fragments exposed to laser beam stretch about 13±1μm. This value is about 0.4 of the particles diameter, which leads to a particle that, now can cover an elliptical area 1.5 times more than the circular area it was covering before.

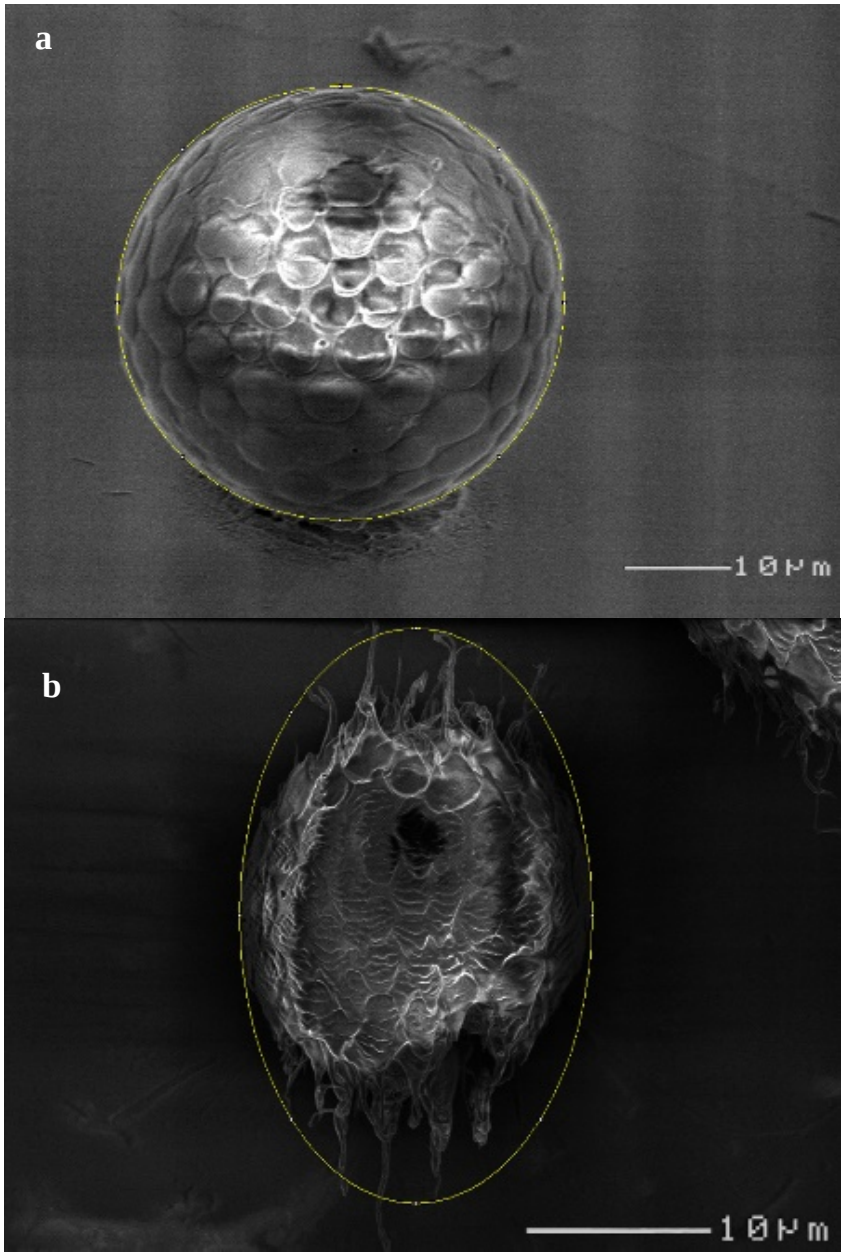

Fig. III.4-7 : a) Coverage area of particle before illumination with laser, b) Coverage area of particle after laser illumination

It should be noted that in this study particles are being investigated as a single particle, but this fact points out that in the case of bulk study, illumination of these particles effect the shape of these particles, their occupied volume and also their effect on the neighboring particle (Fig.III.4-7a,b).

III.4.6. Conclusion

A group of new colloidal azopolymers were synthesized. This particle group possesses a core of PMMA and a fragmented shell of azopolymer, resembling a buckyball. Under laser illumination, this fragmented shell gives rise to a set of unique shape particles such as; porcupine and sea pineapple particles

Conclusions and Perspective

In summary, given the unique properties of different complex ordered and disordered patterns, we reviewed the fabrication of such patterns on azo polymer thin films. Interference of two coherent laser beams has been used to writing surface relief grating on azo-polymer films. Using this property, we have presented the fabrication of surface quasi-crystal structures on azopolymer films and its replication through soft lithography on a transparent elastomer (PDMS). The quasi-crystal structures were prepared simply through a multistep light irradiation via an interference pattern of laser beam without additional manipulation. The printed patterns on PDMS showed the same patterns as the masters and the same relief depths as the stamps. The light diffracted by the PDMS stamp was used to observe the deformation of the surface as a function of its stretching. The PDMS SRGs were used as a tailored surface for the deposition of single nanoparticle in nanocavities. The methods presented here allows the fabrication of cost-effective and efficient deposition surfaces for optical single particle study.

As said and seen, no surface is perfectly flat or ordered at every length scale and they show some degree of roughness. Disordered systems host interesting optical phenomena, which is why disordered photonics has made significant contributions to the field of science and engineering. In this regard, Quasi-random or Gaussian random structures have been proposed as good candidates for energy harvesting.

Here, we have presented a simple and cost effective way to prepare a quasi Gaussian surface and a quasi random grating surface, using a self-photoinduced process on two chiral azopolymer thin films. Creation of a more interesting quasi random grating surface is possible, via combination of a photoisomerization process associated with a good choice of the azopolymer material, in particular with the correct choice of the copolymer function and the grafted azobenzene. The quasi random grating surface has the same advantages, as the quasi Gaussian surface, for light scattering but, as it was

experimentally shown, additionally it allows an induction of an isotropic mode coupling of light into thin film, increasing by 20% its efficiency for light harvesting.

We have highlighted the applicability of the quasi random gratings surface for realistic devices. The replication of the surface pattern on a PDMS surface (a transparent and cost effective material), shows how easily this technique can be used to modify samples like OLEDs or solar cells, for a better efficiency of light diffusion or light harvesting. Furthermore, we note that the primary photoinduced surface can be erased, for re-illumination and regeneration of a new photo structured surface. Finally, the chemical structure of the azobenzene grafted copolymer can be engineered, leading to new observational patterns.

Beside the conventional methods, here we have demonstrated a route to fabricate the ordered nano-patterns from dewetting. These results present an exciting opportunity for manipulating structures and properties of an azopolymer thin film on nanometer scale. In this work, we experimentally presented a facile bottom-up method for fabrication of doughnut shaped nanostructures. The technique chosen for this purpose is dewetting of azopolymer thin film via a solvent-droplet induced method. The produced nanostructures can be classified as nano-doughnuts, consisting of a hole and a surrounding ring. Such structures can be used in fields such as nano-cavities, nano-rectors and sensors. Furthermore, as a result of the unique property of azopolymer thin films leading to massive photoinduced macroscopic motions of polymer chains, nanostructures of azopolymers can be optimized and reshaped via tailored light fields to obtain different modified structures. The exposition of the above films to a coherent polarized beam with an appropriate wavelength results in controlled growth and modification of structures. The next step is the use of the unique property of self-patterning of azopolymer films with different solvents in different conditions of surface ordering and temperature in order to produce desired regular patterns with a controlled dewetting process. This will help to optimize the control of structures to the required geometric forms.

Also, given the importance of polymers and polymeric particles, beside the polymer thin films, a group of new colloidal azopolymers were synthesized. This particle group possesses a core of PMMA and a fragmented shell of azopolymer, resembling a buckyball. Under laser illumination, this fragmented shell gives rise to a set of unique shape particles such as; porcupine and sea pineapple particles, opening new doors for novel applications and study of the phenomena of SRG formation and the basic understanding of the light-matter interaction. Availability of polymeric particles with distinct shapes will prove to be a useful tool in uncovering the role of shape in applications such as biological systems. Particles can be used as models for similar- looking objects, like bacteria, not only in biological applications but also in environmental fields to study bacterial migration in soil or water. In another field, nonspherical particles also may open new applications in advanced materials due to their unique scattering and packing properties. These particles also can be used as research tools or probes in rheology or aerodynamics or as sensors in microrheology studies. The uses and knowledge gained from particles with defined shapes seem limitless, and the availability of a simple method to make such particles will catalyze many new discoveries and technologies.

Future perspectives

One cannot hope to participate in all parts of the endeavor sketched above, especially when taking into account the origin of self-organization in such systems. In the following, we will focus on future works that are related to the current researchs:

- Modification of nano cavity sizes by sample stretching for deposition of any shapes of nanoparticles
- Modification of nano cavity size and shape by stretching the sample from both sides
- Study of transparent elastometer for plasmonic response

- Application of Gaussian and random structures in Solar cells for light trapping
- Possible fabrication of nano-reactor or nano-trap patterns
- Study the possibility of fabrication of unique particle shape

References:

[1] P. Ball, *The Self-Made Tapestry: Pattern Formation in Nature*, 1st Editio. New York: Oxford University Press, 1999.

[2] S. Ahmadi-kandjani, "Réseaux de surface auto-organisés dans les films minces d ' azo-polymères," Université d'Angers, 2007.

[3] G. Theraulaz, J. Gautrais, S. Camazine, and J.-L. Deneubourg, "The formation of spatial patterns in social insects: from simple behaviours to complex structures.," *Philos. Trans. A. Math. Phys. Eng. Sci.*, vol. 361, no. 1807, pp. 1263–1282, 2003.

[4] P. Taylor, J. L. Deneubourg, and S. Goss, "Collective patterns and decision-making," *Ethol. Ecol. Evol.*, vol. 1, pp. 295–311, 1989.

[5] N. R. Franks and A. B. Sendova-Franks, "Brood sorting by ants: distributing the workload over the work-surface," *Behav. Ecol. Sociobiol.*, vol. 30, no. 2, pp. 109–123, 1992.

[6] Y. Zhao and T. Ikeda, *Smart Light-Responsive Materials*. Hoboken, NJ, USA: John Wiley & Sons, Inc., 2009.

[7] F.-W. Schulze, H.-J. Petrick, H. K. Cammenga, and H. Klinge, "Thermodynamic Properties of the Structural Analogues Benzo[c]cinnoline, Trans-azobenzene, and Cis-azobenzene," *Zeitschrift für Phys. Chemie*, vol. 107, no. 1, pp. 1–19, Jan. 1977.

[8] I. Mita, K. Horie, and K. Hirao, "Photochemistry in polymer solids. 9. Photoisomerization of azobenzene in a polycarbonate film," *Macromolecules*, vol. 22, no. 2, pp. 558–563, Mar. 1989.

[9] E. V Brown and G. R. Granneman, "Cis-trans isomerism in the pyridyl analogs of azobenzene. Kinetic and molecular orbital analysis," *J. Am. Chem. Soc.*, vol. 97, no. 3, pp. 621–627, Feb. 1975.

[10] P. Haberfield and M. S. Lux, "Enthalpies of solvent transfer of transition states in cis trans isomerization of azo compounds rotation vs nitrogen inversion mechanism," *J Am Chem Soc*, vol. 90, no. 20, pp. 5804–5806, 1975.

[11] W. J. Priest and M. M. Sifain, "Photochemical and thermal isomerization in polymer matrices: Azo compounds in polystyrene," *J. Polym. Sci. Part A-1 Polym. Chem.*, vol. 9, no. 11, pp. 3161–

3168, 1971.

[12] C. Barrett, a. Natansohn, and P. Rochon, “Cis-Trans Thermal Isomerization Rates of Bound and Doped Azobenzenes in a Series of Polymers,” *Chem. Mater.*, vol. 7, no. 7, pp. 899–903, 1995.

[13] C. Barrett, a Natansohn, and P. Rochon, “Thermal cis-trans isomerization rates of azobenzenes bound in the side chain of some copolymers and blends,” *Macromolecules*, vol. 27, pp. 4781–4786, 1994.

[14] N. Sarkar, A. Sarkar, and S. Sivaram, “Isomerization Behavior of Aromatic Azo Chromophores Bound to Semicrystalline Polymer Films,” *J. Appl. Polym. Sci.*, vol. 81, no. 12, pp. 2923–2928, 2001.

[15] J. J. de Lange, J. M. Robertson, and I. Woodward, “X-Ray Crystal Analysis of Trans-Azobenzene,” *Proc. R. Soc. Lond. A. Math. Phys. Sci.*, vol. 171, no. 946, pp. 398–410, 1939.

[16] G. C. Hampson and J. M. Robertson, “Bond lengths and resonance in the cis-azobenzene molecule,” *J. Chem. Soc.*, pp. 409–413, 1941.

[17] C. J. Brown, “A refinement of the crystal structure of azobenzene,” *Acta Crystallogr.*, vol. 21, no. 1, pp. 146–152, 1966.

[18] T. Naito, K. Horie, and I. Mita, “Photochemistry in polymer solids: 12. Effects of main-chain structures and formation of hydrogen bonds on photoisomerization of azobenzene in various polymer films,” *Polymer (Guildf).*, vol. 34, no. 19, pp. 4140–4145, 1993.

[19] T. Naito, K. Horie, and I. Mita, “Photochemistry in Polymer Solids .11. the Effects of the Size of Reaction Groups and the Mode of Photoisomerization on Photochromic Reactions in Polycarbonate Film,” *Macromolecules*, vol. 24, no. 10, pp. 2907–2911, 1991.

[20] L. Lamarre and C. S. P. Sung, “Studies of physical aging and molecular motion by azochromophoric labels attached to the main chains of amorphous polymers,” *Macromolecules*, vol. 16, no. 11, pp. 1729–1736, Nov. 1983.

[21] T. Hugel, N. B. Holland, A. Cattani, L. Moroder, M. Seitz, and H. E. Gaub, “Single-Molecule Optomechanical Cycle,” *Science (80-.).*, vol. 296, no. 5570, p. 1103 LP-1106, May 2002.

[22] N. B. Holland, T. Hugel, G. Neuert, A. Cattani-Scholz, C. Renner, D. Oesterhelt, L. Moroder, M. Seitz, and H. E. Gaub, “Single Molecule Force Spectroscopy of Azobenzene Polymers:

Switching Elasticity of Single Photochromic Macromolecules," *Macromolecules*, vol. 36, no. 6, pp. 2015–2023, Mar. 2003.

[23] K. G. Yager and C. J. Barrett, "Novel photo-switching using azobenzene functional materials," *J. Photochem. Photobiol. A Chem.*, vol. 182, no. 3, pp. 250–261, 2006.

[24] A. Natansohn, P. Rochon, M. Pezolet, P. Audet, D. Brown, and S. To, "Azo Polymers for Reversible Optical Storage. 4. Cooperative Motion of Rigid Groups in Semicrystalline Polymers," *Macromolecules*, vol. 27, no. 9, pp. 2580–2585, Apr. 1994.

[25] R. Hagen and T. Bieringer, "Photoaddressable Polymers for Optical Data Storage," *Adv. Mater.*, vol. 13, no. 23, pp. 1805–1810, 2001.

[26] P. M. Blanchard and G. R. Mitchell, "A comparison of photoinduced poling and thermal poling of azo-dye-doped polymer films for second order nonlinear optical applications," *Appl. Phys. Lett.*, vol. 63, no. 15, pp. 2038–2040, Oct. 1993.

[27] P. M. B. and G. R. Mitchell, "Localized room temperature photo-induced poling of azo-dye-doped polymer films for second-order nonlinear optical phenomena," *J. Phys. D. Appl. Phys.*, vol. 26, no. 3, p. 500, 1993.

[28] Z. Sekkat, C.-S. Kang, E. F. Aust, G. Wegner, and W. Knoll, "Room-Temperature Photoinduced Poling and Thermal Poling of a Rigid Main-Chain Polymer with Polar Azo Dyes in the Side Chain," *Chem. Mater.*, vol. 7, no. 1, pp. 142–147, Jan. 1995.

[29] X. L. Jiang, L. Li, J. Kumar, and S. K. Tripathy, "Photoassisted poling induced second harmonic generation with in-plane anisotropy in azobenzene containing polymer films," *Appl. Phys. Lett.*, vol. 69, no. 24, pp. 3629–3631, Dec. 1996.

[30] J.-M. N. and C. F. and A.-C. E. and F. Kajzar, "All-optical poling in polymers: dynamical aspects and perspectives," *Pure Appl. Opt. J. Eur. Opt. Soc. Part A*, vol. 7, no. 2, p. 141, 1998.

[31] X. Zhong, X. Yu, Q. Li, S. Luo, Y. Chen, Y. Sui, and J. Yin, "Identification of the alignment of azobenzene molecules induced by all-optical poling in polymer film," *Opt. Commun.*, vol. 190, no. 1, pp. 333–337, 2001.

[32] V. Shibaev, A. Bobrovsky, and N. Boiko, "Photoactive liquid crystalline polymer systems with light-controllable structure and optical properties," *Prog. Polym. Sci.*, vol. 28, no. 5, pp. 729–

836, May 2003.

[33] Y. Yu and T. Ikeda, “Alignment modulation of azobenzene-containing liquid crystal systems by photochemical reactions,” *J. Photochem. Photobiol. C Photochem. Rev.*, vol. 5, no. 3, pp. 247–265, 2004.

[34] N. K. Viswanathan, Y. Kim, S. Bian, J. Williams, W. Liu, L. Li, L. Samuelson, and S. K. Tripathy, “Surface relief structures on azo polymer films,” pp. 1941–1955, 1999.

[35] P. Rochon, E. Batalla, and A. Natansohn, “Optically induced surface gratings on azoaromatic polymer films,” *Appl. Phys. Lett.*, vol. 66, no. 2, pp. 136–138, Jan. 1995.

[36] D. Y. Kim, S. K. Tripathy, L. Li, and J. Kumar, “Laser-induced holographic surface relief gratings on nonlinear optical polymer films,” *Appl. Phys. Lett.*, vol. 66, no. 10, pp. 1166–1168, Mar. 1995.

[37] F. Lagugné Labarthet, T. Buffeteau, and C. Sourisseau, “Analyses of the Diffraction Efficiencies, Birefringence, and Surface Relief Gratings on Azobenzene-Containing Polymer Films,” *J. Phys. Chem. B*, vol. 102, no. 15, pp. 2654–2662, Apr. 1998.

[38] J. A. Delaire and K. Nakatani, “Linear and Nonlinear Optical Properties of Photochromic Molecules and Materials,” *Chem. Rev.*, vol. 100, no. 5, pp. 1817–1846, May 2000.

[39] A. Natansohn and P. Rochon, “Photoinduced Motions in Azo-Containing Polymers,” *Chem. Rev.*, vol. 102, no. 11, pp. 4139–4176, Nov. 2002.

[40] A. Stracke, J. H. Wendorff, D. Goldmann, D. Janietz, and B. Stiller, “Gain Effects in Optical Storage: Thermal Induction of a Surface Relief Grating in a Smectic Liquid Crystal,” *Adv. Mater.*, vol. 12, no. 4, pp. 282–285, 2000.

[41] T. Yamamoto, M. Hasegawa, A. Kanazawa, T. Shiono, and T. Ikeda, “Holographic gratings and holographic image storage via photochemical phase transitions of polymer azobenzene liquid-crystal films,” *J. Mater. Chem.*, vol. 10, no. 2, pp. 337–342, 2000.

[42] J. Wang, P. Xu, X. Li, J. Shen, G. Wu, and B. Zhou, “Optical Properties of Sol-Gel Coatings on Plastic Foils Embossed with Surface-Relief Gratings,” *J. Sol-Gel Sci. Technol.*, vol. 23, no. 1, pp. 73–77, 2002.

[43] C. R. Mendonça, A. Dhanabalan, D. T. Balogh, L. Misoguti, D. S. dos Santos, M. A. Pereira-da-

Silva, J. A. Giacometti, S. C. Zilio, and O. N. Oliveira, “Optically Induced Birefringence and Surface Relief Gratings in Composite Langmuir−Blodgett (LB) Films of Poly[4‘-[[2-(methacryloyloxy)ethyl]ethylamino]-2-chloro-4-nitroazobenzene] (HPDR13) and Cadmium Stearate,” *Macromolecules*, vol. 32, no. 5, pp. 1493–1499, Mar. 1999.

[44] J.-A. He, S. Bian, L. Li, J. Kumar, S. K. Tripathy, and L. A. Samuelson, “Photochemical Behavior and Formation of Surface Relief Grating on Self-Assembled Polyion/Dye Composite Film,” *J. Phys. Chem. B*, vol. 104, no. 45, pp. 10513–10521, Nov. 2000.

[45] Y. He, H. Wang, X. Tuo, W. Deng, and X. Wang, “Synthesis, self-assembly and photoinduced surface-relief gratings of a polyacrylate-based Azo polyelectrolyte,” *Opt. Mater. (Amst).*, vol. 26, no. 1, pp. 89–93, 2004.

[46] L. M. Goldenberg, O. Kulikovska, and J. Stumpe, “Thermally Stable Holographic Surface Relief Gratings and Switchable Optical Anisotropy in Films of an Azobenzene-Containing Polyelectrolyte,” *Langmuir*, vol. 21, no. 11, pp. 4794–4796, May 2005.

[47] H. Nakano, T. Tanino, and Y. Shirota, “Surface relief grating formation on a single crystal of 4-(dimethylamino)azobenzene,” *Appl. Phys. Lett.*, vol. 87, no. 6, p. 61910, Aug. 2005.

[48] Y. Shirota, “Photo- and electroactive amorphous molecular materials-molecular design, syntheses, reactions, properties, and applications,” *J. Mater. Chem.*, vol. 15, no. 1, pp. 75–93, 2005.

[49] E. Ishow, B. Lebon, Y. He, X. Wang, L. Bouteiller, L. Galmiche, and K. Nakatani, “Structural and Photoisomerization Cross Studies of Polar Photochromic Monomeric Glasses Forming Surface Relief Gratings,” *Chem. Mater.*, vol. 18, no. 5, pp. 1261–1267, Mar. 2006.

[50] L.-H. Liu, K. Nakatani, R. Pansu, J.-J. Vachon, P. Tauc, and E. Ishow, “Fluorescence Patterning through Photoinduced Migration of Squaraine-Functionalized Azo Derivatives,” *Adv. Mater.*, vol. 19, no. 3, pp. 433–436, 2007.

[51] X. L. Jiang, L. Li, J. Kumar, D. Y. Kim, V. Shivshankar, and S. K. Tripathy, “Polarization dependent recordings of surface relief gratings on azobenzene containing polymer films,” *Appl. Phys. Lett.*, vol. 68, no. 19, pp. 2618–2620, May 1996.

[52] S. Tripathy, D.-Y. Kim, X. L. Jiang, L. Li, T. Lee, X. Wang, and J. A. Kumar, “Photofabrication

of Surface Relief Gratings Using Photodynamic Polymers," *Mol. Cryst. Liq. Cryst. Sci. Technol. Sect. A. Mol. Cryst. Liq. Cryst.*, vol. 314, no. 1, pp. 245–255, May 1998.

[53] C. Hubert, C. Fiorini-debuisschert, L. Rocha, P. Raimond, and J. Nunzi, "Spontaneous photoinduced patterning of azo-dye polymer films : the facts," *J. Opt. Soc. Am. B*, vol. 24, no. 8, pp. 1839–1846, 2007.

[54] S. Bian, L. Li, J. Kumar, D. Y. Kim, J. Williams, and S. K. Tripathy, "Single laser beam-induced surface deformation on azobenzene polymer films," *Appl. Phys. Lett.*, vol. 73, no. 13, pp. 1817–1819, Sep. 1998.

[55] S. Bian, J. M. Williams, D. Y. Kim, L. Li, S. Balasubramanian, J. Kumar, and S. Tripathy, "Photoinduced surface deformations on azobenzene polymer films," *J. Appl. Phys.*, vol. 86, no. 8, pp. 4498–4508, Sep. 1999.

[56] C. J. Barrett, A. L. Natansohn, and P. L. Rochon, "Mechanism of Optically Inscribed High-Efficiency Diffraction Gratings in Azo Polymer Films," *J. Phys. Chem.*, vol. 100, no. 21, pp. 8836–8842, Jan. 1996.

[57] C. J. Barrett, P. L. Rochon, and A. L. Natansohn, "Model of laser-driven mass transport in thin films of dye-functionalized polymers," *J. Chem. Phys.*, vol. 109, no. 4, pp. 1505–1516, Jul. 1998.

[58] M. S. Ho, A. Natansohn, and P. Rochon, "Azo Polymers for Reversible Optical Storage. 7. The Effect of the Size of the Photochromic Groups," *Macromolecules*, vol. 28, no. 18, pp. 6124–6127, Aug. 1995.

[59] K. Sumaru, T. Yamanaka, T. Fukuda, and H. Matsuda, "Photoinduced surface relief gratings on azopolymer films: Analysis by a fluid mechanics model," *Appl. Phys. Lett.*, vol. 75, no. 13, pp. 1878–1880, Sep. 1999.

[60] K. Sumaru, T. Fukuda, T. Kimura, H. Matsuda, and T. Yamanaka, "Photoinduced surface relief formation on azopolymer films: A driving force and formed relief profile," *J. Appl. Phys.*, vol. 91, no. 5, pp. 3421–3430, Feb. 2002.

[61] J. Kumar, L. Li, X. L. Jiang, D.-Y. Kim, T. S. Lee, and S. Tripathy, "Gradient force: The mechanism for surface relief grating formation in azobenzene functionalized polymers," *Appl.*

Phys. Lett., vol. 72, no. 17, pp. 2096–2098, Apr. 1998.

[62] T. Fukuda, H. Matsuda, T. Shiraga, T. Kimura, M. Kato, N. K. Viswanathan, J. Kumar, and S. K. Tripathy, "Photofabrication of Surface Relief Grating on Films of Azobenzene Polymer with Different Dye Functionalization," *Macromolecules*, vol. 33, no. 11, pp. 4220–4225, May 2000.

[63] N. K. Viswanathan, S. Balasubramanian, L. Li, J. Kumar, and S. K. Tripathy, "Surface-Initiated Mechanism for the Formation of Relief Gratings on Azo-Polymer Films," vol. 5647, no. 98, pp. 6064–6070, 1998.

[64] K. Yang, S. Yang, and J. Kumar, "Formation mechanism of surface relief structures on amorphous azopolymer films," *Phys. Rev. B*, vol. 73, no. 16, p. 165204, Apr. 2006.

[65] O. Baldus, A. Leopold, R. Hagen, T. Bieringer, and S. J. Zilker, "Surface relief gratings generated by pulsed holography: A simple way to polymer nanostructures without isomerizing side-chains," *J. Chem. Phys.*, vol. 114, no. 3, pp. 1344–1349, Jan. 2001.

[66] K. G. Yager and C. J. Barrett, "Temperature modeling of laser-irradiated azo-polymer thin films," *J. Chem. Phys.*, vol. 120, no. 2, pp. 1089–1096, Dec. 2003.

[67] S. Bauer-Gogonea, S. Bauer, W. Wirges, and R. Gerhard-Multhaupt, "Pyroelectrical investigation of the dipole orientation in nonlinear optical polymers during and after photoinduced poling," *J. Appl. Phys.*, vol. 76, no. 5, pp. 2627–2635, Sep. 1994.

[68] O. Baldus and S. J. Zilker, "Surface relief gratings in photoaddressable polymers generated by cw holography," *Appl. Phys. B*, vol. 72, no. 4, pp. 425–427, 2001.

[69] P. L. and C. F. and J.-M. Nunzi, "Anisotropy of the photo-induced translation diffusion of azobenzene dyes in polymer matrices," *Pure Appl. Opt. J. Eur. Opt. Soc. Part A*, vol. 7, no. 1, p. 71, 1998.

[70] P. Lefin, C. Fiorini, and J.-M. Nunzi, "Anisotropy of the photoinduced translation diffusion of azo-dyes," *Opt. Mater. (Amst).*, vol. 9, no. 1, pp. 323–328, 1998.

[71] C. Fiorini, N. Prudhomme, G. de Veyrac, I. Maurin, P. Raimond, and J.-M. Nunzi, "Molecular migration mechanism for laser induced surface relief grating formation," *Synth. Met.*, vol. 115, no. 1, pp. 121–125, 2000.

[72] T. G. Pedersen, P. M. Johansen, N. C. R. Holme, P. S. Ramanujam, and S. Hvilsted, "Mean-field

theory of photoinduced formation of surface reliefs in side-chain azobenzene polymers," *Phys. Rev. Lett.*, vol. 80, no. 1, pp. 89–92, 1998.

[73] I. Naydenova, L. Nikolova, T. Todorov, N. C. R. Holme, P. S. Ramanujam, and S. Hvilsted, "Diffraction from polarization holographic gratings with surface relief in side-chain azobenzene polyesters," *J. Opt. Soc. Am. B*, vol. 15, no. 4, p. 1257, 1998.

[74] M. Srinivasarao, "Nano-Optics in the Biological World: Beetles, Butterflies, Birds, and Moths," *Chem. Rev.*, vol. 99, no. 7, pp. 1935–1962, Jul. 1999.

[75] L. P. Lee and R. Szema, "Inspirations from Biological Optics for Advanced Photonic Systems," *Science (80-.).*, vol. 310, no. 5751, p. 1148 LP-1150, Nov. 2005.

[76] R. Magnusson and S. S. Wang, "New principle for optical filters," *Appl. Phys. Lett.*, vol. 61, no. 9, pp. 1022–1024, Aug. 1992.

[77] Z. V. Vardeny, A. Nahata, and A. Agrawal, "Optics of photonic quasicrystals," *Nat Phot.*, vol. 7, no. 3, pp. 177–187, Mar. 2013.

[78] X. Wang, C. Y. Ng, W. Y. Tam, C. T. Chan, and P. Sheng, "Large-Area Two-Dimensional Mesoscale Quasi-Crystals," *Adv. Mater.*, vol. 15, no. 18, pp. 1526–1528, 2003.

[79] S. P. Gorkhali, J. Qi, and G. P. Crawford, "Electrically switchable mesoscale Penrose quasicrystal structure," *Appl. Phys. Lett.*, vol. 86, no. 1, p. 11110, Dec. 2004.

[80] R. C. Gauthier and A. Ivanov, "Production of quasi-crystal template patterns using a dual beam multiple exposure technique," *Opt. Express*, vol. 12, no. 6, p. 990, 2004.

[81] T. Matsui, A. Agrawal, A. Nahata, and Z. V. Vardeny, "Transmission resonances through aperiodic arrays of subwavelength apertures," *Nature*, vol. 446, no. 7135, pp. 517–521, Mar. 2007.

[82] I. Simonsen, "Optics of surface disordered systems," *Eur. Phys. J. Spec. Top.*, vol. 181, no. 1, pp. 1–103, 2010.

[83] Lord Rayleigh, "On the Dynamical Theory of Gratings," *Proc. R. Soc. London. Ser. A*, vol. 79, no. 532, p. 399 LP-416, Aug. 1907.

[84] I. Simonsen, "Optics of surface disordered systems," *Eur. Phys. J. Spec. Top.*, vol. 181, no. 1, pp. 1–103, Jan. 2010.

[85] P. Sheng, *Introduction to Wave Scattering, Localization and Mesoscopic Phenomena*, Second edi., vol. 17, no. 2. Springer Berlin Heidelberg, 2007.

[86] K. F. Warnick and W. C. Chew, "Numerical simulation methods for rough surface scattering," *Waves in Random Media*, vol. 11, no. 1, pp. R1–R30, Jan. 2001.

[87] A. V Shchegrov, A. A. Maradudin, and E. R. Méndez, "Multiple scattering of light from randomly rough surfaces," *Prog. Opt.*, vol. 46, pp. 117–241, 2004.

[88] O. Katz, P. Heidmann, M. Fink, and S. Gigan, "Non-invasive single-shot imaging through scattering layers and around corners via speckle correlations," *Nat Phot.*, vol. 8, no. 10, pp. 784–790, Oct. 2014.

[89] D. S. Wiersma, "Disordered photonics," *Nat Phot.*, vol. 7, no. 3, pp. 188–196, Mar. 2013.

[90] D. S. Wiersma, "The physics and applications of random lasers," *Nat Phys*, vol. 4, no. 5, pp. 359–367, May 2008.

[91] Y. Yoon, D. Kim, and J.-B. Lee, "Hierarchical micro/nano structures for super-hydrophobic surfaces and super-lyophobic surface against liquid metal," *Micro Nano Syst. Lett.*, vol. 2, no. 1, p. 3, 2014.

[92] E. Akkermans, P. E. Wolf, and R. Maynard, "Coherent Backscattering of Light by Disordered Media: Analysis of the Peak Line Shape," *Phys. Rev. Lett.*, vol. 56, no. 14, pp. 1471–1474, Apr. 1986.

[93] M. Segev, Y. Silberberg, and D. N. Christodoulides, "Anderson localization of light," *Nat Phot.*, vol. 7, no. 3, pp. 197–204, Mar. 2013.

[94] L. Levi, Y. Krivolapov, S. Fishman, and M. Segev, "Hyper-transport of light and stochastic acceleration by evolving disorder," *Nat Phys*, vol. 8, no. 12, pp. 912–917, Dec. 2012.

[95] J.-H. Park, C. Park, H. Yu, J. Park, S. Han, J. Shin, S. H. Ko, K. T. Nam, Y.-H. Cho, and Y. Park, "Subwavelength light focusing using random nanoparticles," *Nat Phot.*, vol. 7, no. 6, pp. 454–458, Jun. 2013.

[96] J. Bingi, A. R. Warrier, and C. Vijayan, "Raman mode random lasing in ZnS-β-carotene random gain media," *Appl. Phys. Lett.*, vol. 102, no. 22, p. 221105, Jun. 2013.

[97] LiuC., A. Di Falco, MolinariD., KhanY., O. S., K. F., and FratalocchiA., "Enhanced energy

storage in chaotic optical resonators," *Nat Phot.*, vol. 7, no. 6, pp. 473–478, Jun. 2013.

[98] R. Dewan, S. Shrestha, V. Jovanov, J. Hüpkes, K. Bittkau, and D. Knipp, "Random versus periodic: Determining light trapping of randomly textured thin film solar cells by the superposition of periodic surface textures," *Sol. Energy Mater. Sol. Cells*, vol. 143, pp. 183–189, 2015.

[99] A. Bozzola, M. Liscidini, and L. C. Andreani, "Broadband light trapping with disordered photonic structures in thin-film silicon solar cells," *Prog. Photovoltaics Res. Appl.*, vol. 22, no. 12, pp. 1237–1245, 2014.

[100] J. Wang, L. Yang, D. Lin, Y. Luo, D. Li, and Q. Meng, "Optical studies of random disorder of colloidal photonic crystals and its evolution in evaporation induced self-assembly," *J. Chem. Phys.*, vol. 137, no. 23, p. 234111, Dec. 2012.

[101] X. Zhang, Q. Di, F. Zhu, G. Sun, and H. Zhang, "Wideband anti-reflective micro/nano dual-scale structures: fabrication and optical properties," *IET Micro & Nano Letters*, vol. 6, no. 11. pp. 947–950, 2011.

[102] E. Moulin, M. Steltenpool, M. Boccard, L. Garcia, G. Bugnon, M. Stuckelberger, E. Feuser, B. Niesen, R. van Erven, J. W. Schüttauf, F. J. Haug, and C. Ballif, "2-D Periodic and Random-on-Periodic Front Textures for Tandem Thin-Film Silicon Solar Cells," *IEEE Journal of Photovoltaics*, vol. 4, no. 5. pp. 1177–1184, 2014.

[103] D. Tan, E. Tuncer, Y. Cao, and P. Irwin, "Nanofiller dispersion in polymer dielectrics," *2012 Annual Report Conference on Electrical Insulation and Dielectric Phenomena*. pp. 916–918, 2012.

[104] O. Matoba, Y. Kitamura, T. Manabe, K. Nitta, and W. Watanabe, "Femtosecond laser fabrication of scattering medium by randomly distributed holes in polymer," in *Optics and Photonics for Information Processing III*, 2009, vol. 7442, p. 74420H–74420H–8.

[105] P. Hsieh, C. Chung, J. F. McMillan, M. Tsai, M. Lu, N. C. Panoiu, and C. W. Wong, "Photon transport enhanced by transverse Anderson localization in disordered superlattices," *Nat Phys*, vol. 11, no. 3, pp. 268–274, Mar. 2015.

[106] T. Ito and S. Okazaki, "Pushing the limits of lithography," *Nature*, vol. 406, no. 6799, pp. 1027–

1031, Aug. 2000.

[107] R. F. Service, “Optical Lithography Goes to Extremes--And Beyond,” *Science (80-.).*, vol. 293, no. 5531, p. 785 LP-786, Aug. 2001.

[108] B. J. Lin, “The future of subhalf-micrometer optical lithography,” *Microelectron. Eng.*, vol. 6, no. 1, pp. 31–51, 1987.

[109] C. Vieu, F. Carcenac, A. Pépin, Y. Chen, M. Mejias, A. Lebib, L. Manin-Ferlazzo, L. Couraud, and H. Launois, “Electron beam lithography: resolution limits and applications,” *Appl. Surf. Sci.*, vol. 164, no. 1, pp. 111–117, 2000.

[110] J. Melngailis, “Focused ion beam technology and applications,” *J. Vac. Sci. Technol. B Microelectron. Process. Phenom.*, vol. 5, no. 2, pp. 469–495, Mar. 1987.

[111] R. D. Piner, J. Zhu, F. Xu, S. Hong, and C. A. Mirkin, “Dip-Pen" Nanolithography,” *Science (80-.).*, vol. 283, no. 5402, p. 661 LP-663, Jan. 1999.

[112] F. Huo, G. Zheng, X. Liao, L. R. Giam, J. Chai, X. Chen, W. Shim, and C. A. Mirkin, “Beam pen lithography,” *Nat Nano*, vol. 5, no. 9, pp. 637–640, Sep. 2010.

[113] X. Liao, K. A. Brown, A. L. Schmucker, G. Liu, S. He, W. Shim, and C. A. Mirkin, “Desktop nanofabrication with massively multiplexed beam pen lithography,” *Nat. Commun.*, vol. 4, p. 2103, Jul. 2013.

[114] E. Mcleod and C. B. Arnold, “Subwavelength direct-write nanopatterning using optically trapped microspheres,” *Nat Nano*, vol. 3, no. 7, pp. 413–417, Jul. 2008.

[115] J. V Barth, G. Costantini, and K. Kern, “Engineering atomic and molecular nanostructures at surfaces,” *Nature*, vol. 437, no. 7059, pp. 671–679, Sep. 2005.

[116] Y. Xia, J. A. Rogers, K. E. Paul, and G. M. Whitesides, “Unconventional Methods for Fabricating and Patterning Nanostructures,” *Chem. Rev.*, vol. 99, no. 7, pp. 1823–1848, Jul. 1999.

[117] M. Schliwa and G. Woehlke, “Molecular motors,” *Nature*, vol. 422, no. 6933, pp. 759–765, Apr. 2003.

[118] J. Bath and A. J. Turberfield, “DNA nanomachines,” *Nat Nano*, vol. 2, no. 5, pp. 275–284, May 2007.

[119] R. F. Ismagilov, A. Schwartz, N. Bowden, and G. M. Whitesides, “Autonomous Movement and Self-Assembly ,” *Angew. Chemie Int. Ed.*, vol. 41, no. 4, pp. 652–654, 2002.

[120] G. A. Ozin, I. Manners, S. Fournier-Bidoz, and A. Arsenault, “Dream Nanomachines,” *Adv. Mater.*, vol. 17, no. 24, pp. 3011–3018, 2005.

[121] J. Wang and K. M. Manesh, “Motion Control at the Nanoscale,” *Small*, vol. 6, no. 3, pp. 338–345, 2010.

[122] A. del Campo and E. Arzt, “Fabrication Approaches for Generating Complex Micro- and Nanopatterns on Polymeric Surfaces,” *Chem. Rev.*, vol. 108, no. 3, pp. 911–945, Mar. 2008.

[123] E. Menard, M. A. Meitl, Y. Sun, J.-U. Park, D. J.-L. Shir, Y.-S. Nam, S. Jeon, and J. A. Rogers, “Micro- and Nanopatterning Techniques for Organic Electronic and Optoelectronic Systems,” *Chem. Rev.*, vol. 107, no. 4, pp. 1117–1160, Apr. 2007.

[124] Z. Nie and E. Kumacheva, “Patterning surfaces with functional polymers,” *Nat Mater*, vol. 7, no. 4, pp. 277–290, Apr. 2008.

[125] G. Reiterf, “Unstable Thin Polymer Films : Rupture and Dewetting Processes,” no. 19, pp. 1344–1351, 1993.

[126] A. Vrij, “Possible mechanism for the spontaneous rupture of thin, free liquid films,” *Discuss. Faraday Soc.*, vol. 42, no. 0, pp. 23–33, 1966.

[127] G. Reiter, “Dewetting as a Probe of Polymer Mobility in Thin Films,” *Macromolecules*, vol. 27, no. 11, pp. 3046–3052, May 1994.

[128] S. Herminghaus, K. Jacobs, K. Mecke, J. Bischof, A. Fery, M. Ibn-Elhaj, and S. Schlagowski, “Spinodal Dewetting in Liquid Crystal and Liquid Metal Films,” *Science (80-.).*, vol. 282, no. 5390, p. 916 LP-919, Oct. 1998.

[129] S. Liu, W. M. Wang, A. L. Briseno, S. C. B. Mannsfeld, and Z. Bao, “Controlled Deposition of Crystalline Organic Semiconductors for Field-Effect-Transistor Applications,” *Adv. Mater.*, vol. 21, no. 12, pp. 1217–1232, 2009.

[130] F. B. Wyart and J. Daillant, “Drying of solids wetted by thin liquid films,” *Can. J. Phys.*, vol. 68, no. 9, pp. 1084–1088, Sep. 1990.

[131] R. Xie, A. Karim, J. F. Douglas, C. C. Han, and R. A. Weiss, “Spinodal Dewetting of Thin

Polymer Films," no. 1, pp. 1251–1254, 1998.

[132] V. S. Mitlin, "Dewetting of Solid Surface: Analogy with Spinodal Decomposition," *J. Colloid Interface Sci.*, vol. 156, no. 2, pp. 491–497, 1993.

[133] V. S. Mitlin, "On dewetting conditions," vol. 89, pp. 97–101, 1994.

[134] G. Reiter, "Dewetting of Thin Polymer Films," *Phys. Rev. Lett.*, vol. 68, no. 1, pp. 75–78, 1992.

[135] U. Thiele, M. Velarde, and K. Neuffer, "Dewetting: Film Rupture by Nucleation in the Spinodal Regime," *Phys. Rev. Lett.*, vol. 87, no. 1, p. 16104, Jun. 2001.

[136] R. Seemann, S. Herminghaus, and K. Jacobs, "Dewetting Patterns and Molecular Forces: A Reconciliation," *Phys. Rev. Lett.*, vol. 86, no. 24, pp. 5534–5537, Jun. 2001.

[137] A. Sharma and R. Khanna, "Pattern formation in unstable thin liquid films under the influence of antagonistic short- and long-range forces," *J. Chem. Phys.*, vol. 110, no. 10, pp. 4929–4936, Feb. 1999.

[138] G. Reiter, A. Sharma, R. Khanna, A. Casoli, and M.-O. David, "The Strength of Long-Range Forces across Thin Liquid Films," *J. Colloid Interface Sci.*, vol. 214, no. 1, pp. 126–128, 1999.

[139] R. S. and S. H. and K. Jacobs, "Gaining control of pattern formation of dewetting liquid films," *J. Phys. Condens. Matter*, vol. 13, no. 21, p. 4925, 2001.

[140] K. Jacobs, S. Herminghaus, and K. R. Mecke, "Thin Liquid Polymer Films Rupture via Defects," *Langmuir*, vol. 14, no. 4, pp. 965–969, Feb. 1998.

[141] G. Reiter, "Dewetting of Thin Polymer Films," vol. 68, no. 1, 1992.

[142] F. Brochard-Wyart and C. Redon, "Dynamics of liquid rim instabilities," *Langmuir*, vol. 8, no. 9, pp. 2324–2329, Sep. 1992.

[143] Lord Rayleigh, "On The Instability Of Jets," *Proc. London Math. Soc.*, vol. s1-10, no. 1, pp. 4–13, 1878.

[144] L. Xue and Y. Han, "Autophobic Dewetting of a Poly(methyl methacrylate) Thin Film on a Silicon Wafer Treated in Good Solvent Vapor," *Langmuir*, vol. 25, no. 9, pp. 5135–5140, May 2009.

[145] C. Redon, F. Brochard-Wyart, and F. Rondelez, "Dynamics of dewetting," *Phys. Rev. Lett.*, vol. 66, no. 6, pp. 715–718, Feb. 1991.

[146] T. Thurn-albrecht and T. P. Russell, “Electrically induced structure formation and pattern transfer,” vol. 403, no. February, pp. 1998–2001, 2000.

[147] E. Schäffer, T. Thurn-Albrecht, T. P. Russell, and U. Steiner, “Electrohydrodynamic instabilities in polymer films,” *Eur. Lett.*, vol. 53, no. 4, pp. 518–524, Feb. 2001.

[148] W. Mönch and S. Herminghaus, “Elastic instability of rubber films between solid bodies,” *Eur. Lett.*, vol. 53, no. 4, pp. 525–531, Feb. 2001.

[149] E. Schäffer and U. Steiner, “Acoustic instabilities in thin polymer films,” *Eur. Phys. J. E*, vol. 8, no. 3, pp. 347–351, Jun. 2002.

[150] K. D. F. Wensink and B. Jérôme, “Dewetting induced by density fluctuations,” *Langmuir*, vol. 18, no. 2, pp. 413–416, 2002.

[151] E. S. and S. H. and R. B. and U. Steiner, “Temperature-gradient–induced instability in polymer films,” *EPL (Europhysics Lett.*, vol. 60, no. 2, p. 255, 2002.

[152] A. Sharma and G. Reiter, “Instability of Thin Polymer Films on Coated Substrates: Rupture, Dewetting, and Drop Formation,” *J. Colloid Interface Sci.*, vol. 178, no. 2, pp. 383–399, Mar. 1996.

[153] A. M. Higgins and R. A. L. Jones, “Anisotropic spinodal dewetting as a route to self-assembly of patterned surfaces,” *Nature*, vol. 404, no. 6777, pp. 476–478, Mar. 2000.

[154] N. Rehse, C. Wang, M. Hund, M. Geoghegan, R. Magerle, and G. Krausch, “Stability of thin polymer films on a corrugated substrate,” *Eur. Phys. J. E*, vol. 4, no. 1, pp. 69–76, 2001.

[155] L. Rockford, Y. Liu, P. Mansky, T. P. Russell, M. Yoon, and S. G. J. Mochrie, “Polymers on Nanoperiodic, Heterogeneous Surfaces,” *Phys. Rev. Lett.*, vol. 82, no. 12, pp. 2602–2605, 1999.

[156] C. Luo, R. Xing, Z. Zhang, J. Fu, and Y. Han, “Ordered droplet formation by thin polymer film dewetting on a stripe-patterned substrate,” *J. Colloid Interface Sci.*, vol. 269, no. 1, pp. 158–163, 2004.

[157] B. Yoon, H. Acharya, G. Lee, H.-C. Kim, J. Huh, and C. Park, “Nanopatterning of thin polymer films by controlled dewetting on a topographic pre-pattern,” *Soft Matter*, vol. 4, no. 7, pp. 1467–1472, 2008.

[158] S. Luan, Z. Cheng, R. Xing, Z. Wang, X. Yu, and Y. Han, “Patterning organic luminescent

materials by solvent-assisted dewetting and polymer-bonding lithography," *J. Appl. Phys.*, vol. 97, no. 8, p. 86102, Apr. 2005.

[159] R. Xing, C. Luo, Z. Wang, and Y. Han, "Dewetting of polymethyl methacrylate on the patterned elastomer substrate by solvent vapor treatment," *Polymer (Guildf).*, vol. 48, no. 12, pp. 3574–3583, 2007.

[160] L. Courbin, E. Denieul, E. Dressaire, M. Roper, A. Ajdari, and H. A. Stone, "Imbibition by polygonal spreading on microdecorated surfaces," *Nat. Mater.*, vol. 6, no. 9, pp. 661–664, 2007.

[161] Z. Zhang, Z. Wang, R. Xing, and Y. Han, "How to form regular polymer microstructures by surface-pattern-directed dewetting," *Surf. Sci.*, vol. 539, no. 1, pp. 129–136, 2003.

[162] C. Luo, R. Xing, Z. Zhang, J. Fu, and Y. Han, "Ordered droplet formation by thin polymer film dewetting on a stripe-patterned substrate," *J. Colloid Interface Sci.*, vol. 269, no. 1, pp. 158–163, Jan. 2004.

[163] H. A. Biebuyck and G. M. Whitesides, "Self-Organization of Organic Liquids on Patterned Self-Assembled Monolayers of Alkanethiolates on Gold," *Langmuir*, vol. 10, no. 8, pp. 2790–2793, Aug. 1994.

[164] G. Krausch, "Surface induced self assembly in thin polymer films," *Mater. Sci. Eng. R Reports*, vol. 14, no. 1, p. v-94, 1995.

[165] M. Boltau, S. Walheim, J. Mlynek, G. Krausch, and U. Steiner, "Surface-induced structure formation of polymer blends on patterned substrates," *Nature*, vol. 391, no. 6670, pp. 877–879, Feb. 1998.

[166] C. Bauer and S. Dietrich, "Phase diagram for morphological transitions of wetting films on chemically structured substrates," *Phys. Rev. E*, vol. 61, no. 2, pp. 1664–1669, Feb. 2000.

[167] S. Herminghaus, A. Fery, and D. Reim, "Imaging of droplets of aqueous solutions by tapping-mode scanning force microscopy," *Ultramicroscopy*, vol. 69, no. 3, pp. 211–217, 1997.

[168] J. Heier, E. J. Kramer, S. Walheim, and G. Krausch, "Thin Diblock Copolymer Films on Chemically Heterogeneous Surfaces," *Macromolecules*, vol. 30, no. 21, pp. 6610–6614, Oct. 1997.

[169] R. García, M. Calleja, and F. Pérez-Murano, "Local oxidation of silicon surfaces by dynamic

force microscopy: Nanofabrication and water bridge formation," *Appl. Phys. Lett.*, vol. 72, no. 18, pp. 2295–2297, Apr. 1998.

[170] K. Kargupta and A. Sharma, "Templating of Thin Films Induced by Dewetting on Patterned Surfaces," *Phys. Rev. Lett.*, vol. 86, no. 20, pp. 4536–4539, May 2001.

[171] G. Nisato, B. D. Ermi, J. F. Douglas, and A. Karim, "Excitation of Surface Deformation Modes of a Phase-Separating Polymer Blend on a Patterned Substrate," *Macromolecules*, vol. 32, no. 7, pp. 2356–2364, Apr. 1999.

[172] H. Celio, E. Barton, and K. J. Stevenson, "Patterned Assembly of Colloidal Particles by Confined Dewetting Lithography," *Langmuir*, vol. 22, no. 26, pp. 11426–11435, Dec. 2006.

[173] B. K. Yoon, J. Huh, H.-C. Kim, J.-M. Hong, and C. Park, "Ordered Patterns of Microimprinted Bilayer Polymer Films with Controlled Dewetting and Layer Inversion," *Macromolecules*, vol. 39, no. 3, pp. 901–903, Feb. 2006.

[174] M. K. Kwak, K. H. Shin, E. Y. Yoon, and K. Y. Suh, "Fabrication of conductive metal lines by plate-to-roll pattern transfer utilizing edge dewetting and flexographic printing," *J. Colloid Interface Sci.*, vol. 343, no. 1, pp. 301–305, Mar. 2010.

[175] I. Karapanagiotis, D. F. Evans, and W. W. Gerberich, "Leveling and Dewetting Processes of Nanoindentation-Induced Defects on Thin Polymer Films," *Macromolecules*, vol. 34, no. 11, pp. 3741–3747, May 2001.

[176] I. Karapanagiotis, W. W. Gerberich, and D. F. Evans, "Early Dewetting Stages of Thin Polymer Films Initiated by Nanoindentation," *Langmuir*, vol. 17, no. 8, pp. 2375–2379, Apr. 2001.

[177] I. Karapanagiotis, D. F. Evans, and W. W. Gerberich, "Dynamics of the leveling process of nanoindentation induced defects on thin polystyrene films," *Polymer (Guildf).*, vol. 43, no. 4, pp. 1343–1348, Feb. 2002.

[178] C. Luo, R. Xing, and Y. Han, "Ordered pattern formation from dewetting of polymer thin film with surface disturbance by capillary force lithography," *Surf. Sci.*, vol. 552, no. 1, pp. 139–148, 2004.

[179] Y. S. Kim and H. H. Lee, "Selective Dewetting for General Purpose Patterning," *Adv. Mater.*, vol. 15, no. 4, pp. 332–334, 2003.

[180] S.-J. Choi, D. Tahk, and H. Yoon, “Spontaneous dewetting-induced residue-free patterning at room temperature,” *J. Colloid Interface Sci.*, vol. 340, no. 1, pp. 74–81, Dec. 2009.

[181] C. Luo, R. Xing, and Y. Han, “Ordered pattern formation from dewetting of polymer thin film with surface disturbance by capillary force lithography,” *Surf. Sci.*, vol. 552, no. 1–3, pp. 139–148, Mar. 2004.

[182] S. Stolnik, L. Illum, and S. S. Davis, “Long circulating microparticulate drug carriers,” *Adv. Drug Deliv. Rev.*, vol. 16, no. 2, pp. 195–214, 1995.

[183] B. G. Subramanian and V. N. Manoharan, “Ordered Macroporous Materials by Colloidal Assembly : A Possible Route to Photonic Bandgap Materials,” *Adv. Mater.*, vol. 11, no. 15, pp. 1261–1265, 1999.

[184] B. Luppi, T. Cerchiara, F. Bigucci, R. Basile, and V. Zecchi, “Polymeric nanoparticles composed of fatty acids and polyvinylalcohol for topical application of sunscreens,” *J pharm pharmacol*, vol. 56, no. 3, pp. 407–411, 2004.

[185] M. Elsabahy, G. S. Heo, S.-M. Lim, G. Sun, and K. L. Wooley, “Polymeric Nanostructures for Imaging and Therapy,” *Chem. Rev.*, vol. 115, no. 19, pp. 10967–11011, Oct. 2015.

[186] T. G. Mason, K. Ganesan, J. H. van Zanten, D. Wirtz, and S. C. Kuo, “Particle Tracking Microrheology of Complex Fluids,” *Phys. Rev. Lett.*, vol. 79, no. 17, pp. 3282–3285, Oct. 1997.

[187] D. R. Paul and L. M. Robeson, “Polymer nanotechnology: Nanocomposites,” *Polymer (Guildf).*, vol. 49, no. 15, pp. 3187–3204, Jul. 2008.

[188] R. H. Ottewill, *An Introduction to Polymer Colloids*. Dordrecht: Springer Netherlands, 1990.

[189] T. Sugimoto, “Preparation of monodispersed colloidal particles,” *Adv. Colloid Interface Sci.*, vol. 28, pp. 65–108, 1987.

[190] J. W. Goodwin, J. Hearn, C. C. Ho, and R. H. Ottewill, “Studies on the preparation and characterisation of monodisperse polystyrene laticee,” *Colloid Polym. Sci.*, vol. 252, no. 6, pp. 464–471, 1974.

[191] Y. Yin and Y. Xia, “Self-Assembly of Monodispersed Spherical Colloids into Complex Aggregates with Well-Defined Sizes, Shapes, and Structures,” *Adv. Mater.*, vol. 13, no. 4, pp. 267–271, 2001.

[192] T. Lopez-Leon, V. Koning, K. B. S. Devaiah, V. Vitelli, and A. Fernandez-Nieves, “Frustrated nematic order in spherical geometries,” *Nat Phys*, vol. 7, no. 5, pp. 391–394, May 2011.

[193] D. Dendukuri, S. S. Gu, D. C. Pregibon, T. A. Hatton, and P. S. Doyle, “Stop-flow lithography in a microfluidic device,” *Lab Chip*, vol. 7, no. 7, pp. 818–828, 2007.

[194] J. P. Rolland, B. W. Maynor, L. E. Euliss, A. E. Exner, G. M. Denison, and J. M. DeSimone, “Direct Fabrication and Harvesting of Monodisperse, Shape-Specific Nanobiomaterials,” *J. Am. Chem. Soc.*, vol. 127, no. 28, pp. 10096–10100, Jul. 2005.

[195] S. Xu, Z. Nie, M. Seo, P. Lewis, E. Kumacheva, H. A. Stone, P. Garstecki, D. B. Weibel, I. Gitlin, and G. M. Whitesides, “Generation of monodisperse particles by using microfluidics: control over size, shape, and composition,” *Angew Chem Int Ed Engl*, vol. 44, no. 5, pp. 724–728, 2005.

[196] D. Dendukuri, K. Tsoi, T. A. Hatton, and P. S. Doyle, “Controlled Synthesis of Nonspherical Microparticles Using Microfluidics,” *Langmuir*, vol. 21, no. 6, pp. 2113–2116, Mar. 2005.

[197] C. C. Ho, R. H. Ottewill, A. Keller, and J. A. Odell, “Monodisperse ellipsoidal polystyrene latex particles: Preparation and characterisation,” *Polym. Int.*, vol. 30, no. 2, pp. 207–211, 1993.

[198] L. Zheng, P. Huang, L. Zhang, D. Guo, and Q. Yan, “Facile Fabrication of Anisotropic Colloidal Particles with Controlled Shapes and Shape Dependence of Their Elastic Properties,” *Part. Part. Syst. Charact.*, vol. 33, no. 11, pp. 842–850, 2016.

[199] C. C. H, A. Keller, J. A. Odell, and R. H. Ottewill, “Preparation of monodisperse ellipsoidal polystyrene particles,” *Colloid Polym. Sci.*, vol. 479, no. 1993, pp. 469–479, 1986.

[200] K. M. Keville, J. M. Caruthers, and E. I. Franses, “Characterization of dimensions of ellipsoidal microparticles via electron microscopy,” *J. Microsc.*, vol. 142, no. 3, pp. 327–340, 1986.

[201] C. C. Ho, M. J. Hill, and J. A. Odell, “Morphology of ellipsoidal latex particles,” *Polymer (Guildf).*, vol. 34, no. 10, pp. 2019–2023, 1993.

[202] M. K. Klein, N. Klinkenberg, S. Schuetter, N. Saenger, P. Pfleiderer, and A. Zumbusch, “PMMA/PMMA Core–Shell Particles with Ellipsoidal, Fluorescent Cores: Accessing Rotational Dynamics,” *Langmuir*, vol. 31, no. 9, pp. 2655–2661, Mar. 2015.

[203] Y. Li, Y. Deng, Y. He, X. Tong, and X. Wang, “Amphiphilic Azo Polymer Spheres, Colloidal

Monolayers, and Photoinduced Chromophore Orientation," *Langmuir*, vol. 21, no. 14, pp. 6567–6571, Jul. 2005.

[204] Y. Li, Y. He, X. Tong, and X. Wang, "Photoinduced Deformation of Amphiphilic Azo Polymer Colloidal Spheres," *J. Am. Chem. Soc.*, vol. 127, no. 8, pp. 2402–2403, Mar. 2005.

[205] Y. Li, Y. Deng, X. Tong, and X. Wang, "Formation of Photoresponsive Uniform Colloidal Spheres from an Amphiphilic Azobenzene-Containing Random Copolymer," *Macromolecules*, vol. 39, no. 3, pp. 1108–1115, Feb. 2006.

[206] E. Ortyl, S. Zielinska, R. Barillé, Y. Almohamed, and J.-M. Nunzi, "Instantaneous photoinduced patterning of an azopolymer colloidal nanosphere assembly," *Opt. Mater. Express*, vol. 6, no. 9, p. 2925, Sep. 2016.

[207] R. Barillé, P. Tajalli, S. Kucharski, E. Ortyl, and J.-M. Nunzi, "Photoinduced deformation of azopolymer nanometric spheres," *Appl. Phys. Lett.*, vol. 96, no. 16, p. 163104, 2010.

[208] Y. Xia and G. M. Whitesides, "Soft lithography," *Annu. Rev. Mater. Sci.*, vol. 28, pp. 153–184, 1998.

[209] J. Bingi and V. M. Murukeshan, "Speckle lithography for fabricating structures and black silicon structures," *Nat. Publ. Gr.*, vol. 5, no. 18452, pp. 1–9, 2015.

Appendix A:

IV.1. Introduction

In a first experiment we characterized, via optical diffraction, the microscopic elongation of nanocavities, induced by a macroscopic stretching of the elastomeric quasi-crystal. This leads to a tunable periodicity of the diffraction grating and consequently the manipulation of the size of nanocavities formed on the surface of elastomer

Beside the experimental results of the 2D Quasi-crystal structures and their replicas on PDMS, few simulations were also done to obtain a mathematical description and evaluation of the structures and their evolution.

IV.1.1. Mathematical Description of the SRG

The PDMS surface acts as a phase grating. Indeed, PDMS istransparent in the visible part of the spectrum and consequentlydoesn't absorb light, however, it changes its phase.

The main hypothesis for this mathematical description of thesample is that the SRGs created by the light interference patterncreate sinusoidal height modulation on the azo-polymer surface.These modulation are then replicated on the PDMS surface.

IV.1.1.1. 1Dsinusoidal phase grating

At 1D, the surface can be depicted as in fig.IV.1-1.The transmittance of the grating can be written

$$t_g(x) = \exp\left[j\frac{m}{2}\sin\left(2\pi\frac{x}{\Lambda}\right)\right] \qquad \text{(IV.1-1)}$$

With :

- $j = \sqrt{-1}$
- $m = 2\pi\dfrac{(n_{PDMS} - 1)s}{\lambda_r}$ (IV.1-2)

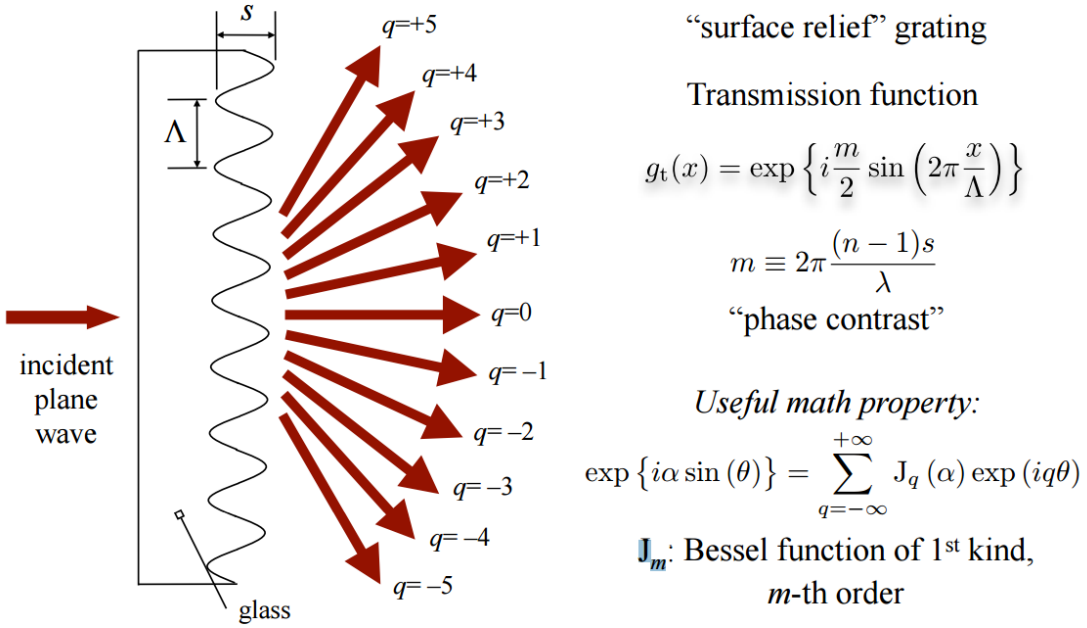

Fig. IV.1-1 : Modeling of the 1D sinusoidal phase grating surface. From George Barbastathis, Colin Sheppard, and Se Baek Oh.2.71 Optics. Spring 2009. Massachusetts Institute of Technology: MIT OpenCourseWare, https://ocw.mit.edu. License: Creative Commons BY-NC-SA.

is the phase contrast of the grating with :

1. n_{PDMS} isthe refractive index of PDMS (taken as 1.4)

2. λ_r the reading wavelength

3. s the peak-to-peak amplitude of the grating (its heightin nm)

· Λ is the pitch of the grating

· x is the abscissa along the 1D grating.

Indeed, the phase shift correpond to the amount of PDMSthat the wave has crossed. If we take, for phase reference, thelowest point on the sinusoid, then the additional thickness d ofcrossed PDMS for a point at[1]x is equal[2]to:

$$d(x) = \frac{s}{2}\sin(2\pi \frac{x}{L}) + (\frac{s}{2})$$

The associated phase shift is equal to:

$$\Delta\Phi_{PDMS} = 2\pi\, n_{PDMS} \frac{d(x)}{\lambda_r}$$

Interferences arise from phase shift of two wave and consequently we have to compare the phase shift of a beam crossingthe thickness d(x) of PDMS to the phase shift of a beam crossingthe same amount of air (n_{air}= 1)

$$\Delta\Phi_{air} = 2\pi\, n_{air} \frac{d(x)}{\lambda_r} = 2\pi \frac{d(x)}{\lambda_r}$$

In the end, the total phase shift is:

$$\Delta\Phi = 2\pi \frac{(n_{PDMS} - 1)}{\lambda_r} d(x) = 2\pi \frac{(n_{PDMS} - 1)}{\lambda_r} \frac{s}{2}\sin\left(2\pi \frac{x}{L}\right) = \frac{m}{2}\sin\left(2\pi \frac{x}{L}\right) \qquad \text{(IV.1-3)}$$

and consequently tg(x) is:

$$t_g(x) = \exp[j\Delta\Phi] = \exp\left[j \frac{m}{2}\sin\left(2\pi \frac{x}{L}\right)\right]$$

This expression can be rewritten[3]using bessel function, J, of the first kind:

---

[1]Taking for the origin of the x axis such as sin(x) = 0

[2]sinus is comprised between -1 and 1, or between 0 and 2 with the shift,hencethe division by 2 for s/2

[3]we have the identity :

$$\exp[j\beta \sin(\theta)] = \sum_{q=-\infty}^{\infty} J_q(\beta)\exp[jq\theta]$$

$$t_g(x) = \sum_{q=-\infty}^{+\infty} J_q\left(\frac{m}{2}\right)\exp\left[jq2\pi\frac{x}{\Lambda}\right] \qquad \text{(IV.1-4)}$$

Physically, each q term of the sum correspond to a plane wave propagating with the angle $\sin\theta = q\frac{\lambda_r}{\Lambda}$, that is to say onediffraction order of the grating.

Fraunhoffer's diffraction pattern is the Fourier transform ofthe transmittance of the object. The Fourier transform of thefunction exp [jx$_0$] is:

$$TF\left[\exp\left[j2\pi\frac{1}{\Lambda}x\right]\right] = \delta\left(k_x - \frac{1}{\Lambda}\right) = \delta\left(k_x - f_r\right) \qquad \text{(IV.1-5)}$$

Where:

- k_x is the relative variable[4] in the Fourier space : it is an angular frequency.
- δ is Dirac function.
- $f_r = \frac{1}{\Lambda}$ is the spatial frequency of the grating

The Fourier transform of the transmittance can be written as:

$$TF\left(t_g(x)\right) = TF\left[\sum_{q=-\infty}^{+\infty} J_q\left(\frac{m}{2}\right)\exp\left[jq2\pi\frac{x}{\Lambda}\right]\right] = \sum_{q=-\infty}^{+\infty} J_q\left(\frac{m}{2}\right)TF\left[\exp\left[jq2\pi\frac{x}{\Lambda}\right]\right] \qquad \text{(IV.1-6)}$$

Consequently, the light vibration amplitude U(k_x) is (viaequation IV.1-5) :

$$U(k_x) = TF\left(t_g(x)\right) = \sum_{q=-\infty}^{+\infty} J_q\left(\frac{m}{2}\right)\delta\left(k_x - \frac{q}{\Lambda}\right) \qquad \text{(IV.1-7)}$$

---

[4]

$$a(x) = \int_{-\infty}^{+\infty} A(k_x)\, e^{j2\pi k_x x}\, dk_x$$

If we put a screen at distance D from the diffracting object,the spatial frequency k_x give rise to a measurable distance. More precisely, the function $\delta\left(k_x - \frac{q}{\Lambda}\right)$ is a point in the angular frequency space. It means than a plane wave (i.e. a beam) is propagating out of the grating with the angular frequency $k_x = q\Lambda$,or, stated differently, with the angle θ_q such as:

$$\sin\theta_q = q\frac{\lambda_r}{\Lambda}$$

The beam creats a spot on the screen at position X as:

$$\tan\theta_q = \frac{X}{D}$$

Finally, the special frequency $k_x = \frac{1}{\Lambda}$ creates a position X such as:

$$X = D\tan\left[\arcsin\left(q\frac{\lambda_r}{\Lambda}\right)\right] \qquad \text{(IV.1-8)}$$

Conversely, if we measure X, we have access to the spatial frequency $f_r = \frac{1}{\Lambda}$ via:

$$\frac{1}{\Lambda} = \frac{1}{q\lambda_r}\sin\left[\arctan\left(\frac{X}{D}\right)\right] \qquad \text{(IV.1-9)}$$

The screen where the diffraction pattern is formed has the same axis of frequency kx with a magnification factor given by formula IV.1-8. If we go back to the electrical field (eq IV.1-7), we obtain the normalized intensity with the square of the electrical field. Strictly speaking, we have:

$$I(k_x) = |U(k_x)|^2 = \left[\sum_{q=-\infty}^{+\infty} J_q\left(\frac{m}{2}\right)\delta\left(k_x - \frac{q}{\Lambda}\right)\right]^2$$

In principle, we should consider all double products of the form $J_0\,J_1$. However, thanks to the delta function all these double products are canceled out because the different points, q/Λ, in the frequency space are never superposed and consequently they can't be non-zero at the same time. Consequently, we have:

$$I(k_x)=\left(\sum_{q=-\infty}^{\infty} J_q\left(\frac{m}{2}\right)\delta\left(k_x-\frac{q}{\Lambda}\right)\right)^2 \approx \sum_{q=-\infty}^{\infty}\left(J_q\left(\frac{m}{2}\right)\delta\left(k_x-\frac{q}{\Lambda}\right)\right)^2 \qquad \text{(IV.1-10)}$$

Which, if we limit the sum to the first terms, gives:

$$I(k_x)=\underbrace{J_0^2\left(\frac{m}{2}\right)\delta(0)}_{Order\ 0}+\underbrace{J_{-1}^2\left(\frac{m}{2}\right)\delta\left(k_x+\frac{1}{\Lambda}\right)}_{Order\ -1}+\underbrace{J_1^2\left(\frac{m}{2}\right)\delta\left(k_x-\frac{1}{\Lambda}\right)}_{Order\ 1}+\ldots$$

IV.1.1.2. 2D sinusoidal phase grating

We have to adapt the transmittance (eqIV.1-1) :

$$t_g(x,y)=\exp\left[j\frac{m}{2}\sin\left(2\pi\frac{\cos(\alpha)\,x+\sin(\alpha)\,y}{\Lambda}\right)\right] \qquad \text{(IV.1-11)}$$

α is the angle of the grating relative to the axis x. Which can be rewritten[5] as:

$$t_g(x,y)=\exp\left[j\frac{m}{2}\sin\left(\mathbf{K}_{ff}\,\mathbf{r}\right)\right] \qquad \text{(IV.1-12)}$$

With:

- K_{ff}, the wave vector of the grating with :

$$\mathbf{K}_{ff}=\frac{2\pi}{\Lambda}\left(\cos\alpha\,\mathbf{e}_x+\sin\alpha\,\mathbf{e}_y\right)$$

[5]vectors are in bold

· r = $xe_x + ye_y$, the position vector on the plan defined bythe 2D grating.

Using once again the Bessel functions:

$$t_g(x,y) = \sum_{q=-\infty} J_q\left(\frac{m}{2}\right)\exp\left[jq K_{ff} r\right] = \sum_{q=-\infty} J_q\left(\frac{m}{2}\right)\exp\left[jq\,2\pi \frac{\cos(\alpha)\,x}{\Lambda}\right]\exp\left[jq\,2\pi \frac{\sin(\alpha)\,y}{\Lambda}\right] \quad \text{(IV.1-13)}$$

Then, the Fourier transform of the grating becomes:

$$U(k_x,k_y) = \sum_{q=-\infty} J_q\left(\frac{m}{2}\right)\delta\left(k_x - \frac{\cos(\alpha)}{\Lambda}\right)\delta\left(k_y - \frac{\sin(\alpha)}{\Lambda}\right)$$

For each order q, we have, in the frequency space, a point atcoordinates (cos α/Λ, sin α/Λ). For instance, for α = 0, that isto say a grating with a vector K_{ff} parallel to the axis x, or stateddifferently; with vertical fringes (along y), we have a point atcoordinate (1/Λ, 0), that is to say on axis x.

As before, this point in the angular frequency space gives torise to a beam that creates a spot on a screen, placed at distance D, at the coordinate (X, Y) such as:

$$X = D\tan\left[\arcsin\left(q\frac{\lambda_r \cos\alpha}{\Lambda}\right)\right]$$

$$Y = D\tan\left[\arcsin\left(q\frac{\lambda_r \sin\alpha}{\Lambda}\right)\right] \quad \text{(IV.1-14)}$$

And we also have:

$$\frac{1}{\Lambda} = \frac{1}{q\cos\alpha\, l_r}\sin\left[\arctan\left(\frac{X}{D}\right)\right] = \frac{1}{q\sin\alpha\, l_r}\sin\left[\arctan\left(\frac{Y}{D}\right)\right] \qquad \text{(IV.1-15)}$$

$$I(k_x,k_y) = \sum_{q=-\infty}^{+\infty}\left[J_q\left(\frac{m_i}{2}\right)\delta\left(k_x - \frac{q\cos\alpha}{\Lambda}\right)\delta\left(k_y - \frac{q\sin\alpha}{\Lambda}\right)\right]^2$$

IV.1.1.3. Sum of 2D sinusoidal phase gratings

Assuming there are no interactions between the N gratings, we have to sum the transmittances of all of them:

$$t_g(x,y) = \sum_{i=0}^{N}\exp\left[j\frac{m_i}{2}\sin\left(2\pi\frac{\cos(\alpha_i)\,x + \sin(\alpha_i)\,y}{\Lambda_i}\right)\right] = \sum_{i=0}^{N}\exp\left[j\sin\left(\frac{m_i}{2}K_{ff}\,r\right)\right] \qquad \text{(IV.1-16)}$$

Then:

$$U(k_x,k_y) = \sum_{i=0}^{N}\sum_{q=-\infty}^{+\infty} J_q\left(\frac{m_i}{2}\right)\left[\delta\left(k_x - \frac{q\cos(\alpha_i)}{\Lambda_i}\right)\delta\left(k_y - \frac{q\sin(\alpha_i)}{\Lambda_i}\right)\right]$$

And finally:

$$I(k_x,k_y) = \sum_{i=0}^{N}\sum_{q=-\infty}^{+\infty}\left[J_q\left(\frac{m_i}{2}\right)\delta\left(k_x - \frac{q\cos\alpha_i}{\Lambda_i}\right)\delta\left(k_y - \frac{q\sin\alpha_i}{\Lambda_i}\right)\right]^2$$

In our experiment, as soon as N > 2, the orders with q > 1are note visible anymore and we can write[6]:

$$I(k_x,k_y) \approx \sum_{i=0}^{N} J_0^2\left(\frac{m_i}{2}\right)\delta(0) + J_1^2\left(\frac{m_i}{2}\right)\left[\delta\left(k_x + \frac{\cos\alpha_i}{\Lambda_i}\right)\delta\left(k_y + \frac{\sin\alpha_i}{\Lambda_i}\right) + \delta\left(k_x - \frac{\cos\alpha_i}{\Lambda_i}\right)\delta\left(k_y - \frac{\sin\alpha_i}{\Lambda_i}\right)\right] \qquad \text{(IV.1-17)}$$

[6]With $J_{-1}^2(x) = J_1^2(x)$

IV.1.1.4. Sinusoidal grating amplitude from intensity measurements

From the intensity of the diffracted spots, we get a relative scalebetween the different value of s_i. If we want an absolute scalefor the s_i, we have to measure the ratio, γ_i, of the intensity ofthe order 0 beam, I_0, and the intensity of one of the first orders,$I_1(i)$, beam, that is to say :

$$g_i = \frac{I_1(i)}{I_0} = \frac{J_1^2\left(m_i/2\right)}{\sum_{i=0}^{N} J_0\left(m_i/2\right)^2}$$

Then, we can make two estimations:

- The diffraction efficiency is very small. All the light's energy is with the 0th order and consequently all $J_0(m_i/2)^2$ Term are almost equal :

$$\sum_{i=0}^{N} J_0\left(m_i/2\right)^2 \approx N J_0\left(m/2\right)^2$$

Where m is the mean phase contrast.

Consequently:

$$g_i = \frac{I_1(i)}{I_0} \approx \frac{J_1^2\left(m_i/2\right)}{N J_0\left(m/2\right)^2} \qquad \text{(IV.1-18)}$$

- The phase contrast values, m_i, are also small and we can use the asymptotic form[7]of the Bessel function J_1 :

$$J_1^2(x) \approx \frac{x^2}{4} \qquad \text{(IV.1-19)}$$

If we summarize:

---

[7] $J_a(x) \approx \frac{1}{\Gamma(a+1)}\left(\frac{x}{2}\right)^a$ With α = 1 and Γ (2) = 1, consequently we have $J_1^2(x) \approx \left(\frac{x}{2}\right)^2$, which is very good approximation up to x = 0.25 (less than 2% of relative error)

· From the measurement of γ_i (cf eq. IV.1-18), via a numerical resolution (for instance dichotomy), we have access to the phase contrast, m_i, of grating i and consequently to the absolute peak-to-peak amplitude, s_i, of grating i, from the formula IV.1-2.

· The relative peak-to-peak amplitude, s_i and s_j, between two sinusoidal gratings can be deduced from their relative intensities, I_j and I_i, respectively, using the formula IV.1-19 :

$$s_j = \sqrt{\frac{I_j}{I_i}} s_i \qquad \text{(IV.1-20)}$$

Let's stress the fact that this relation is not linear.

IV.2. Optical Height Measurement of the SRG

As explained from the previous section, the relative intensity measurement between the 0th order of diffraction and one of the diffracted spots permit us to measure the height of one of the sinusoidal gratings composing the SRG.

These measurements were done with a Si photodiode (Thor-labs DET100A). Since the 0th order beam is 4 order of magnitude more intense than the diffracted spot, the intensity measurement for the 0th beam requires a calibrated attenuation of the reading laser. We have used two partially crossed polarizer and applied Malus law to precisely determine this attenuation.

Experimentally, we have found, for a 6-fold PDMS SRG a value of $\gamma_1 = 1.1.10^{-4} \pm 1.10^{-5}$, leading to $s_1 = 5 \pm 0.5$ nm.

The absolute values of s_2 and s_3 are obtained via the intensity of the diffraction pattern with the camera and through applying formula IV.1-20.

The PDMS surface is then reconstructed from the diffraction pattern and the height of the cavities are around 15nm, which isin good agreement with the AFM measurements.

IV.3. AFM and optical measurements on PDMS replica of azopolymer SRG

The AFM measurement of the PDMS replica of a 8-fold quasi-crystal structure, (similar to the sample presented on Fig.III.1-1e)) is shown on Fig.IV.3-1. The PDMS surface is a fairly good reproduction of the initial SRG as suggested by the eight spots pattern on the FFT of the AFM image. The height distribution is a Gaussian centered on 32nm.

Fig.IV.3-2 shows the comparison of the FFT of AFM image of azo-SRG (a), the FFT of AFM image of the PDMS replica (b), and the optical measurement of the diffraction pattern obtained on the PDMS replica. The three figures, that correspond to a 8-fold quasi-crystal structure, are very similar. Moreover, the mathematical reconstruction of the PDMS SRG via the optical diffraction measurements leads to the same surface structure as the AFM measurement (Fig.IV.3-1).

Additionally, we have measured the ratio of the intensity of the zeroth order non diffracting optical spot to each of the other diffraction spots. This measurement leads to an optical measurement of the physical height of each SRG, which is in good agreement with the experimental AFM measurements (Fig.IV.3-1).

Consequently, we can say that AFM and optical measurements of the diffraction patterns lead to the same results after characterization of the surfaces of these samples. Nonetheless, optical measurements have one major advantage: these measurement are faster and thus permit one to study the modification of the quasi-crystal during the stretching of the PDMS sample in real time.

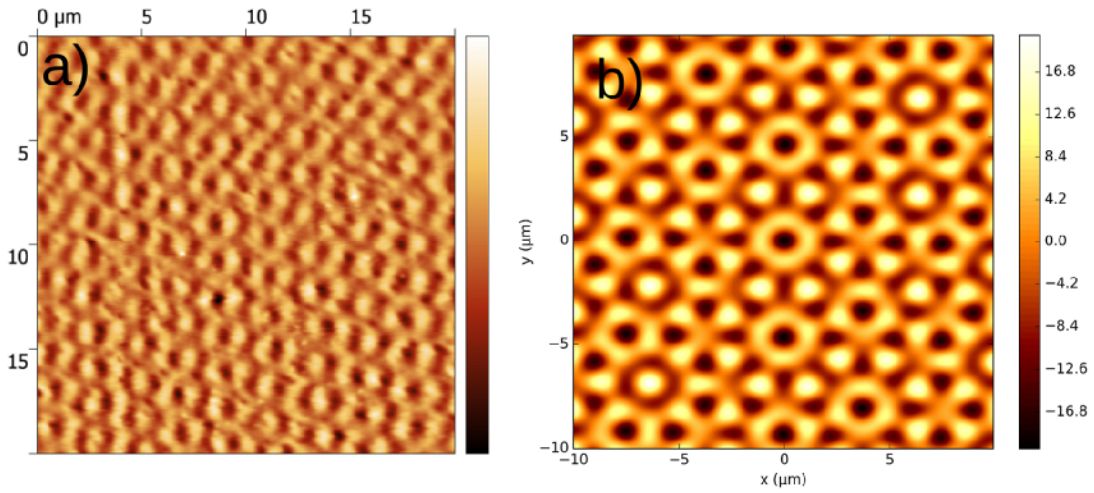

Fig. IV.3-1 : Surface of a 8-fold PDMS quasi-crystal a) measuredwith AFM b) reconstructed from optical measurements.

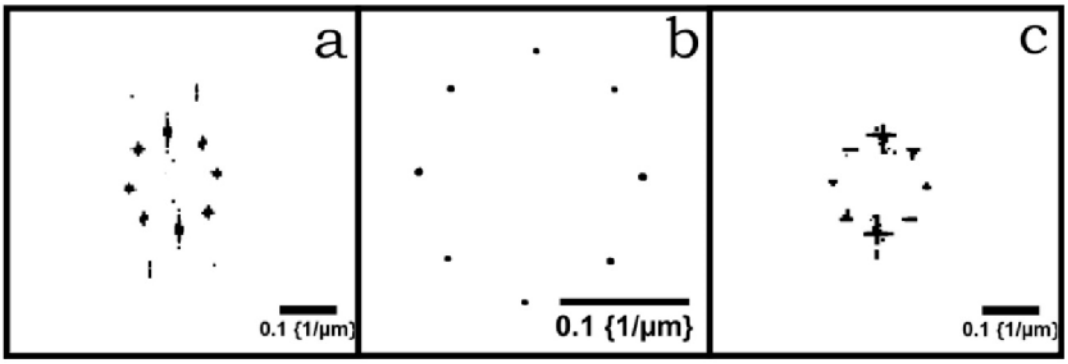

Fig. IV.3-2 : a) FFT of the azopolymer 8-fold quasi-crystal surface measured by AFM. b)Optical Diffraction pattern of a 8-fold quasi-crystal. c) FFT of the PDMS replica of 8-foldquasi-crystal surface measured by AFM

IV.4. Quantitative analysis of the evolution of the nanocavities dimensions with stretching the PDMS quasi-crystal

A more detailed analysis of the diffraction pattern, shown in section 3.1.4, is conducted in order to have a more deep understanding of the reconfiguration of the quasi-crystal during stretching. In particular, for each spot, we measure:

1. The distance from the center, in order to recover the pitch of the i-th SRG, Λ_i

2. The angle between its position relative to the x axis, in order to recover the angle, α_i, of the corresponding SRG.

3. The intensity, in order to determine the height, s_i , of the corresponding SRG.

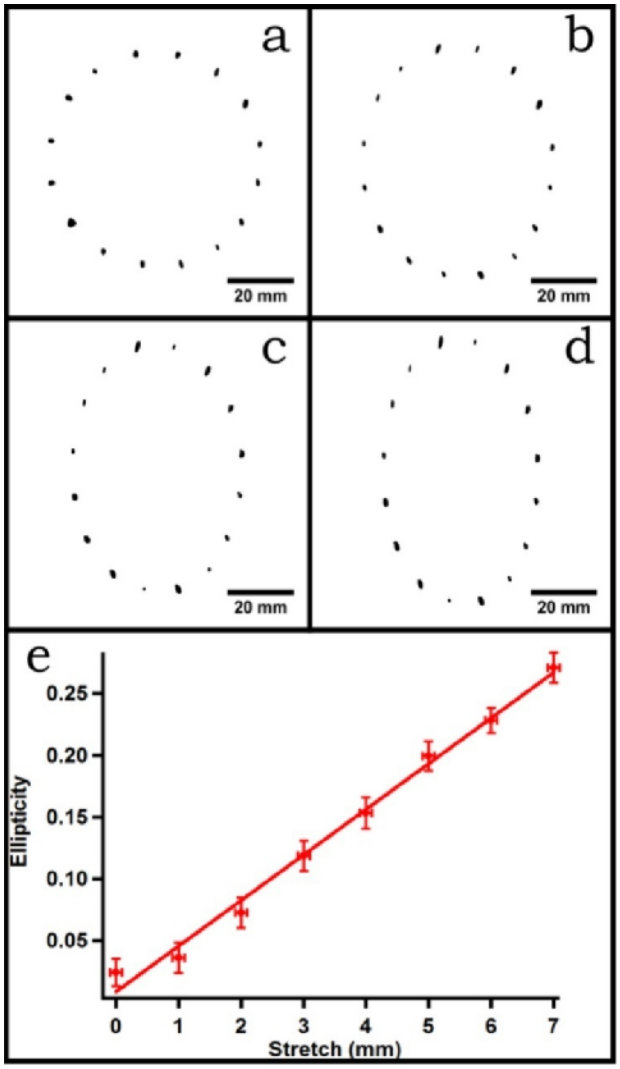

Fig. IV.4-1 : a) Initial diffraction pattern for a 16-fold quasi-crystal structure. b,c,d) Diffractionpattern of a 16-fold quasi-crystal after respectively 2mm, 4mm and 6mm of stretch in adirection corresponding to the horizontal direction of the picture e) Evolution the diffractionpattern ellipticity with the stretch

The optical measurements $\{\alpha_i, s_i, \Lambda_i\}$ are used as parameters for the equation IV.5-1. In one optical measurement, we are able to reconstruct the surface of the stretched PDMS quasi-crystal.

Using the methods explained in section, we have access to the dimensions of each kind of nanocavities formed on the surface of the PDMS replica.

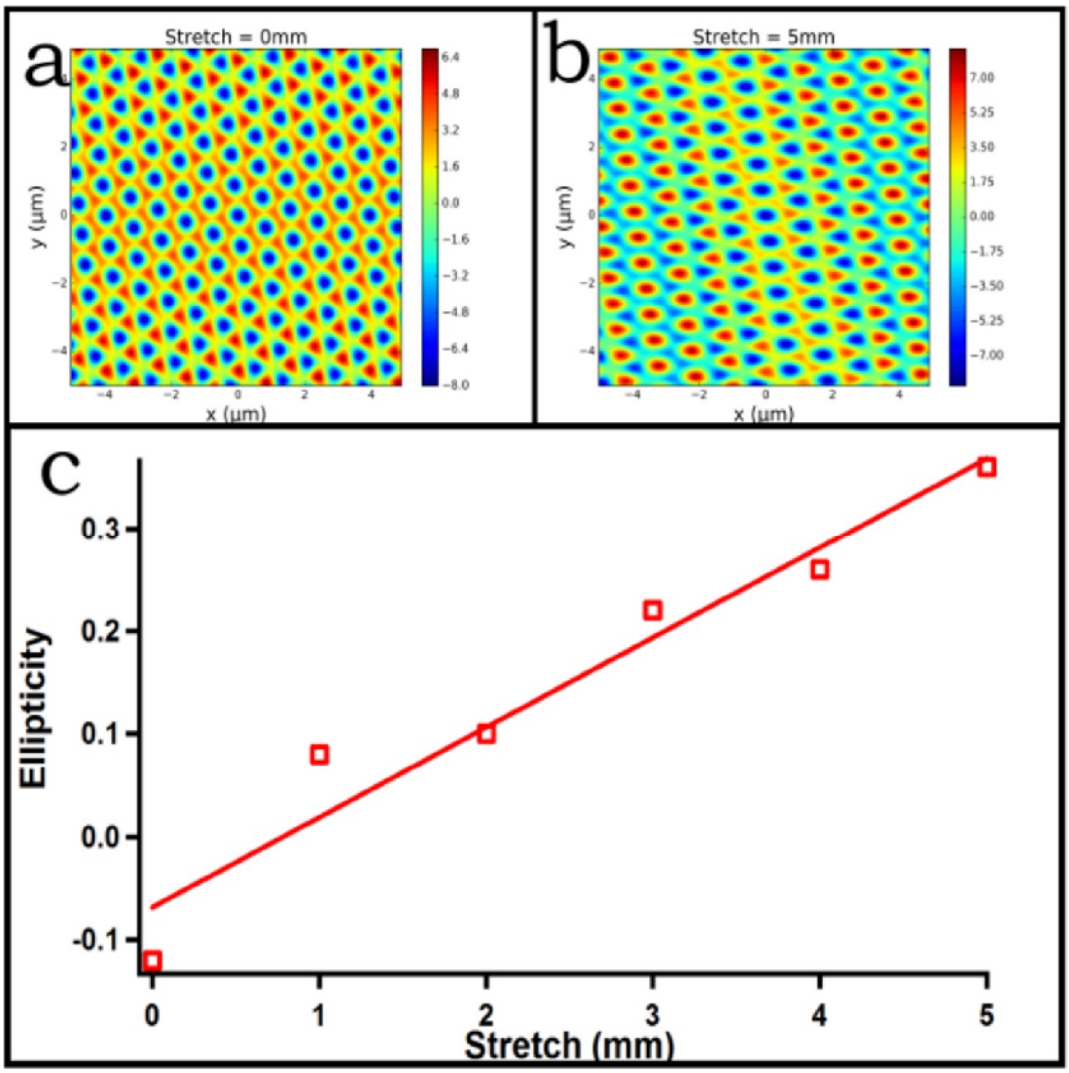

Fig. IV.4-2 : 3-fold quasi-crystal SRG on PDMS with no stretch (a) and 5mm of stretch (b),reconstructed from optical diffraction measurement. (c) Evolution of the ellipticity of thecentral nanocavity with the stretch ; the long axis of the ellipsoid goes from to 280nm to400nm and the short axis from 320 to 260nm.

We have performed these measurements on different kind of SRGs. Fig.IV.4-2 presents the evolution of the topography of the 6-fold quasi-crystal SRG on PDMS, reconstructed from the optical measurements. A 6-fold quasi-crystal structure is particularly interesting for single particle deposition applications. Indeed, the azo surface of 6-fold quasi-crystal pattern is made of evenly spaced hills that transfer to evenly spaced valley for to the PDMS replica (see Fig.III.1-2 d&e).

From Fig.IV.4-2 a&b we can see that the macroscopic stretching directly translate to a microscopic stretching of the cavities. Fig.IV.4-2c shows the quasi-linear evolution of the ellipticity of the nanocavities during streching. For instance, for 5mm of stretch, the central nanocavity is elongated by 40% in the direction of stretching and is compressed by 20% in the direction perpendicular to the stretching.

A similar evolution is seen with a 4-fold quasi-crystal structure, with an interesting transition from cavity to a canal during the stretching (Fig.IV.4-3). However, the situation is more complicated for n-fold (n > 8) SRGs. As it can be seen in Fig.IV.4-5, evolution of the surface of a 8-fold quasi-crystal SRG on PDMS leads to a complex remodeling of the surface. This effect is mainly due to the fact that cavities can coalesce during this process, cavities can transform to hills and vice versa. Whereas, it complicates the particle deposition process, it would be interesting to see if this remodeling of the surface would permit performing a sub-micron transportation of single nanoparticle from one cavity to another.

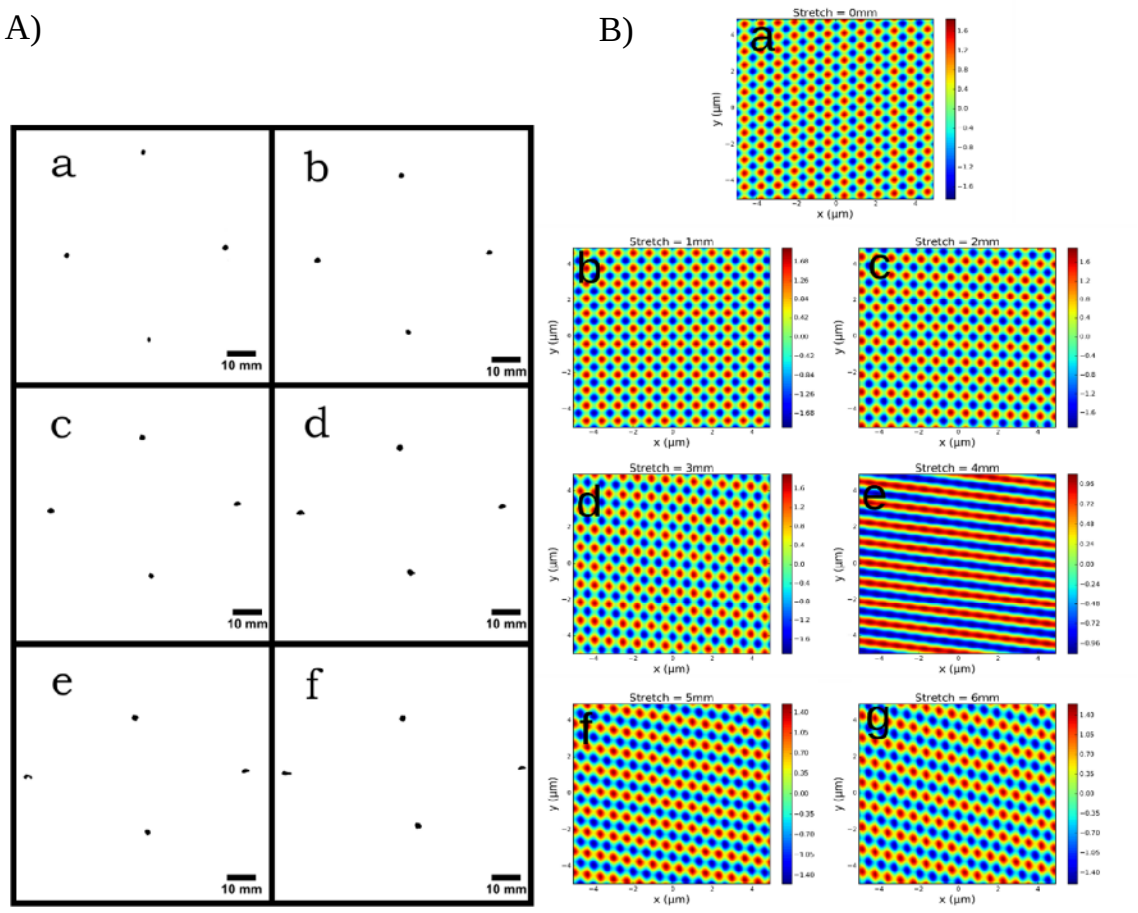

Fig. IV.4-3 : A) Evolution of 4-fold PDMS SRG diffraction patternwith stretching. a) no stretching b-g) stretching 1 mm to 6mm B) Evolution of the 4-folds quasi-crystal SRG on PDMS with a) 0mm, b) 1mm, c) 2mm, d) 3mm, e) 4mm, f) 5mm and g) 6mm of stretching

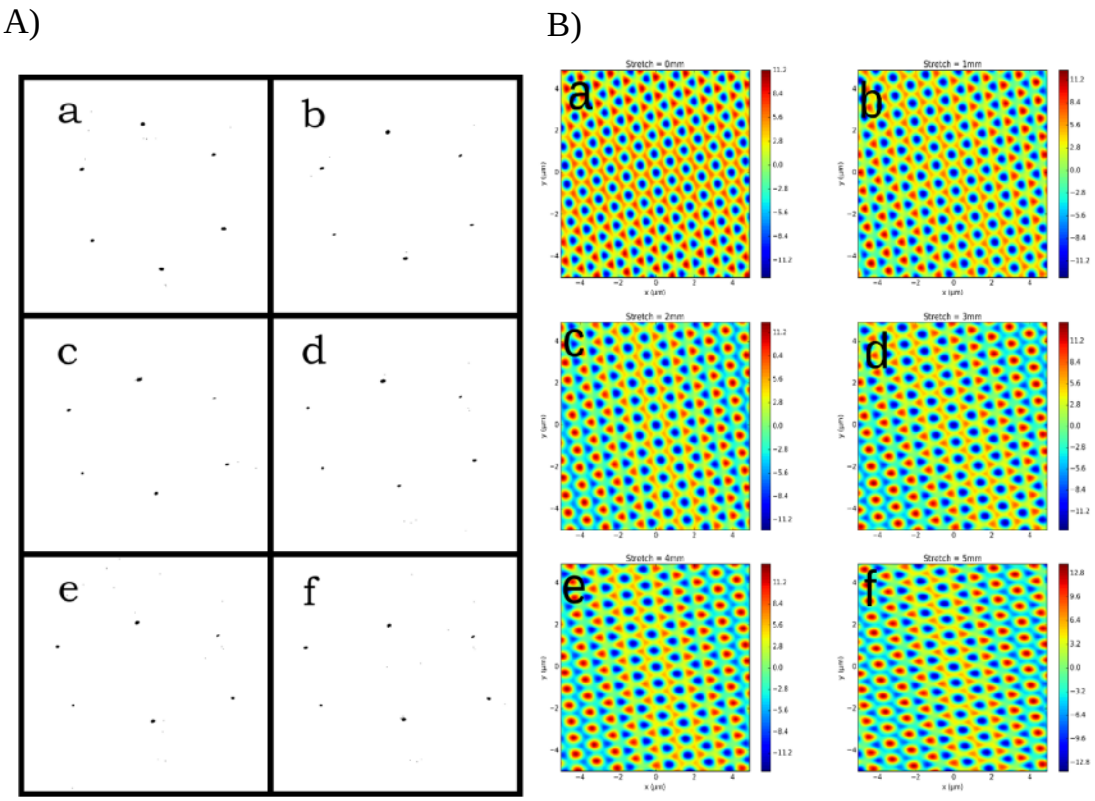

Fig. IV.4-4 : A) Evolution of 6-fold PDMS SRG diffraction patternwith stretching. a) no stretching b-g) stretching 1 mm to 5mm B) Evolution of the 6-folds quasi-crystal SRG on PDMSwith a) 0mm, b) 1mm, c) 2mm, d) 3mm, e) 4mm and f) 5mm ofstretching

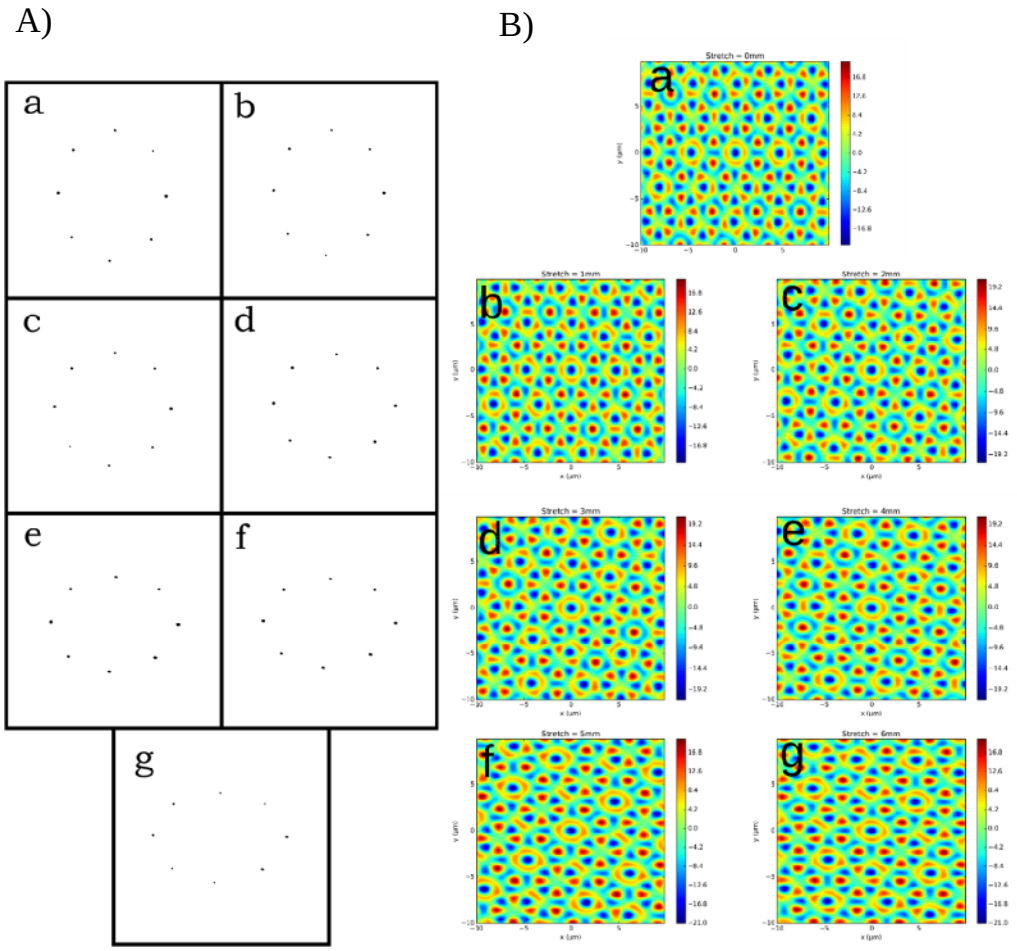

Fig. IV.4-5 : A) Evolution of 8-fold PDMS SRG diffraction patternwith stretching. a) no stretching b-g) stretching 1 mm to 6mm B) Evolution of the 8-folds quasi-crystal SRG on PDMSwith a) 0mm, b) 1mm, c) 2mm, d) 3mm, e) 4mm, f) 5mm and g)6mm of stretching

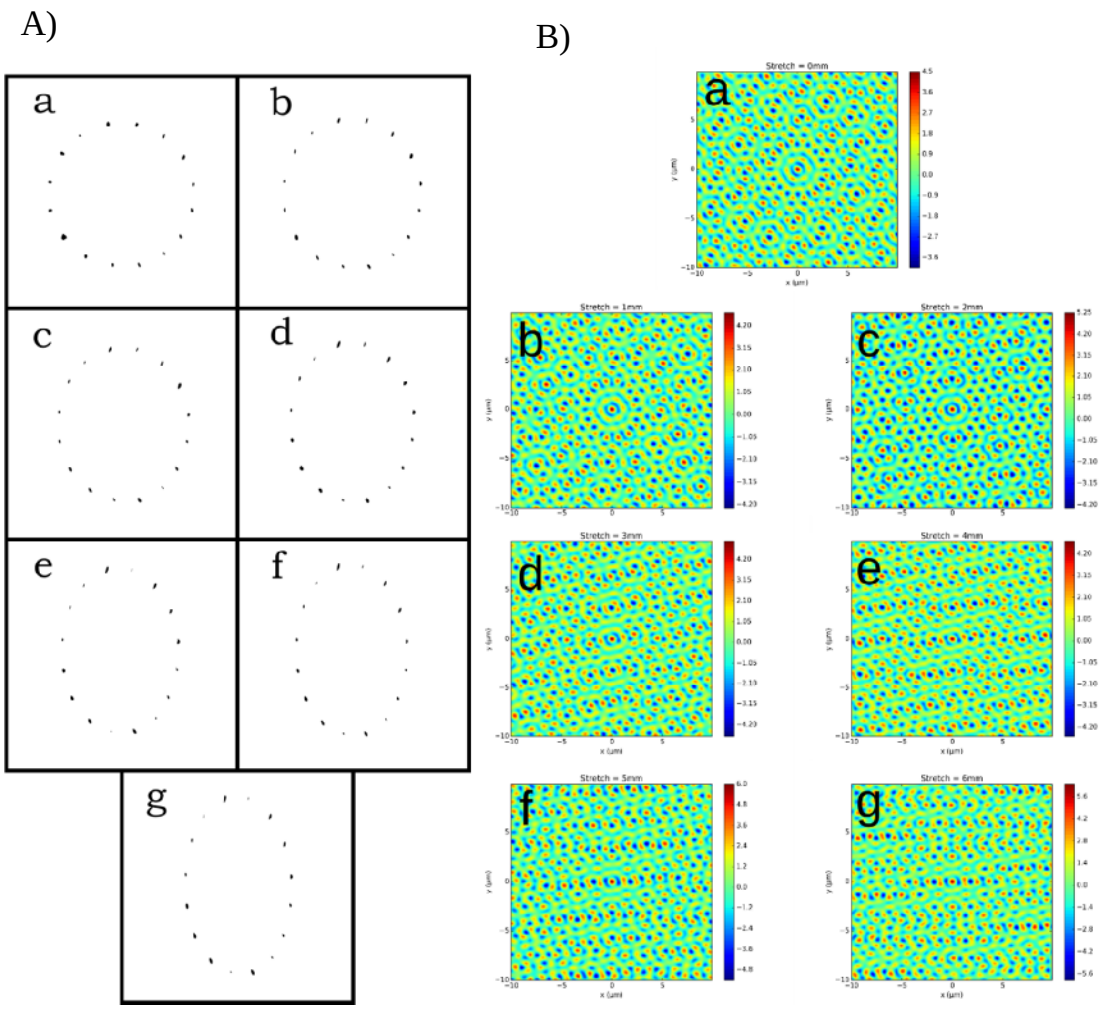

Fig. IV.4-6 : A) Evolution of 16-folds PDMS SRG diffraction pattern a)no stretching b-g) stretching 1 mm to 6mm, B) Evolution of the 16-folds quasi-crystal SRG on PDMSwith a) 0mm, b) 1mm, c) 2mm, d) 3mm, e) 4mm, f) 5mm and g)6mm of stretching

IV.5. Method for extraction of cavities' dimension on the PDMS sample

The PDMS surface structure, in theory, could be obtained through the Fourier Transform of the experimental diffraction pattern. However, this approach leads to very pixelated images, from which it is very hard to get quantitative measurements of the cavity sizes on the PDMS surface.

A more practical approach is to take into account the fact that we already know that a structured surface can be described as a sum of sinusoidal gratings. From the measured Λ_i ,α_i and s_i we can mathematically describe the surface S(x, y) of the grating as :

$$S(x,y)=\sum_{i=1}^{N} s_i \cos\left(2\pi \frac{x\cos\alpha_i + y\sin\alpha_i}{\Lambda_i}\right) \qquad \text{(IV.5-1)}$$

Contrary to the Fourier Transform of the diffraction pattern, the S(x, y) profile can be reconstructed with an arbitrary precision. In order to find the size of the nano-cavities, we first have to find their positions. That is to say the minima of S(x, y). First, we list the critical points $\{(x_c, y_c)\}$ of S(x, y), where both partial derivative are zero, with respect to x and y. Then, we apply a second derivative test for the functions of two variables:

$$D(x_c,y_c)=\frac{\partial^2 S}{\partial^2 x}(x_c,y_c)\frac{\partial^2 S}{\partial^2 y}(x_c,y_c)-\left[\frac{\partial^2 S}{\partial x \partial y}(x_c,y_c)\right]^2 \qquad \text{(IV.5-2)}$$

In order to know if the given critical point (x_c ,y_c) corresponds to a minimum (D > 0 and $\frac{\partial^2 S}{\partial^2 x} > 0$ a maximum (D > 0 and $\frac{\partial^2 S}{\partial^2 x} < 0$ or a saddle point (D < 0).

Once a minimum is found, we create a list of close maxima and neighboring saddle points, that is to say maxima and saddle points with a distance smaller than the distance between the current minimum and the other closest minima.

The last step to obtain a quantitative estimation of the size of this nanocavities is to find the minimum-volume covering ellipsoid that encloses all the neighboring maxima and saddle points. For this purpose, we used the Moshtag's MVEE 28 (minimum volume enclosing ellipsoid) algorithm.

A flowchart of the algorithm is shown in Fig.IV.5-1. The procedures were implemented in the Python programming language (Python 3.5.1), with the numpy (version 1.10.4) and scipy (0.17.0) modules.

The source code of our home made software, Quasi Crystal Diffraction Pattern Analysis (qcdpa), can be found at : https://github.com/MLoum/qcdpa

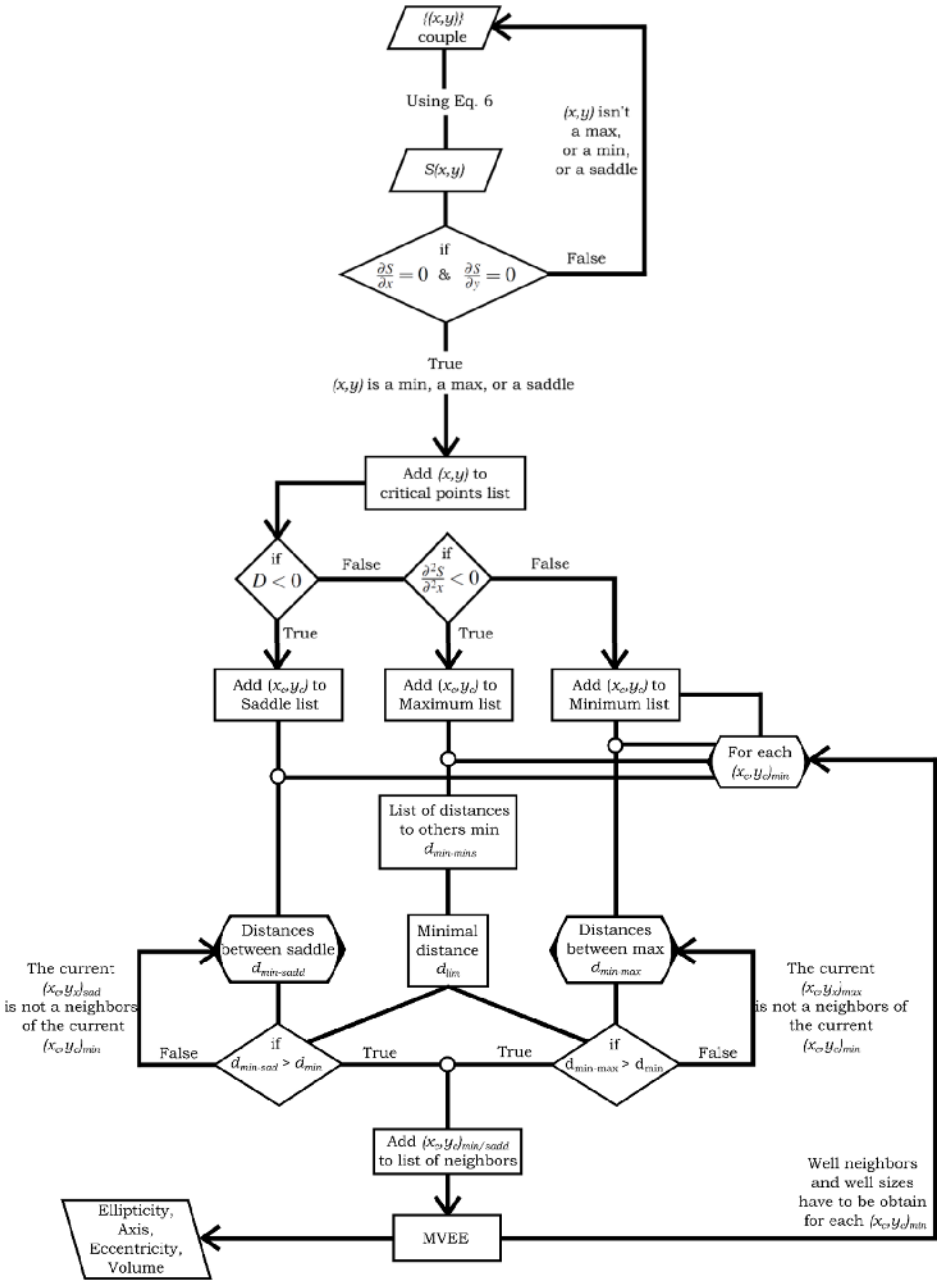

Fig. IV.5-1 : Flow chart of the nanocavities' analysis algorithm.

IV.6. Simulation of the random Gaussian surface

In order to confirm that the photoinduced surface on the thin film is a random surface, obtained with a stochastic process and resulting from an acting random molecular surface process, we simulated the Gaussian surface pattern, considering the same lateral correlation length as the experimental measurements.

The simulated surface is characterized using terms from probability theory, such as; height distribution function (hdf) or the statistical moments of mean and variance (or rms height [σ]). The surface variations in the lateral directions are described by the auto covariance function (acf), which describes the covariance (correlation) of the surface with translationally shifted versions. The correlation length (τ) is the typical distance between two similar features (e.g. hills or valleys). Simulation of the random rough surface with a Gaussian statistics is done using a method outlined in, where an uncorrelated distribution of surface points, using a random number generator (i.e. white noise), is convolved with a Gaussian filter to obtain correlation. This convolution is most efficiently performed using the discrete Fast Fourier Transform (FFT) algorithm. Basically, the simulated surface can be generated by

$$z_{p.q} = \sum_{k=0}^{M-1} \sum_{l=0}^{N-1} h_{k\ell} \eta_{p+k,q+\ell} \qquad \text{(VI.6-1)}$$

With p = 0,1,2,…,(M-1), q = 0,1,2,…,(N-1). h_{kI}, called the FIR filter (Gaussian filter), is the coefficient defining the system and h is a series of Gaussian random numbers. Thus, a M x N point surface with a given m x n ACF is generated. m and n should be less than M and N. We take $h_{r,s}$ and $H_{k,I}$ as:

$$H_{k,\ell} = \sum_{r=0}^{m-1} \sum_{s=0}^{n-1} h_{r,s} exp\left(i2\pi \left[\frac{kr}{m} + \frac{ls}{n}\right]\right) \quad \text{(IV.6-2)}$$

$$h_{r,s} = \frac{1}{mn} \sum_{k=0}^{m-1} \sum_{\ell=0}^{n-1} H_{k,\ell} exp\left(-i2\pi \left[\frac{kr}{m} + \frac{ls}{n}\right]\right) \quad \text{(IV.6-3)}$$

With k_r = 0, 1, 2, …., (m-1) and $\mathbf{l}_s$ = 0, 1, 2, …, (n-1). The FFT of equation1 gives:

$$Z_{k,\mathbf{l}}(w) = H_{k,\mathbf{l}}(w) A_{k,\mathbf{l}}(w) \quad \text{(IV.6-4)}$$

Where, $A_{k,\mathbf{l}}(w)$ is the FFT of h and $H_{k,\mathbf{l}}$ is the transfer function. We take the inverse FFT of $Z_{k,\mathbf{l}}(w)$ to obtain the simulated random surface.

The result of the simulations is given in fig.IV.6-1. It is seen that we are unable to find information of short range or very short range periodicities in the simulated surface structure, like in the measured AFM surface (Fig.III.2-1). By taking the fast Fourier transform (FFT) of the surface corresponding to the image in frequency domain, these short range periodicities are particularly probed in this simulation and in the experiment. fig.IV.6-1b shows the FFT spectrum of the simulated random surface, which is a random distribution of data points in frequency domain and is confined to a circular range of k-vectors, similar to the random photoinduced surface (Fig.III.2-1b).

This 2D Fourier transform does not show any specific frequency distributions, characterized by two symmetrical spots generally attributed to short range periodicity, confirming the absence of short range periodicities.

This figure is in agreement with Fig.III.2-1b, confirming the similarity between these two surfaces. Hence, the name of quasi random surface for the self-photostructuration of azopolymer 1 is justified.

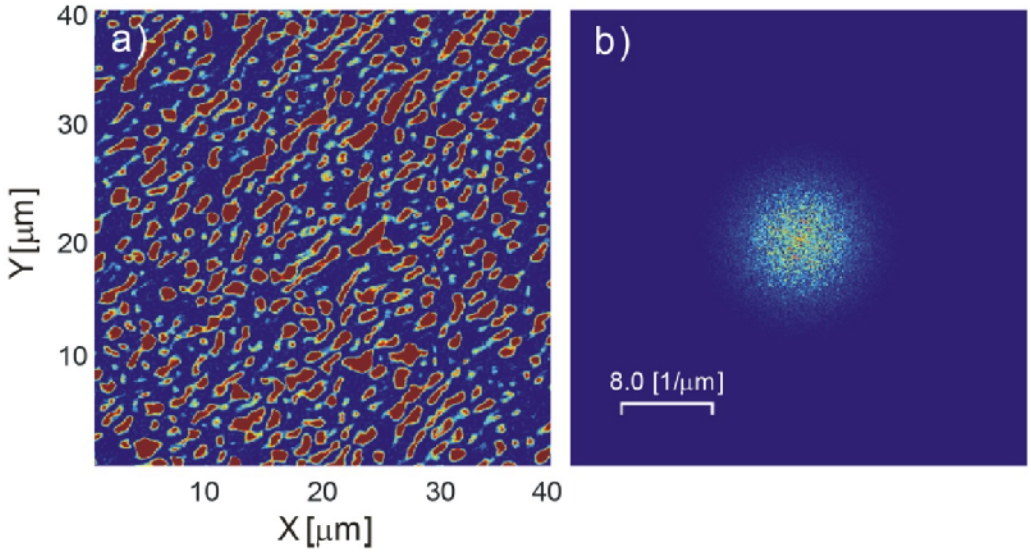

Fig. IV.6-1 : a) Simulation of a Gaussian surface considering the parameter of the photoinduced surface with the azopolymer 2, b) Fourier transform of the simulated surface.